ASSESSMENT OF A WAKE VORTEX

FLIGHT TEST PROGRAM

By Selden B. Spangler, Marnix F. E. Dillenius,
Richard G. Schwind and Jack N. Nielsen
Nielsen Engineering & Research, Inc.

NEAR TR 48

July 1974

TABLE OF CONTENTS

ASSESSMENT OF A WAKE VORTEX FLIGHT TEST PROGRAM

By Selden B. Spangler, Marnix F. E. Dillenius,
Richard G. Schwind and Jack N. Nielsen
Nielsen Engineering & Research, Inc.

SUMMARY

An investigation was made of a proposed flight test program by the Ames Research Center, NASA to measure the characteristics of wake vortices behind a T-33 aircraft. A number of facets of the flight tests were examined to define the parameters to be measured, the anticipated vortex characteristics, the mutual interference between the probe aircraft and the wake, the response of certain instruments to be used in obtaining measurements, the effect of condensation on the wake vortices, and methods of data reduction.

On the basis of the investigation, it is recommended that the probe aircraft (a Learjet) make horizontal passes through the vortex wake, entering the wake at right angles to its length. Since the generating and probe aircraft are similar in speed, size, and weight, the motions of the probe aircraft approaching and passing through the wake are not severe and the corrections to the hot-wire data due to aircraft motion should be small. In addition to the basic hot-wire measurements of the velocity field in the vortices, it is recommended that supporting data be obtained to define the environment in which the vortices persist and dissipate. Specific recommendations on the type of data and means of measurement are given. A data reduction method was developed to reconstruct the velocity field and essential features of the vortex, based on knowledge of the velocity components along some flight path through the vortex. Finally, it is noted that very little information is available on the dissipation of vortices, and measurements in this region would be most valuable as an aid in understanding the dissipation mechanisms.

INTRODUCTION

This report presents the results of a study to assist the Ames Research Center staff in defining a flight test program to critically evaluate theories for trailing vortex behavior and decay. The objective

of the study is to examine the various aspects of the proposed flight
test program to establish requirements for data and to make recommendations
concerning test procedures, instrumentation, and data reduction. The back-
ground for this work consists of theoretical analysis on trailing vortices
done under contract to the Air Force (Contract F44620-70-C-0052) and
experimental work on measurement of trailing vortex characteristics with
hot-wire probes in the Ames Research Center 40- by 80-Foot Wind Tunnel
(Contract NAS2-6719).

A number of problems connected with the flight tests were investigated.
The various theories and analyses of trailing vortices were examined to
define the parameters that should be measured. Investigations were made
of atmospheric turbulence, the mutual interference between the probe air-
craft and the vortex system, effects of condensation on the vortex, the
response of certain instruments, and methods of data reduction. The
results of these investigations are described in the various sections of
this report. In addition, a section is included describing the NEAR
experience with the 40- by 80-Foot Wind Tunnel program to the extent that
it could be instructive in planning and executing the flight test program.

LIST OF SYMBOLS

b	wing span
c	speed of sound or chord
c_p	specific heat at constant pressure
$\bar{c}$	wing mean aerodynamic chord
C_D	wing drag coefficient, based on S_w
C_ℓ	rolling moment coefficient, defined as the rolling moment divided by $qS_w\bar{c}$
d	distance of a crossflow plane of interest downstream of the wing
e	voltage output of a hot-wire probe
$E(k)$	one-dimensional power spectral density for atmospheric turbulent velocity fluctuations along the aircraft direction of flight

f	frequency, Hz
G(k)	one-dimensional power spectral density for atmospheric turbulent velocity fluctuations normal to the aircraft direction of flight
I_o	total enthalpy, defined by equation (11)
k	inverse of the wave length, or thermal conductivity
K	vortex strength parameter, vr
m	mass
m_ℓ	slope of the line normal to the resultant velocity vector V_r. $m_\ell = \tan \Theta_\ell$ (figure 8)
M	molecular weight
Nu	Nusselt number
N_{Pr}	Prandtl number
p	static pressure
q	free-stream dynamic pressure, $1/2\ \rho U^2$
r	radius
r_i	outer radius of vortex eye region, figure 1
r_j	outer radius of vortex logarithmic region, figure 1
r_o	radius at which K has reached 99 percent of its asymptotic value, figure 1
r_1	radius for peak tangential velocity, figure 1
Re	Reynolds number, based on hot-wire diameter unless otherwise indicated
t	time
T	static temperature
S_w	wing area
u,v,w	vortex velocities in a cylindrical coordinate system, u radial, v tangential, and w axial

u', v', w' fluctuating velocity components of atmospheric turbulence, u' in direction of aircraft motion, v' lateral to direction of aircraft motion and horizontal, and w' vertical

u_a, v_a, w_a steady perturbation velocities induced around the Learjet aircraft, u_a axial, positive forward, v_a lateral, positive to starboard, w_a vertical, positive down

U aircraft flight speed or wind-tunnel speed

V_n component of the vortex induced perturbation velocity normal to the probe flight path for a horizontal probe traverse in the crossflow plane

V_r vector sum of V_n and V_s

V_s component of the vortex induced perturbation velocity coaxial with the probe flight path for a horizontal probe traverse in the crossflow plane

V_t vortex tangential velocity (equal to V_r)

W weight

x, y, z axis system with origin at the fuselage nose, x positive forward along fuselage centerline, y spanwise positive to left, and z positive down

Z, Y coordinate system in the crossflow plane of the trailing vortex wake, Y positive to the right, Z positive down when looking upstream (figure 8)

α aircraft angle of attack

α' perturbation angle due to turbulence, equation (6)

α_c angle between V_t and V_n. Tan $\alpha_c = V_s/V_n$ (figure 8)

Γ_o vortex circulation strength at r_o

Γ_1 vortex circulation strength at r_1

$\overline{\delta^2}$ mean square displacement of the vortex from its mean position due to turbulence

Θ_ℓ angle between the Z axis and the radius vector to the apparent vortex center, measured from the positive Z axis in the counterclockwise direction (figure 8)

Θ_s angle between the Z axis and the local tangent to the flight path, measured from the positive Z axis in the counterclockwise direction. Its tangent is the slope of probe flight path, (figure 8).

4

λ_s scale length of turbulence

μ viscosity

ν kinematic viscosity

ρ mass density

σ rms turbulence velocity, normalized by U

ω absolute humidity

Subscripts

a   air

ax   axial component

c   vortex centerline

m   mean

sat   saturation value

w   wire or water vapor

∞ condition at a large radial distance from the vortex

WIND TUNNEL EXPERIENCE ON WAKE VORTEX MEASUREMENTS

In January and June of 1972, tests were conducted in the Ames Research Center 40- by 80-Foot Wind Tunnel to measure velocity profiles in the trailing vortex system behind two wings. The instrumentation used consisted of a three-wire DISA hot-wire probe. NEAR personnel were intimately involved in the design, execution, and data reduction in these tests. The experience gained in these tests, insofar as it may have a bearing on the proposed flight test program, is briefly described in this section.

Two rectangular wings were used: an 8-foot span with 18-inch chord and a 32-inch span with 6-inch chord (one-third scale). The wings were mounted in the center of the tunnel cross section and angles of attack of 8° and 12° were tested. Both wings contained smoke generators consisting of electrically heated tubes through which mineral oil was forced. The smoke exited the wing on the under surface very close to the tips at about mid-chord. From visual observations, the smoke was essentially

completely entrained into the vortex system in a thin annulus at about the core radius as long as the oil flow was steady. If the oil flow "chugged", puffs of smoke would appear which would be contained within a cylinder of perhaps 5 or 6 core radii concentric with the core, and these puffs would be convected downstream without any apparent dissipation or radial diffusion within the run length from the test section down to the turning vanes of the tunnel.

The hot-wire probe was mounted on a rotating arm so that it would pass through the vortex sufficiently rapidly that the vortex could not move significantly during the passage time of the probe. The signals were taken out of the arm through slip rings and recorded on magnetic tape. The minimum noise level obtained on the tape recorder alone (in a well-adjusted condition) with a 2-volt, full-scale range was about 10 millivolts. The hot-wire probe was calibrated before each run, since the calibration was found to change slightly between runs (from hour to hour). Calibration points at five to ten speeds were taken, since there was some scatter in defining the straight line relation between $(volts)^2$ and $(velocity)^{1/2}$. All calibration and vortex data were taken without smoke so as not to foul the wires on the probe.

Some conditions were experienced which exceeded the acceptance half-angle of the probe, which was 35°. The arm was rotated at a speed such that the tangential velocity equalled the tunnel air speed. The probe was then mounted at 45° to the plane of arm rotation, such that the nominal relative velocity was aligned with the probe axis. Under certain combinations of high wing angle of attack (high Γ), probe location and probe direction entering the vortex center, the vector sum of the tunnel velocity, the probe translation relative velocity and the peak tangential velocity in the vortex produced a velocity making an angle with respect to the probe axis as great as 40°.

During the course of the tests, it was found to be extremely useful to have an oscilloscope with a "memory" display feature in parallel with the tape recorder and connected to one of the three wires. Since the vortex meander in the tunnel (due to turbulence) caused only a small proportion of the passes to be core penetrations, the use of the oscilloscope provided an excellent means of determining when core penetrations began to occur as the instrumentation tower containing the rotating arm

6

was translated across the tunnel. Later, some oscilloscope photographs
were taken of the outputs of the wires as recorded on analog tape in order
to provide data for a manual check of the data reduction program for trans-
forming the velocity components from the probe to the vortex coordinate
system. An example of a set of scope photographs is shown in figure 1.

The data reduction method involved having the analog information on
the magnetic tapes digitized and entered directly into a computer for
calculating the corrected velocities. It was found that there is a com-
bination of minimum tape recorder speed and digitizing rate necessary to
give adequate definition of the trailing vortex velocity profile. When
the signals for the vortex, shown in figure 1, were digitized, there were
seven points in the core. This is probably the minimum allowable definition
for the tangential velocity profile, but it is inadequate for the axial
velocity profile. This vortex was generated by the 32-inch span wing, and
the profile is 55 chords downstream. The core diameter is 0.68 inch. The
probe traversed through the vortex at 90 feet per second. The tape record
was generated at 60 inches per second and played back at one-eighth that
speed. The digitizer cycle time was 1 millisecond. As a check on the
digitization process, a sine wave was recorded on the tape prior to
recording the hot-wire data on each run.

NOMINAL FLIGHT VORTEX CHARACTERISTICS

Certain decisions have been made by Ames Research Center concerning
the aircraft to be used and some flight parameters. On the basis of
these data, calculations have been made to define the wake characteristics.
The results are summarized in this section.

The generating aircraft is a T-33 without tip tanks. The pertinent
characteristics of this aircraft are given in Table I. The flight tests
are to be conducted at 12,500 feet altitude at a speed of 300 feet per
second. The results of reference 1 indicate that the T-33 wing planform
should have a nearly elliptic span load distribution. With this assumption,
the trailing vortex span is $\pi/4$ of the wing span. The equation relating
the lift on the bound vortex to the aircraft weight provides the following
relation for the circulation strength

$$\Gamma_o = \frac{4W}{\pi b \rho U} \tag{1}$$

7

For an NACA standard atmosphere (Table II), the circulation strength of the vortices laid down by the T-33 is 819.5 feet^2 per second. The initial vortex span is 29.4 feet.

The specification of the characteristics of a wake vortex follow the theoretical model of a vortex developed in reference 2. The nomenclature is illustrated in figure 2. The vortex is divided into four regions for purposes of specifying the circulation and velocity distribution. There is a solid-body-rotation core (the eye), outside of which are the logarithmic and outer regions. The outer boundary of the latter is the radius (r_o) at which the vortex strength has achieved 99 percent of its asymptotic value. Beyond r_o, the vortex has the classical potential vortex form.

The initial vortex characteristics after roll-up (some 2 to 4 spans downstream of the wing) were estimated on the basis of test results obtained in the 40- by 80- and 7- by 10-Foot Wind Tunnels. For the 8-foot span rectangular wing at a lift coefficient of about 1, a value of r_1 = 1.1 inches was measured 55 chords downstream of the wing. The vortex radius did not appear to change with distance downstream, as visualized by smoke. For tests in the 7- by 10-Foot Wind Tunnel, Corsiglia and Chigier found at comparable distances downstream and at the same angle of attack that the vortex core radius for a Convair 990 swept-wing model was approximately twice that of a rectangular wing. This difference is attributed to the influence of span load distribution on the rolling-up process, since the swept wing had more nearly an elliptical span load distribution than the rectangular wing. Further, tests in the 40- by 80-Foot Wind Tunnel on the 8-foot span wing and a 32-inch span wing indicated the vortex core radius to be approximately proportional to the span. Thus, the 1.1-inch radius, scaled up to the T-33 span and doubled to account for the influence of span load distribution, yields a value for the flight tests of 0.86 foot. This value may be somewhat high but it will be used as the nominal T-33 wake vortex radius, r_1, in the remainder of the calculations.

As a part of the analysis of data taken from the 40- by 80-Foot Wind Tunnel tests, the velocity distributions taken through the core by hot-wire probes were examined to obtain the circulation distributions. On the basis of these measurements, the radius ratio r_1/r_o was found to be about 0.4. Therefore, with Γ_o, r_1, and r_o known, Γ_1 can be obtained

from equation (6) of reference 2,

$$\frac{K_o}{K_1} = 0.76 - 0.928 \ln \frac{r_1}{r_o} \tag{2}$$

The following results are obtained:

$$\Gamma_o = 819.5 \text{ feet}^2 \text{ per second}$$

$$\Gamma_1 = 509 \text{ feet}^2 \text{ per second}$$

$$v_1 = 94 \text{ feet per second}$$

$$r_1 = 0.86 \text{ foot}$$

$$r_o = 2.15 \text{ feet}$$

These values would obtain 55 chords, or about 370 feet, behind the T-33 wing. On the basis of the wind-tunnel tests, these values would not change appreciably up to 800 feet behind the aircraft. No systematic measurements exist for longer distances downstream.

Axial velocity profiles measured in the 40- by 80-Foot Wind Tunnel at 55 chords downstream of the 32-inch span wing indicate a maximum axial velocity defect of about 15 feet per second for a free-stream velocity of 90 feet per second. The entire defect occurs within a cylinder having a radius approximately equal to r_o. Insufficient data have been reduced to determine the manner in which this defect changes with free-stream velocity and wing lift. It should be noted that the axial velocity profile could have large gradients and a complicated structure. The wind-tunnel measurements at 55 chords show a profile similar to the sketch
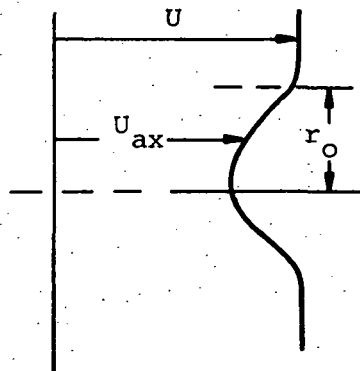
whereas smoke studies made near the ground show regions near r_o where one annulus of flow is moving upstream and one annulus downstream relative to an observer on the ground.

Several things can happen to change the vortex spacing and radius. The vortex pair moves vertically downward by self induction. Buoyancy effects begin to occur due to altitude changes or engine wake ingestion which can have the net effect of continuing the downward motion, causing a leveling off of the vortex pair or causing the vortices to rise again, depending on the atmospheric temperature profile and the gas temperature in the vortices (engine air ingestion). MacCready (ref. 3) indicates cases over the ocean where vortices have continued to descend (at least at low altitude) whereas most other observations (over land) have indicated leveling and/or rising of the vortices after an initial descent. The vortex spacing and strength could change the order to 10 to 20 percent due to the influence of the buoyancy forces over a typical vortex wake life- time (ref. 2). The vortex radius would tend to increase, probably rather slowly, with vortex age due to diffusion outward of the vorticity. The rate at which this happens depends on atmospheric turbulence and is not predictable with confidence at this time.

The persistence of the vortices also depends greatly on atmospheric turbulence. Typical persistency times range from 60 to 150 seconds, which in distance correspond to approximately 3-1/2 to 8-1/2 miles at 300 feet per second.

Turbulence tends to promote breakup of the vortex system either by a Crow instability, in the event of energy in the turbulence having wave lengths comparable to the vortex span, or by single vortex bursting due to axial pressure gradients. Persistency of 120 to 140 seconds was obtained behind a Boeing 747 over land at 4000 feet altitude (ref. 4) and of 40 to 70 seconds behind a DeHavilland DHC-2 at 1000 feet altitude in "relatively calm" air over land (ref. 5). In the latter tests, increasing turbulence levels changed the dissipation mode from single vortex dissi- pation to the Crow instability. Contrail tests reported in reference 6 on a T-33 aircraft indicate contrail lengths as long as 20,000 feet, al- though the speed and altitude of the aircraft are not specified. If flights are to be made over the ocean, it is probable that the turbulence levels are somewhat lower than over the land, and a reasonable estimate for the vortex trail length would be 60 to 90 seconds, or 3-1/2 to 5 miles.

10

ATMOSPHERIC TURBULENCE MEASUREMENTS

It is recognized that atmospheric turbulence plays a significant role in both the time to dissipation of a vortex and the mechanism of dissipation. At present, however, no rational method for predicting the effect of turbulence on vortex dissipation has been developed. It is desirable, nonetheless, to obtain measurements of atmospheric turbulence levels (as well as other atmospheric conditions) during the flight tests to completely document the environmental conditions and provide data for subsequent theories which will be able to treat the influence of turbulence.

Turbulence wave lengths long compared to the generating aircraft span can generally be expected to be important in deforming the trailing vortices and amplifying instabilities of the Crow type. Very short wave length turbulence will determine the turbulent shear, $\overline{u'v'}$, at the edge of the vortices, and so is important for determining the expansion in diameter of each trailing vortex. It is important therefore to determine how to measure the atmospheric turbulence, yet keep the effort to be expended on its measurement in correct perspective when compared to the most important task of obtaining high quality vortex velocity profiles.

Figure 3 is a power spectrum for atmospheric turbulence. It results from a composite of information from references 7, and 8. Only relative units are given on the ordinate, as the whole curve will shift up or down with increasing or decreasing turbulence intensity. Fortunately, the turbulence wave lengths that are of concern for the present study are 1000 feet and less. The turbulent structure in these wave lengths is independent of how the much larger eddies were produced, and this range is known then as the universal equilibrium range. This range is divided into two parts. The upper portion down to 0.1-foot wave length is the inertial subrange. The energy there decreases as $k^{-5/3}$, where k is the inverse of wave length. At shorter wave lengths, where viscous dissipation is important, the energy decrease with k is often approximated with k^{-7} (ref. 9). A negligible fraction of the total turbulence energy is in this dissipation region, although this turbulence may still be important to vortex diffusion.

Since the shape of the turbulence spectrum in the range of wave lengths of interest to the trailing vortex problem is known, but the over-all level of the curve is unknown, only one measurement is needed to define the curve. The simplest measurement would appear to be the root-mean-square of the turbulence signal from one hot wire over a specified frequency range. The following analysis has been made to determine rms signal levels that can be expected and to identify problems with this measurement.

MacCready (ref. 7) has compared and quantified atmospheric turbulence levels with pilot's qualitative reports of its effect on the aircraft, i.e., "zero," "light," "moderate," etc. It is generally expected that trailing vortices persist longest at the lowest turbulence levels, so the turbulence rms levels should be low where the planned flight tests are performed. Selecting the limit between "zero" and "light" turbulence from Cessna 180 tests, the turbulence spectrum in the inertial subrange (0.1-foot to 1000-foot wave lengths) as sensed by an aircraft with velocity U, feet per second, can be described by (ref. 7):

$$\frac{3}{4} G(k) = E(k) = 0.585 \times 10^{-3} U^{2/3} f^{-5/3} \tag{3}$$

The frequency is f, Hz; $E(k)$ is the one-dimensional power spectral density for longitudinal velocity fluctuations (ft^2/sec), and $G(k)$ is that for the lateral fluctuations. Although the turbulence is isotropic, the velocity fluctuations measured from a moving vehicle are not true energies and thus differ slightly for different components (ref. 10). If the aircraft did not respond to this turbulence or the effect of its movement were subtracted out, then a single hot wire perpendicular to the aircraft axis would measure $E(k)$.

Integrating equation (3) between two frequencies f_1 and f_2 gives the mean square between those frequencies:

$$\overline{u'^2}\bigg|_{f_1}^{f_2} = \int_{f_1}^{f_2} E(f) df = -0.876 \, U^{2/3} (f_1^{-2/3} - f_2^{-2/3}) \tag{4}$$

For $U = 300$ feet per second, $f_1 = 0.2$ Hz, and $f_2 = 200$ Hz, the rms turbulence level is

$$\frac{\sqrt{\overline{u'^2}}}{U} = 0.11\%$$

As a point of reference, this is a low turbulence level for a wind tunnel. Using the method of calculation described immediately below, the turbulence level in the 40- by 80-Foot Wind Tunnel has recently been found to be 0.45%.

Good hot-wire sensitivity and low instrumentation noise is necessary to properly measure the above turbulence level. The constant temperature hot-wire anemometer sensitivity is determined from its operating equation

$$e^2 = A + Bu^{1/2} \tag{5}$$

where e is volts, u is the instantaneous velocity component perpendicular to the wire, and A and B are operating constants. Larry Olsen recently used a DISA hot wire in a test in the Ames 40- by 80-Foot Wind Tunnel that is similar to that planned for the flight tests: a 10-micron diameter platinum-rhodium wire with plain ends (not gold plated). At an overheat ratio of 1.6, he measured 9 volts at 30 feet per second, and 12 volts at 250 feet per second; thus B = 5.57. Differentiating equation (5) and rearranging,

$$\sqrt{\overline{e'^2}} = \left(\frac{B}{4eU^{1/2}}\right) \sqrt{\overline{u'^2}} \tag{6}$$

For U = 300 feet per second, e = 12.3 volts, and for the above turbulence level, the rms signal will be 0.9 millivolts. It would be desirable to measure turbulence levels down to about one-third this level of transition between "zero" and "light" turbulence, i.e., 0.3 millivolts.

The DISA 55D35RMS Voltmeter (Large-Scale Aerodynamics has three of these) has a much lower frequency limit than other rms meters; its limit is 0.1 Hz. Its smallest full-scale reading is 1 millivolt, so the turbulence level can be measured with this meter. A problem arises, however, with the rolloff of an rms meter. For the DISA meter it is conjectured to look as presented below.
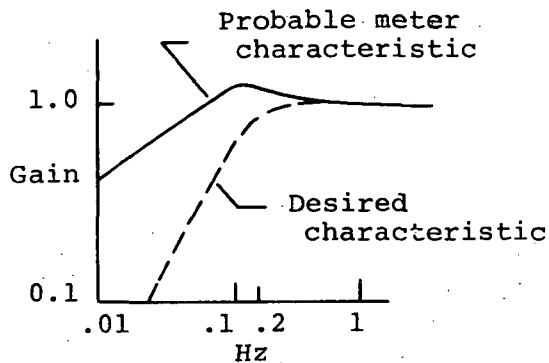
Since the turbulent spectrum energy level keeps rising rapidly below the lower frequency limit that is selected, the lower limit should be filtered to obtain a characteristic such as shown with the dotted line. Once this characteristic is known, the above integration should be redone. There is negligible energy above the upper frequency limit, so there is no need for a cut-off filter there unless it is to eliminate instrumentation noise.

It should be noted that the noise level of a magnetic tape recorder is too great to allow the hot-wire signal to be recorded and the rms value determined later. Under good laboratory conditions, the minimum noise level for a good tape recorder set for a 2-volt range (typical of the range needed for the above hot-wire sensitivity) will be about 10 milli-volts rms. It is therefore recommended that the rms level of at least one channel, preferably all three, of the triple sensor hot-wire anemo-meter be read directly in the flight test experiment during straight and level flight outside of the vortex. (The readings need not be simultaneous, but may be switched through one meter.) The DISA rms meter has an external plug for the mean square value, and this output could be recorded, if preferred.

The noise level on the DISA model 55D05 battery-operated constant temperature hot-wire anemometer is advertised to be approximately 0.8 millivolts rms at full band width. The band width of the anemometer depends on the probe wire diameter and measuring conditions, but will probably be at least 50 KHz. It is expected that the instrument noise

14

level can be greatly reduced by using a high frequency filter at 5 to 10 KHz, and thus still make possible the measurement to the above listed turbulence levels.

The above analysis for the response of the hot-wire anemometer to the atmospheric turbulence assumes that the hot wire is mounted on a perfect platform that does not respond to the turbulence. The short period frequency of the Learjet is 0.6 Hz, and the boom natural frequency is about 11 Hz, both within the integration band width used above. The data can be examined after the flight for energy at these frequencies and some smoothing can be done if it appears necessary.

Another possibility that should be considered is operation of the data recording system at higher sensitivity levels compatible with measurement of turbulence velocities for enough periods of time away from the vortex wake to attempt to establish ambient turbulence levels.

The vanes on the boom also respond to the lateral turbulence components v' and w'. Again making the simplifying assumption that the platform on which the vanes are mounted does not respond to the turbulence, as for the previous analysis, the output signal from the vanes is easily determined. Denoting the perturbation angle of the flow due to turbulence in the vertical direction as α', then

$$\alpha' = \tan^{-1} \frac{w'}{U + u'} \simeq \frac{w'}{U} \tag{7}$$

The vanes only respond accurately to the frequencies up to 15 Hz. Changing the upper frequency limits in the integration performed in connection with equation (4) from 200 to 15 Hz reduces the integral by 2 percent. Including the 4/3 factor for lateral turbulence,

$$\sqrt{\overline{\alpha'^2}} = 0.0014 \quad \text{radians}$$

For the vane angle transducer sensitivity of one volt per 10°, there results

$$\sqrt{\overline{\alpha'^2}} = 8.2 \quad \text{millivolt rms}$$

During the series of tests on trailing vortices in the 40- by 80- and the 7- by 10-Foot Wind Tunnels, it was observed that the vortices were undergoing significant lateral oscillations which appeared to increase in amplitude with increasing distance downstream of the wing. This behavior was believed to be induced by turbulence in the tunnels. Motion pictures were taken of the vortex motion and some statistical analysis was done on the photography. In addition, a theory was developed to explain the results. The details of this work are reported in reference 11. Since the work yields some indication of the anticipated random motion of the vortices in flight, the major results are reported here.

The motion of the vortices in the tunnels was found to be quite random. The correlation between the vertical and horizontal deviations from the mean position of a vortex was found to be quite high, however, which might indicate that some organized form of motion such as a "cork-screw" form was occurring. The rms values of the displacement of the vortex from its mean position $(\overline{\delta^2})$ were calculated at several locations and are shown as the data points in figures 4(a) and 4(b), for the 40- by 80-and 7- by 10-Foot Wind Tunnel tests respectively. The turbulence velocity levels, σ, are measured values for the two tunnels. The data in figure 4(a) are for both the 8-foot and the 32-inch span wings and show that the rms displacement is independent of the wing scale. The reason for the difference between right and left vortices is not known, but may be a result of a consistent variation across the tunnel of turbulence level.

A theory was developed for the vortex motion at a distance d downstream of the wing, based on the premises that the vortex is a filament which has the transverse velocity locally of the turbulence at that point and the vortex does not respond to high frequency turbulence. The results of the analysis indicate that the root-mean-square deviation of the vortex varies with d as shown.

$$\frac{\sqrt{\overline{\delta^2}}}{\sigma} = d\sqrt{\frac{2}{\pi} \arctan \frac{\lambda_s}{d}} \tag{8}$$

where λ_s is a scale wave length of the turbulence. For cases where λ_s/d is large (small d or large λ_s), the arctan is $\pi/2$ and

16

$$\frac{\sqrt{\overline{\delta^2}}}{\sigma} = d \qquad\qquad (9)$$

Equation (8) is represented as the lines in figure 4, with the values of the parameters shown. The values of the turbulence scale selected were values approximating the cross section dimensions of the tunnels, which are shown to cause reasonably good agreement with the data.

The theory can be applied to the flight test conditions, provided the form of the power spectrum is known. Using the model from reference 7 for the inertial subrange, the results of figure 5 were obtained. These results indicate that the rms displacements reach the order of the wing semispan for light turbulence with typical values of the turbulence length scale at distances of 2 to 4 miles aft of the aircraft. Provided that single vortex bursting has not occurred within this distance, this calculation would indicate the minimum distance required to permit the "touching" of the two vortices and the subsequent formation of vortex rings, in accordance with the Crow instability model.

DATA REQUIREMENTS FOR THE FLIGHT TESTS

A principal objective of the flight test program is to obtain velocity profile measurements of wake vortices as an input to the problem of calculating the severity of aircraft-wake encounters. In addition, it is desirable to obtain sufficiently detailed measurements of both the vortices and the environment to permit evaluation of theories describing the formation, motion, and dissipation of wake vortices. For this purpose, existing theories have been examined to determine the kinds of data required either as input or as a means of evaluating the predictive capability. The theories examined were the following:

(a) The NEAR, Inc. vortex structure theory, reference 2.

(b) The work of McCormick, reference 12.

(c) The NASA work of Baldwin and Chigier, reference 13.

(d) The instability theory of Crow, reference 14.

(e) The NEAR, Inc. theory on buoyancy effects, reference 2.

(f) The buoyancy work of Scorer and Davenport, reference 15.

(g) The buoyancy work of Tombach, reference 16.

The data fall into three categories: airplane data, wake vortex data and meteorological data. The description of these data, together with a discussion of means of obtaining the data, is given below.

Airplane Data

The airplane data required are those necessary to define the circulation strength of the wake vortex system of the generating aircraft (the T-33). In accordance with equation (1), the following information is required:

(1) Aircraft weight at the time the wake is being generated.

(2) Aircraft air speed during a probe period.

(3) Air density at the altitude of the generating aircraft.

(4) Some indication of the constancy of the flight path of the generating aircraft. The ideal quantity would be a recording of vertical acceleration. The pilot's assessment would probably be satisfactory. For example, it has been shown (ref. 5) that small pitch oscillations of an aircraft at the correct frequency can decrease the time to onset of the Crow instability by a factor of 2. The object in the ARC tests is to maintain a constant wing lift (e.g., no vertical accelerations) so as to lay down a uniform wake.

(5) Some indication of the accuracy with which the air speed is maintained during a run. If the quantity is recorded, the records would provide an indication of the excursions. Again, the pilot's assessment would probably be satisfactory since this is not a critical area.

Trailing Vortex Data

The data required on the trailing vortices consist of velocity and temperature traverses through the vortices, auxiliary information to fix the location of the traversing station relative to the generating aircraft, and some photographic coverage. The considerations involved are discussed below.

18

The principal measurements to be obtained are three components of velocity through the vortex. These are to be obtained with a three-wire DISA hot-wire probe mounted on the nose boom of the Learjet. From the NEAR, Inc. hot-wire experience in the 40- by 80-Foot Wind Tunnel tests, several things are worthy of comment.

A portion of the core flow in the vortices may be made up of engine exhaust air, which is hotter than the ambient and therefore a potential source of error for the hot-wire measurements. The rate at which the engine exhaust mixes with the ambient air in the presence of the vortex system is not predictable at this time. A rough estimate was made assuming only a coflowing turbulent jet exists, and the calculations indicated that a 170 to 1 dilution of exhaust gases would occur within approximately 1700 engine exhaust radii, which is about one mile. If the engine exhaust temperature is 1000° F at the tailpipe, the mixed gas temperature is about 20° F at one mile, or some 6° above ambient. Thus a reasonable part of the vortex wake region of interest may have temperature differences above ambient that must be accounted for in the hot-wire data reduction, since 1° C temperature difference causes an error in velocity of about 2 percent. It is also of interest to know what the temperature profiles are in the vortex in order to apply buoyancy theories to the vertical motion of the vortex pair.

With respect to correction of the hot-wire results for temperature, Bradshaw (ref. 17) recommends that the calibrations be plotted in terms of Nusselt number (Nu) versus Reynolds number (Re) for the temperature conditions of the calibration procedure. Operation at other temperatures can then be evaluated through use of theoretical behavior for the effect of temperature on these parameters. The Reynolds number of the flow over a 10-micron wire at standard atmospheric conditions at 12,500 feet reaches a maximum of 45 in the vortex. This value is just at the transition region where the wake behind a cylinder begins to oscillate and affect the heat transfer. For a Reynolds number up to 44, Bradshaw recommends the heat transfer relation

$$Nu \left(\frac{T_m}{T_a} \right)^{-.17} = 0.24 + 0.56 \ Re^{0.45} \qquad (10)$$

where

$$Nu = H/\pi \ell k (T_w - T_a)$$

and

H = heat transfer rate to the fluid

ℓ = wire length

k = conductivity of air

T_w = wire temperature

T_a = air temperature

T_m = average of wire and air temperature

and Re and Nu are evaluated at T_m.

The Learjet carries a single wire probe for the measurment of temperature. Since this wire must have sufficient response to follow variations through the vortex, its thermal inertia characteristics were calculated to determine if a d.c. bridge might offer satisfactory response. Using the same wire type as for the three-wire probe, the wire time constant is about 3.5 milliseconds. However, for a 5-percent error in following a sinusoidal temperature oscillation, the maximum allowable frequency is only 15 Hz, which is too low for the vortex penetration case. Therefore, constant-current hot-wire anemometer electronics will be necessary to amplify and compensate the wire signal to obtain reasonable temperature frequency response (1000 Hz is adequate).

The acceptance angle of the hot-wire probe was a problem in the wind-tunnel tests. In the flight tests, however, with a Learjet velocity of 300 feet per second and a maximum tangential velocity in the vortex of 94 feet per second, the flow angles on the probe should not exceed 17.4°, which is well below the acceptance angle of 35°.

It should be noted that traversing directly through the center of an axisymmetric vortex will not produce a symmetric trace on a wire of the three-wire probe, even if it is aligned in the plane perpendicular to the vortex. For instance, for the above peak tangential velocity and traverse speed, and for typical values of A = 50 and B = 5.5 (eq. (5)), the voltage of the larger peak (or deflection on an oscilloscope) should

20

be 1.79 times that of the smaller peak. This is due to two factors that add, the nonlinearity between velocity and voltage in a hot-wire characteristic, and the nonlinear effect of angle change on the hot wire, as sketched here. The velocity components perpendicular to the wire for $\theta = 17.4°$, $0°$, and $-17.4°$ for $U = 300$ feet per second are 232,245 and 300 feet per second, respectively.

$\theta = 17.4°$

$17.4°$ 54.7
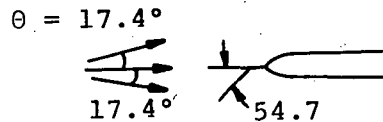
These velocities with the nonlinear velocity-voltage characteristic provide the unequal peak voltage measurements.

Calibration of the probe should be done at five to ten velocities in order to establish the voltage-velocity calibration curve, since there is always some scatter in the data. It would also be desirable to calibrate several times during a flight because of the possibility of smoke or particle impact changing the wire characteristics.

It was noted earlier that an oscilloscope with a "memory" feature was used to monitor the output of the wire that most nearly sensed tangential velocity in the wind-tunnel tests. It is recommended that this be done in the Learjet in order to determine when core penetrations are made, since so much more information is available with a core penetration than without.

Further, it was noted earlier that high tape recording speeds were used in the tunnel tests so that the tape could be slowed in the digitizing process to gain definition in the velocity profile in the core region. For flight test conditions of 300 feet per second, a core diameter of 1.7 feet, a digitizing cycle time of 2 milliseconds and no tape speed reduction or playback, the number of data points in the core would be only 2.9. Therefore, a 2 to 1 tape slowdown is absolutely necessary, and a 4 to 1 slowdown is desirable, particularly for measuring the axial velocity profile. If the minimum digitizing speed is 1-7/8 ips, then a recording speed of 7-1/2 ips is preferable when flying through the vortices.

Another possible limitation on the tape recording is the frequency response. The basic sine wave component of the tangential velocity profile of the trailing vortex for the above conditions is 87 Hz. For 1-percent accuracy in recording this signal, the recorder must be capable of recording 13 times this fundamental frequency, or 1.1 KHz. An fm tape recorder operating with a carrier frequency of 13.5 KHz (standard) at 7-1/2 ips has a frequency limit of 1.25 KHz. Thus 7-1/2 ips appears to be the minimum acceptable tape speed for recording vortex information unless the digitizing cycle period is reduced and the analog tape recorder has extended band width.

It is necessary to determine the location of the wake traverse relative to the generating aircraft. It is understood that some airborne DME equipment can be obtained from Langley Research Center which will provide a separation distance measurement to within about 30 feet. It is desirable also to measure the vertical distance that the vortices have moved between the time they were laid down and the time the Learjet passes through the vortices. The objective here is to obtain information on the vertical translation of the vortices to evaluate buoyancy theories. The vertical motion of the vortices should be the order of several hundred to one thousand feet maximum. If the T-33 is able to fly at a perfectly constant altitude, the vertical translation is the difference in altitude between the two aircraft at the time of vortex entry by the Learjet. Since each altitude is measured individually and differenced, measurement of each altitude to ± 10 feet will provide ± 20 feet on the difference or about 5- to 10-percent accuracy which should be sufficient. Since the difference is the major feature of interest, the altimeters in the two aircraft can be adjusted to read identically with the aircraft side-by-side prior to beginning testing. In order to ascertain whether the T-33 is flying a constant altitude, the pilot can radio altimeter readings to the Learjet for voice recording periodically, so that his altitude history can be reconstructed.

With regard to the number and location of the axial stations which are probed, it would appear desirable to have one station as close to the generating aircraft as is feasible (perhaps 1/2 mile), three or four stations in the stable portion of the vortex, and one or more in the breakup region. This would amount to spacings between probe stations of

the order of one-half to one mile depending on the distance to vortex breakup. The last station (breakup) is deserving of some comment.

From the standpoint of alleviating the wake vortex problem, an understanding of the dissipation mechanism is of great importance. The instability mechanism predicted by Crow (ref. 14) agrees with observations of vortex breakup, but his theory does not postulate how the instability develops, what influence atmospheric turbulence has on the development, nor what happens when the flow gets highly nonlinear in the breakup and ring formation region. No measurements have been made of the velocity distributions in the ring formation region to determine the potential hazard to passage of aircraft. Also, in the case of single vortex dissipation, no measurements have been made to indicate whether a bursting or a more rapid vorticity diffusion process is responsible for the dissipation.

We would suggest that consideration be given to making some traverses in the dissipation region. The exact approach to how these should be made would probably have to be decided upon during the test program when the dissipation mechanism has been observed. It would probably be desirable to make traverses just upstream of the dissipation event and within the region where dissipation has occurred.

Certain photographic coverage is considered essential. The first category is coverage to determine the development of the Crow instability and the dissipation mechanism. The wave length of the vortex oscillations for maximum growth rate of the Crow instability is 6.6 spans, or about 200 feet. It is recommended that the Learjet or another chase plane be flown parallel to the vortex system at 300 feet per second either just above or just below the vortex trail and movies be taken looking forward and slightly down (or up). The vortex lateral motion as derived from these movies will represent the time variation of the vortex oscillations at a fixed distance behind the aircraft. It is suggested that this coverage be obtained at three or four axial stations behind the generating aircraft for cases where the dissipation is due to a Crow instability and where it is due to single vortex bursting or diffusion. A single camera can be used, and the variation of the separation distance between the vortices will appear very close to its true perspective in the photography. Measurements from the photographs can be related to a time average of this

distance to obtain fractional deviations and their frequency. It is recognized that this photography may be difficult to obtain due to overall deformation or twisting of the vortex system due to large scale turbulence, buoyancy effects, etc. Nevertheless, little, if any, such systematic data has been obtained, and it is worth some effort to collect such data.

Other categories of photographic coverage would include photography to document the form and details of vortex dissipation and the influence of the Learjet on the vortex system at and shortly after the instant of passage of the aircraft through the vortex. The former is of interest in order to gain greater understanding of the details of the dissipation region. Coverage would be desirable both from a side view and a top view. The coverage of the Learjet penetration is of interest in terms of assessing the influence of the aircraft on the stability of the vortex. On the basis of the 40- by 80-Foot Wind Tunnel tests, it is expected that the Learjet should not cause vortex breakup, since the size of the "probe" relative to the vortex core is not greatly different in the two cases.

Meteorological Data

It is essential to document the meteorological conditions in which the vortex measurements are made, since they have an important part in determining the motion and dissipation of the vortex system. The considerations involved in measuring turbulence were discussed in a previous section. In addition to these data, information is desirable on the temperature and pressure at the test altitude, and the manner in which the temperature varies with altitude within, say, 500 feet above to 1500 feet below the test altitude; i.e., the range over which the vortex system might be expected to translate vertically.

From the standpoint of calculating buoyancy effects on the vortex vertical translation, it would be desirable to know whether or not vertical velocities are present in the atmosphere. The vertical velocity components with wave lengths of 1000 feet or less can be obtained from the turbulence measurements, with the assumption of isotropy, which is probably a reasonable assumption. The longer wave lengths, which in the limit become a uniform vertical velocity (at least over the length scale of the vortex), are difficult to measure because the aircraft tends to follow these. In addition, since the mutual induction velocity of the vortex pair is the

order of 5 feet per second, the long wave length vertical velocities of interest are small compared to the forward speed of the aircraft. It may be possible by examining angle of attack, altitude, and vertical acceleration data outside the vortex to back out long wave length vertical air velocity data, and it is suggested this be considered in connection with any buoyancy calculations made with the data.

Another measurement of considerable potential importance is humidity. In a subsequent section of this report, the influence of condensation on vortex behavior is discussed. It is noted there that tests at low altitudes under humid and/or hazy conditions (ref. 5) have shown distances to vortex breakup of one-third those obtained in clear weather. While these tests did not identify the mechanism responsible for the early breakup, it is possible that high humidity is responsible, at least in part. Therefore it is recommended that humidity measurements be made on board the Learjet at several times throughout a flight test and within the vortex, if possible. The latter location is of interest because of the possibility of high water vapor content due to ingestion of engine exhaust air.

INTERACTION BETWEEN THE PROBE AIRCRAFT AND THE VORTEX WAKE

The flow disturbance around the aircraft in steady flight will induce velocity components at the probe which will appear as biases changing with angle of attack. Also, the probe aircraft will respond to the flow field induced by the vortex wake, and the resulting motion will induce a velocity relative to the hot-wire probe which must be removed from the data and could cause problems in aiming the aircraft so as to penetrate the core. Finally, the presence of the aircraft will cause the vortex to move or deform, which could affect the measurements. Some estimates of the sizes of these effects were made to attempt to anticipate problems in this area.

Steady Flow Disturbance Due to the Aircraft

The perturbation flow field around the Learjet in a steady flow at several angles of attack was calculated using an existing potential flow program for a wing-body combination. The program is limited to an axisymmetric body shape. Consequently, the correct area distribution was

used, but the Learjet fuselage was modeled as an axisymmetric body. The program fits a source and doublet distribution to the fuselage and a vortex lattice to the wing. The tip tanks were not modeled because their influence should be small. The details of the configurations were obtained from reference 18.

Results for the perturbation velocities over the forward part of the Learjet are shown in figures 6 and 7. Figure 6 shows longitudinal and vertical velocity components in the vertical plane of symmetry for $0°$ and $10°$ angle of attack at various distances above and below the fuselage centerline. The vertical distance scale has been greatly expanded to simplify the presentation. At the hot-wire location ($x = 5$ feet), the axial (u_a) component is about 3 percent of free stream (6 feet per second) and essentially does not change with angle of attack, since it is due to a fuselage-thickness effect. The vertical component (w_a) is zero at $\alpha = 0$ and increases to about 1/2 percent of free stream (1.5 feet per second) at $\alpha = 10$ degrees due to a wing-induced upwash. These velocities are small compared to the peak tangential velocities in the vortex. In particular, if the angle of attack is perturbed due to vortex-induced motion of the aircraft, the only influenced component will be the upwash velocity, whose magnitude changes so little that its effect on the probe readings can be neglected. Figure 7 shows u_a and w_a velocities in a vertical plane 10-1/4 feet from the plane of symmetry (60-percent span station). These results are of interest principally in estimating vortex deformation due to the passage of the aircraft and show the upwash forward of, and downwash behind, the wing and the acceleration ($- u_a$) over the wing and deceleration under the wing.

Aircraft Motion Induced by the Vortex System

The Learjet will respond to the flow field induced by the vortex system. The potential problems are control of the attitude of the aircraft and the relative velocities induced at the hot-wire probe by aircraft motion. For the case where the aircraft flies along the vortex and penetrates by descending or ascending through the vortex, the worst case is that in which the aircraft finds itself in the center of one vortex with a large induced roll, as shown in the sketch.
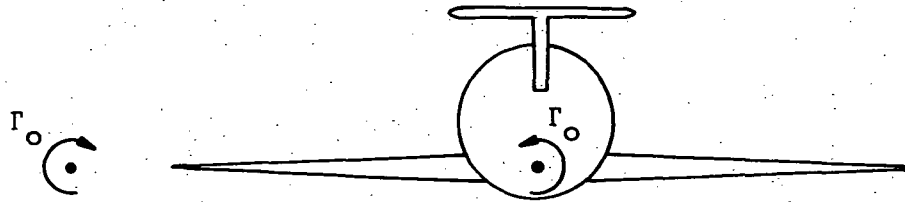
An estimate of the induced rolling moment due to both vortices acting on the aircraft was made assuming a wing alone to be centered on one vortex. Potential vortices with solid body rotation inside r_1 were used to obtain spanwise upwash distributions along the wing panels, and strip theory was used with a uniform section lift coefficient along the span to obtain the vortex-induced lift distribution and the resultant rolling moment. A value of $C_\ell = 0.3$ was calculated. The control roll moment available through differential aileron deflection was estimated assuming 20° of aileron deflection, a change in section angle of zero lift with change in aileron deflection angle of 0.6, and a section lift coefficient slope of 0.07 per degree (equal to the wing lift coefficient slope). The resulting rolling moment coefficient, calculated again using strip theory, is $C_\ell = 0.36$. If the assumptions are reasonable, these results indicate the Learjet does have sufficient control effectiveness to maintain a zero bank angle in the vortex, but the two values are so close that there are likely to be large excursions in roll attitude as the aircraft enters the vortex in spite of the skill of the pilot. Although the attitude of the aircraft will be monitored so as to extract the aircraft dynamics from the hot-wire signals, it is felt that the marginal control situation is not conducive to satisfactorily controlling the trajectory of the aircraft as it makes the vortex penetration.

For a case in which the aircraft approaches the vortex system horizontally at right angles to the wake, the aircraft will pitch and heave as it passes through the vortex. An estimate of the vertical acceleration was made assuming the wake-vortex-induced lift on the Learjet to be given by the vertical velocity induced at the wing quarter-mean-aerodynamic-chord by the two vortices, combining this velocity with U to get an angle of attack (see fig. 8(a)), and causing the resulting perturbation wing lift to act on the aircraft weight. A plot of the resulting acceleration is shown in figure 8(b). The values are low and should not cause any problems on aircraft loading. The acceleration was integrated to obtain

27

vertical velocities in order to estimate the difficulty that the pilot might have in adjusting his height to hit the center of the vortex. The Learjet would sustain an upward velocity component of only 0.65 foot per second by the time the probe reached the vortex. Since the accelerations are significant only within 50 feet of the vortex, the aircraft height relative to the vortex should change, for a speed of 300 feet per second, only a few inches at most due to the vortex-induced upwash.

An estimate was also made of the pitching rate induced on the aircraft by its interaction with the vortex. Two approaches were examined. In the first, it was assumed that a pitching moment was imposed equal to the moment on the Learjet in a uniform flow at an angle of attack equal to the local angle at the quarter-mean-aerodynamic-chord (fig. 8(a)). From reference 18, the pitching moment coefficient slope of the complete aircraft about $\bar{c}/4$ is -0.02 per degree. For the center of mass at the same location and a moment of inertia in pitch of 20,000 pounds-feet per second^2, an angular velocity of -9×10^{-4} degrees per second (nose down) is reached at the time the nose boom intersects the vortex. This value is highly dependent on the assumed center of mass but is so small that any effects due to rotation are negligible. The other approach taken assumed that the only region of the aircraft acted upon by the vortex-induced upwash is the nose of the aircraft, since the gradient in upwash is high near the vortex and drops off rapidly (fig. 8(a)). Slender-body theory gives the lift curve slope on an expanding body as 2, based on the maximum cross section area. Applying this concept to the Learjet with the assumption that this lift acts 15 feet forward of $\bar{c}/4$, one computes an angular velocity of 0.5 degrees per second when the boom probe enters the vortex core. This value is also negligibly small in terms of either causing the aircraft to miss the core during the vortex penetration or causing relative velocities at the probe.

Effect of the Aircraft on Vortex Deformation and Stability

The penetration of the Learjet into the vortex wake of the T-33 has one and possibly two effects on the vortices: deformation of the line vortices and vortex bursting. No calculations of these phenomena were considered justified because of their difficulty. However, some qualitative observations can be made.

In the case of a horizontal probe path normal to the vortices, the results of figure 6 indicate that there is insufficient disturbance ahead of the Learjet to cause any vortex motion or deformation prior to the entry of the hot-wire probe into the near vortex. Assuming that both vortices still lie in a horizontal plane and measurements through both vortices are possible during the passage of the aircraft, the near vortex will not be affected appreciably until the hot-wire probe is some 3 or 4 feet past the near vortex center. The near vortex will then deform to pass over, or possibly under, the aircraft in accordance with the pertur- bation velocity field induced by the aircraft. The deformed vortex will in turn induce some deformation of the far vortex before the hot-wire probe enters the far vortex. Since the vortex span is 29 feet, the near vortex will be in the region of the wing trailing edge when the probe enters the far vortex and will have been displaced about 3 feet vertically. It is felt that this deformation should not cause a large effect on the far vortex, and the chances for obtaining good data on the far vortex are reasonably good.

Insofar as bursting is concerned, the tests in the 40- by 80-Foot Wind Tunnel indicated that passage of the probe through the vortex caused no observable oscillations or bursting of the vortex. The probe in that case had a diameter of about half the core diameter, whereas in the flight test case, the "probe" (the Learjet) is about four times the core diameter. It is possible that the vortex deformation will set up disturbances which would enhance the onset of the Crow instability after passage of the aircraft.

For a coaxial probe in which the aircraft ascends or descends through one vortex, the influence of the aircraft on the vortex at the hot-wire location is more difficult to predict. Although the aircraft disturbance at the hot-wire location is very small, it is possible that the presence of the fuselage downstream could cause a large disturbance in the vortex which could propagate upstream to affect the flow at the hot-wire location. We are not aware of any data which would shed any light on this problem.

FLIGHT TEST PROBE PROCEDURE

The two methods of probing the vortex wake that are under conside-
ration are a horizontal traverse at right angle to the vortex, as illus-
trated on the left below, and a vertical traverse down (or up)
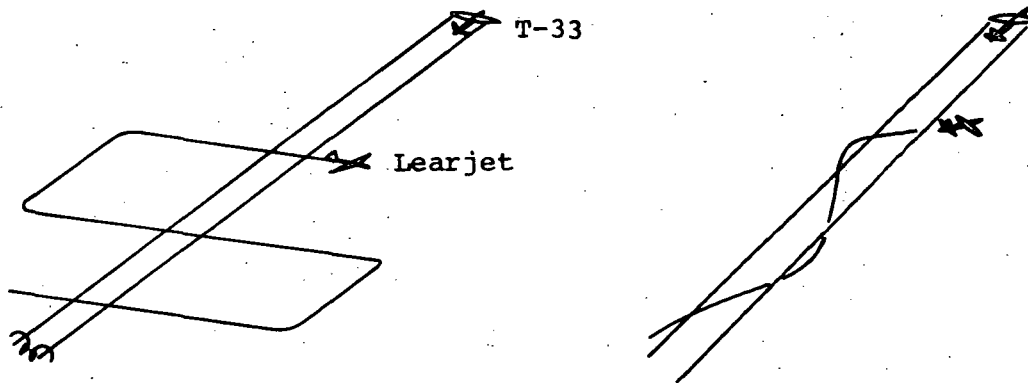
through the vortex as shown on the right. In the first case the Learjet
must fly faster than the T-33 on the upwind legs so that when it turns to
cross the vortex wake, the intersection with the wake occurs at about the
desired distance aft of the T-33 on each pass. In the second case, the
Learjet may fly at essentially a constant speed just over 300 feet per
second to keep the intersection point a given distance behind the T-33.
The navigation problem is more difficult with the crossing technique.

It would appear that the crossing procedure is the more desirable of
the two for three reasons. First, it appears from the controllability
calculation previously described that it may be difficult to control the
attitude and trajectory of the Learjet if it has to fly into the core
aligned with it because of the large induced rolling moment. Secondly,
it is probably easier to obtain a core penetration with a crossing tra-
jectory because the vortex will appear relatively stationary to the pilot,
whereas with the aligned probe, the vortex will appear to move from side
to side beneath the aircraft due to standing waves in the vortex. Thirdly,
a crossing probe will provide some information on both vortices in one
pass, whereas the aligned probe will provide information on only one
vortex. These advantages would appear to outweigh the disadvantages in
the crossing probe of the more difficult navigation problem and a greater
time between probes. It is suggested, however, that some of the probes
in the vortex breakup region be obtained with the aligned probe technique,

30

or possibly the Learjet be flow at a constant altitude in the breakup region, since this procedure would provide some qualitative pilot reaction to the degree of turbulence in this region as well as quantitative data.

The number of axial stations along the wake where data are to be obtained was discussed in a previous section. It is suggested that sufficient passes be made at a given nominal distance behind the T-33 to obtain at least one core penetration and, better two penetrations for each distance. The oscilloscope records would provide indications of a core penetration.

EFFECT OF CONDENSATION ON VORTEX CHARACTERISTICS

Condensation trails (contrails) have long been recognized as one of the most vivid means of visualizing trailing vortex wakes from aircraft at high altitudes. A considerable amount of research was conducted in the 1950's and early 1960's on means of suppressing contrails (refs. 6 and 19, for instance). This work was concerned principally with the physics of condensation and sublimation rather than the fluid mechanics of vortices, and consequently has shed little light on the influence of condensation on the structure and persistence of vortex wakes. Recently, however, Chevalier (ref. 5) reported on some low altitude flight wake vortex experiments in which he noted on days of high haze and/or moisture content that vortex breakup occurred in about one-third the distance required on clear days. While no measurements were made of the meteorological conditions (temperature, humidity, turbulence, etc.), the dominant effect seemed to be humidity. At the present time there is no theory, or even a qualitative model, to explain this effect.

It is well known from Hilsch tube experiments that an energy separation occurs in rotating flows. The fluid in the center has a lower static pressure and total temperature than that in the outer flow. If moisture is present, the possible effects of moisture are a condensation in the center of the vortex due to the drop in static temperature, a heat release due to condensation, transfer of momentum from the gas to the liquid droplets, and a radial flow of this momentum in the liquid particles. Some preliminary calculations were made of these effects in order to compare the T-33 flight conditions with other flight conditions where certain

observations have been made and to determine if some mechanism of insta-
bility could be found. Three cases were compared: the T-33 at 12,500
feet, a DCH-2 aircraft at 1,000 feet (Chevalier's experiment, ref. 5) and
a B-47 at 35,000 feet (experiments reported in ref. 6 demonstrating con-
trail lengths of up to 120 seconds). The pertinent conditions are listed
in Table III. These calculations were made ignoring the heat and moisture
input from the jet engine exhaust (which was not present in Chevalier's
experiment) which is too difficult to include at the present time.

An excellent summary of the equations governing the flow in a vortex
is given in reference 20. In order to make the calculations tractable,
the form of these equations for negligible temperature variations and
compressibility effects and for zero fluctuations (laminar flow) was used
(eq. (3) of ref. 20). These equations would apply to the core but not
necessarily to the outer flow which is turbulent.

The radial static pressure gradient in the vortex is given by

$$\frac{\partial p}{\partial r} = \rho \frac{v^2}{r} \tag{11}$$

Expressions for the variation of the velocity with radius are given in ref-
erence 2. To minimize the computation time, the vortex was divided into
three regions: a core with outer radius r_i, a portion of the logarithmic
region from r_i to r_1, and a potential vortex outside of r_1. Expres-
sions for the velocity variation in these regions are available in ref-
erence 2, as follows

$$
\left.
\begin{array}{ll}
0 < r < r_i & \dfrac{K}{K_1} = 1.47 \left(\dfrac{r}{r_1}\right)^2 \\[2ex]
r_i < r < r_1 & \dfrac{K}{K_1} = 1 + 0.928 \ln\left(\dfrac{r}{r_1}\right) \\[2ex]
r_1 < r < \infty & v = \dfrac{\Gamma_o}{2\pi r}
\end{array}
\right\} \tag{12}
$$

Using these expressions, the static pressure difference between the vortex
center and the free stream can be calculated from equation (11).

The static temperature distribution in the vortex was estimated using the energy equation. This has the form (ref. 20)

$$\rho \left(\frac{\partial I_o}{\partial t} + u \frac{\partial I_o}{\partial r} + w \frac{\partial I_o}{\partial z} \right) - \frac{\partial p}{\partial t} =$$

$$\frac{1}{r} \frac{\partial}{\partial r} \left[\frac{\mu}{N_{Pr}} r \frac{\partial I_o}{\partial r} + \mu (N_{PR} - 1) r \left(v \frac{\partial v}{\partial r} + w \frac{\partial w}{\partial r} \right) - \mu v^2 \right] \quad (13)$$

where I_o is the total enthalpy,

$$I_o \equiv c_p T + \frac{1}{2} (u^2 + v^2 + w^2) \quad (14)$$

In order to use this expression, the following assumptions were made:

(1) the flow is steady; i.e., $\partial/\partial t = 0$

(2) the Prandtl number is one

(3) the terms involving u (the radial velocity) and $\partial/\partial z$ (axial gradients) are small and can be neglected.

These assumptions reduce equation (13) to the following

$$r \frac{\partial I_o}{\partial r} - v^2 = 0 \quad (15)$$

Again through the use of equation (12), the variation of total enthalpy through the vortex can be obtained. One interesting result of these calculations is that the variation in total enthalpy in the core region is due entirely to the velocity variation, and the static temperature is constant.

Condensation can occur within the vortex if the relative humidity of the ambient air in which the vortex is formed is sufficiently high that the drop in temperature in the vortex would tend to increase the relative humidity above one. The absolute humidity ω is

$$\omega \equiv \frac{m_w}{m_w + m_a} = \frac{1}{1 + (p_a/p_w)(M_a/M_w)} \quad (16)$$

where p_a and p_w are the partial pressures of air and water vapor, respectively, in the mixture. The absolute humidity at saturation is the value of ω for $p_w = p_{sat}(T)$. Thus, if the ambient air is saturated at $p_{sat}(T_\infty)$ and T_1 is lower than T_∞, $\omega_{sat}(T_1)$ will be lower than $\omega_{sat}(T_\infty)$ and the difference represents the amount of water vapor which must be condensed when the (saturated) ambient air is entrained in the core as the vortex is formed. Saturation pressures at low temperatures were obtained from reference 15 and are reproduced in figure 9. Since the predicted temperature differences between ambient and the core are small, the slopes of the saturation pressure curve of figure 9 were used to calculate changes in humidity at the nominal temperatures of interest.

If condensation does occur within the vortex, heat is released and tends to warm the air-water vapor mixture in the core. When the amount of water vapor condensed per pound of mixture is known, the heat of evaporation and the specific heat of the gas mixture can be used to calculate a temperature rise in the core gas mixture.

If water vapor condenses in the core and is centrifuged outward due to its higher density, the core suffers a loss in momentum. The amount of the loss depends on the velocity imparted to the condensed water. The water droplets will assume tangential and axial velocities equal (essentially) to the values of the air at the point where the vapor condenses. If the centrifugal separation occurs slowly enough, the droplets will assume the local tangential velocity as they move outward. Assuming this to be the case, the angular momentum per unit mass of core flow assumed by the droplets is the product of their mass per mass of core flow and v_1. One can compute the total angular momentum of the air in the core per mass of air in the core as

$$\frac{\text{core ang. mom.}}{\text{core mass}} = \frac{\int_0^{r_1} \rho u v \, dr}{\int_0^{r_1} \rho u \, dr} \tag{17}$$

For purpose of making this calculation, u was considered constant within r_1. The ratio of the droplet momentum to the core momentum can then be obtained. Using equations (12) for the velocity distribution in the core

and logarithmic region out to r_1, one obtains for the momentum ratio 1.53 times the mass of vapor condensed per mass of core mixture.

The results of the calculations described above are shown in Table IV for the three conditions noted previously. The DCH-2 has a low wing loading compared to the other two aircraft and therefore a low vortex strength (Table III). Even though the ambient pressure and temperature are highest for this case because of the low altitude, the low vortex strength causes only small changes in pressure and temperature between the vortex center and ambient. As a result, the various calculated effects of condensation are very small compared to the other two cases.

The B-47E has the highest vortex strength and therefore the greatest relative influence on condensation in the core. However, there is an order of magnitude less water vapor in the saturated condition at 35,000 feet than at 12,500 feet. Consequently, the absolute magnitude of the condensation effects is smaller than for the T-33 case. It is of interest to note that Pilié (ref. 19) gives a lower limit of water droplet concentration for contrail visibility of 10^{-5} pounds per pound. While this figure may be applicable only under ideal conditions and therefore somewhat low, the three cases show condensed water concentrations of this order. Finally, it should be noted that in the B-47E case, the ambient water vapor level is so low that the water content in the jet engine exhaust, which was neglected in these calculations, is going to have a very large effect on condensation in the wake vortex system.

These calculated results are not conclusive. In the DCH-2 case where Chevalier (ref. 5) observed a much earlier vortex dissipation in moist conditions (20 seconds) than in dry conditions (1 to 2 minutes) and where the engine (a piston engine) has little moisture input to the vortex wake, the calculated effects of condensation are so small that no obvious mechanism of dissipation is apparent. In the B-47E case where sufficient condensation has been observed to occur to cause the wake to be visible for up to 15 miles or so, condensation does not appear to be a dominant factor in vortex dissipation. Since Chevalier did not make any measurements of either the ambient atmospheric conditions or the vortex wake, it is not possible to determine the precise mechanism acting on his vortices under his "early morning fog or haze" condition which caused early dissipation. It is felt, however, that the T-33 case will be more like

the B-47E case than Chevalier's case for several reasons:

- The tests to be performed with the T-33 will be made under conditions of good visibility (i.e., low humidity) for safety purposes and for purposes of locating the wake so the Learjet can effect wake penetrations.

- The work reported in reference 6 discussed contrail lengths behind T-33 aircraft of up to 20,000 feet, although the altitude and atmospheric conditions are not described. This work also does not note any distinctive differences between the T-33 contrails and the contrails of the other aircraft examined (F-86, F-100, B-47, B-52).

- The 12,500-foot altitude is sufficiently different than the 1,000-foot altitude of Chevalier's tests that the local environment is not dominated by effects of ground heat transfer, airborne particles, inversion layers, ground-generated pollutants, fog, and the like.

Consequently, it is felt that early dissipation of the sort noted by Chevalier is not likely to occur with the T-33 tests.

One interesting possibility is suggested by Chevalier's tests. If there is an unknown dissipative mechanism present as Chevalier's tests suggest, it would be most important to define that mechanism for possible consideration as an aircraft-borne dissipator device. ARC might consider the possibility of performing lower altitude tests both in clear weather and in high humidity conditions (providing acceptable visibility and safety conditions) over Moffett Field where some atmospheric measurements can be made either by radiosonde or the Learjet instruments to attempt to duplicate Chevalier's results.

VORTEX VELOCITY DATA REDUCTION

The Learjet will pass through the T-33 wake vortex system and obtain a record of the voltage outputs of the three wires of the probe along some path traversed by the probe. This section is concerned with the manner in which this data is analyzed to obtain information on the vortex characteristics. It is assumed that a horizontal traverse at right angles to the

wake will be made. Thus, the path of the probe will be a straight or curved line lying in a plane essentially normal to the vortex filament (denoted the crossflow plane). Further, it is assumed that some prior operation on the data will be done to convert the hot-wire voltages to velocities, to transform the three velocity components into a system having axes parallel to the principal axes of the probe aircraft, and to remove the velocity components at the hot wire due to aircraft motion. The resulting data will be velocity components normal to and coaxial with the path line followed by the aircraft in the crossflow plane and a third component normal to the crossflow plane (along the vortex axis). Finally, it is assumed that time on the magnetic tape record and the aircraft velocity components can be related such that two coordinates of the path of the hot-wire probe through the vortex system in an arbitrary coordinate system in the crossflow plane can be established. Thus, the velocity components at any point along this path line can be obtained from the data.

The first part of this section contains a discussion of the types of vortex penetrations that can be achieved and the reconstruction of the vortex velocity system from the measured velocity components along the probe path. The second part then deals with the description and use of a computer program associated with the velocity reconstruction procedure. Only the two velocity components in the crossflow plane are considered in the following discussion.

Methods for Reconstruction of the Vortex Characteristics

Penetration of a vortex in a crossflow plane can be categorized as follows. When the probe flight path passes closer to the vortex center than its core radius, (r_1), a core penetration is said to result. A pass that misses the vortex center by more than the core radius is called a noncore penetration. In either case, the component of the vortex-induced perturbation velocity normal to the probe flight path, V_n, will exhibit a well-defined maximum and minimum. If a wing-tip vortex has circular, concentric streamlines with negligible radial velocity, and if there are small influences from the opposite tip vortex, the peaks should be equal and opposite as shown in the sketch below.
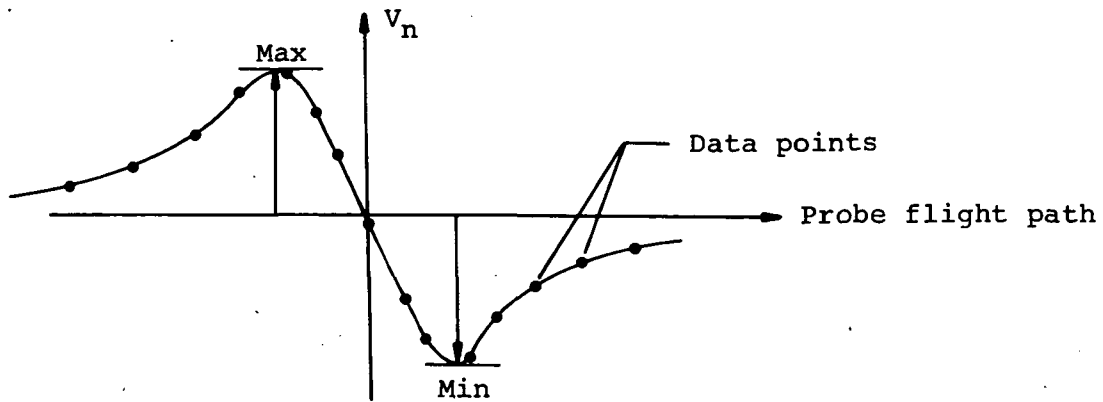
Downwash induced by the opposite vortex would tend to shift the profile in the vertical direction so that asymmetry results. It should be noted that in the absence of any motion of the vortex center in the crossflow plane during the probe time, the component of the perturbation velocity along the probe flight path, V_s, should not change sign during the penetration.

The resultant perturbation velocity is obtained from a vector addition of the components along and normal to the probe flight path. By erecting normals to the resultant velocity vectors, the vortex center can be located as shown in the sketch below.
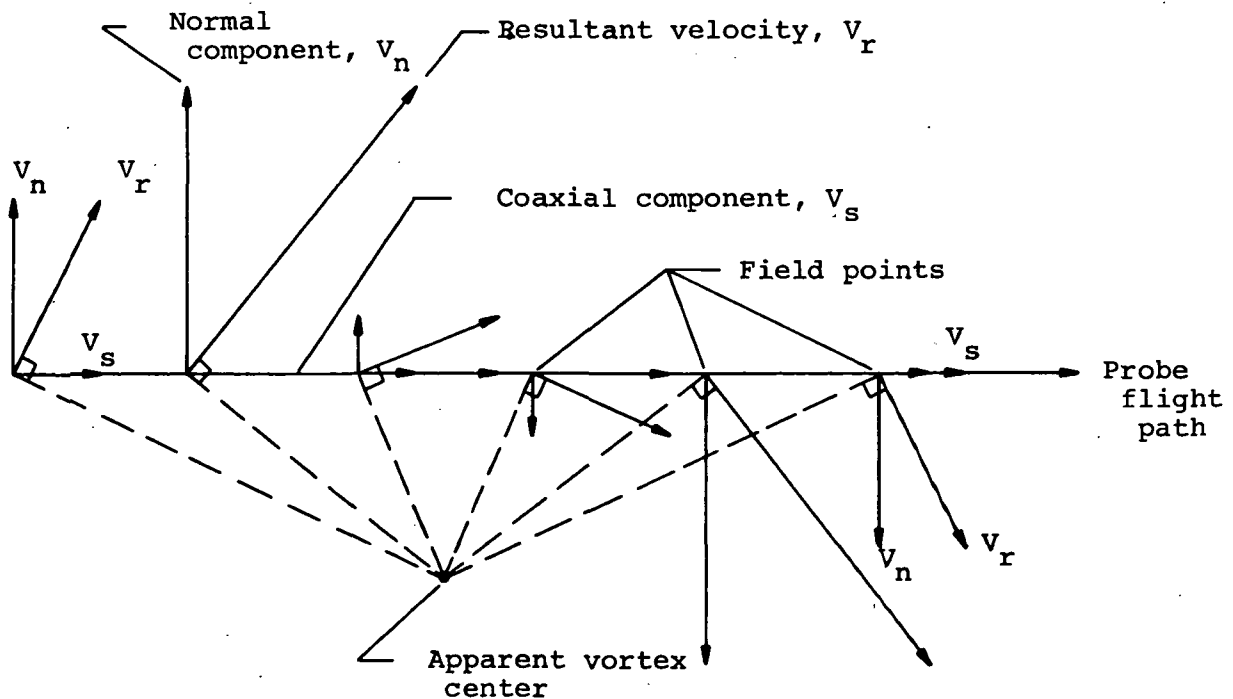
From a knowledge of the vortex center and the resultant velocities, a curve of the variation of tangential velocity V_t with radius can be determined. In fact, the tangential velocities V_t are the resultant velocities V_r.

The two types of vortex penetration can now be distinguished. For the case of a core penetration, the results will assume the appearance of the curve shown below. In this sketch the tangential velocity is plotted versus radius. Positive values of V_t have an upward component, and negative values a downward component. No data points occur for values of the radius less than that for closest approach to the center. One sees well-defined maximum and minimum peaks in the tangential velocity variation. The radial location where these occur is termed r_1. The radius of closest approach must be less than r_1 for a core penetration to occur and for a well-defined maximum to occur.
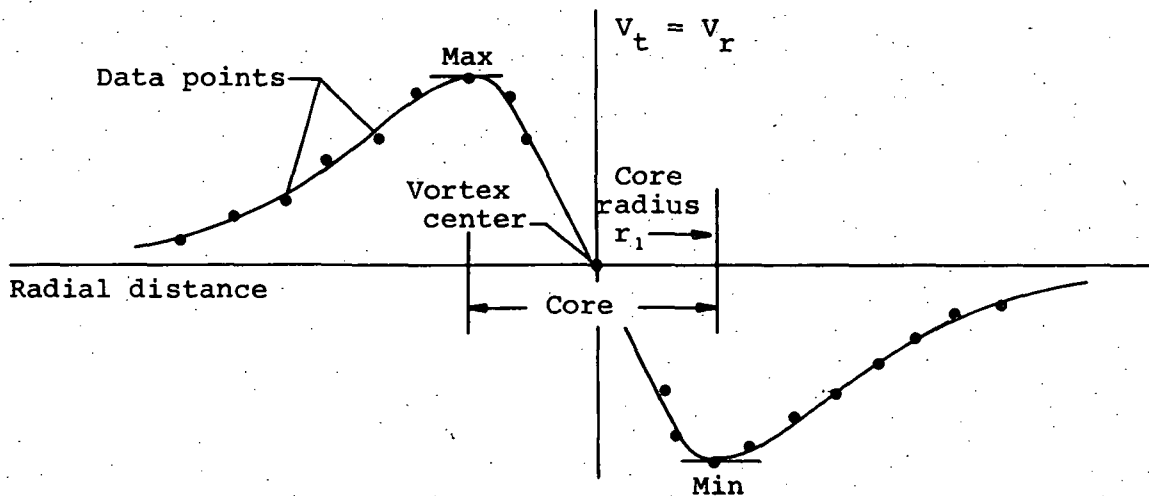
The peaks in the vortex tangential velocity V_t must be clearly indicated before the core size can be estimated. In other words, some data points must exist on either side of the maximum and the minimum.

If the probe does not enter the core, the same form of resultant velocity and vortex center determination may be used to construct a curve of tangential velocity versus radius. However, this curve will not show the well-defined maximum and minimum velocities, as shown below, since data will not be available at or within the core radius.

$V_t = V_r$

Radial distance

Data points
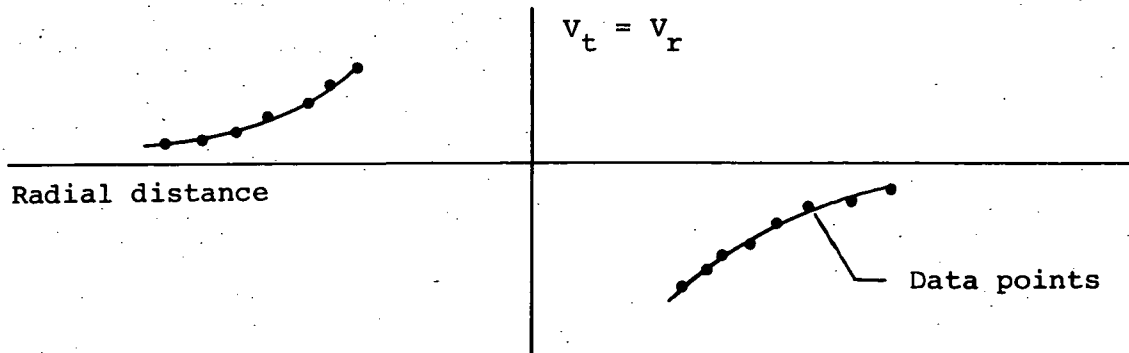
The method for performing the analysis just described is as follows. The axis system in the crossflow plane is shown in figure 10, together with the positive sense of the normal and coaxial velocity components, V_n and V_s. The origin and the direction of the positive sense of the Z,Y coordinate system are somewhat arbitrary, in accordance with the following considerations. Figure 10 shows a left-to-right traverse, looking along the vortex towards the generating aircraft. The coordinate system shows Z generally down and Y to the right. It is suggested that an origin of this coordinate system be fixed for each set of data from a pass through the wake. The location of the origin is completely arbitrary and serves only to permit assignment of two length coodinates to the data taken at every instant of time during passage through the wake by means of the air-craft accelerometer data. The Z and Y axes do not have to be truly vertical and horizontal but only approximately so. However, the general arrangement of Z down and Y to the right should be maintained for all passes, whether right-to-left or left-to-right, in order to provide con-sistent signs and senses of rotation of the vortices in the data reduction.

Pertinent angles necessary for the determination of the slopes of the normals to the resultant velocity vectors V_r at field points (Z,Y) are also shown in figure 10. Two such lines emanating from points (Z_i, Y_i) and (Z_j, Y_j) are seen to intersect at point (Z_{ij}, Y_{ij}). The expressions for the intersection point coordinates are given by

$$Z_{ij} = -\frac{\left(Y_i - m_{\ell_i} Z_i\right) - \left(Y_j - m_{\ell_j} Z_j\right)}{m_{\ell_i} - m_{\ell_j}}$$

$$Y_{ij} = -m_{\ell_i}\left(Z_i - Z_{ij}\right) + Y_i \quad (18)$$

The slope of line i is given by m_{ℓ_i} and the slope of line j is given by m_{ℓ_j}. These slopes are determined from the following expressions:

$$m_{\ell_i} = \tan \Theta_{\ell_i} \qquad \Theta_{\ell_i} = \alpha_i + \Theta_{s_i}$$

$$\Theta_{s_i} = \tan^{-1}\left(\frac{\Delta Y}{\Delta Z}\right)_i \qquad \alpha_{c_i} = \tan^{-1}\left(\frac{V_s}{V_n}\right)_i \quad (19)$$

and $(\Delta Y/\Delta Z)_i$ is the slope of the flight path at the i'th point, obtained from the coordinates of points along the path adjacent to the i'th point.

If there are N data points given along a probe flight path, the number of unique intersection points is equal to $1/2\ N(N-1)$. Ideally, all intersection points should coincide. In actuality, a collection of points is generated and after exclusion of those points that are obviously in error, a suitable averaging scheme can be called upon to generate the apparent vortex center from the set of (Z_{ij}, Y_{ij}) coordinate pairs. In the ideal case, lines drawn from the apparent vortex center to the field points where the resultant velocity vectors are constructed will be normal to those vectors. In practice, these lines will be near normal to the velocity vectors and their lengths are approximately equal to the radial distances from the vortex center to the tangential velocity vectors.

The magnitude of the total circulation Γ_o of the vortex can be determined from a potential vortex model using the vortex tangential velocities and the radial distances from the apparent vortex center. The approach followed here makes use of the following assumptions:

(1) The vortex can be characterized by circular, concentric stream-
    lines in the crossflow plane.

(2) The radial velocity in the crossflow plane is negligible.

(3) The downwash effect from the opposite vortex is small.

(4) The vortex center does not move appreciably during the duration
    of the traverse.

These assumptions appear reasonable based on the following considerations. The small "intersection areas" obtained from the vortex center analysis of the wind-tunnel hot-wire data indicate that any radial velocities that do exist are small compared to the tangential velocities. Visual observations of the vortex size indicated no change in core diameter within 100 chords of the wing, which also indicates small radial velocities. Since the velocity induced by one vortex of the pair at the other is only 5 percent of the maximum tangential velocity of that other vortex, the noncircularity of this effect should be small in determining vortex centers and circulations. This effect can be included later if it is found to be significant. Finally, the time to traverse the vortex is less than 0.01 second so that the vortex displacement in this time increment should be negligible.

Since the potential vortex velocity distribution joins the inner velocity model at a radius (r_o) about 2.5 times the core radius (fig. 2), the following expression can be used for the calculation of a set of circulation values for those points having radii greater than 2.5 r_1

$$\Gamma_{o_i} = 2\pi r_i V_{t_i} \tag{20}$$

The average over the set of Γ_{o_i}'s yields a value for the total circulation or vortex strength Γ_o.

Trailing Vortex Crossflow Program

The purpose of this section is to describe the program which reduces the trailing vortex velocity data taken in some crossflow plane to a tabulation of vortex tangential velocities as a function of radial distance from the apparent vortex center. The program also computes an average total circulation associated with the vortex in the crossflow plane.

Fundamentally, the program is based on the assumption that the vortex possesses circular, concentric streamlines with negligible radial velocity. The effects of the opposite tip vortex and vortex center motion are not accounted for.

In the following, the program and its input and output will be described in detail. At the end of this section, a sample case illustrates how the program handles a segment of data recently taken in the 40- by 80-Foot Wind Tunnel at the Ames Research Center.

42

Calculation procedure.- The computer program proceeds through various stages as follows. After run identification and input of certain variables, a set of field point coordinates and vortex perturbation velocity components coaxial and normal to the probe flight path in the crossflow plane are read in for one vortex traverse. The maximum and minimum values of the normal component and the corresponding field point coordinates are determined from the set of supplied data for later use. The program prints all of the input data and prints the peak values of the normal component velocity encountered during the traverse under consideration.

The program proceeds to compute resultant velocities (V_r) at all the input data points using the coaxial and normal velocity components. Since the induced velocities become very small at large distances from the vortex and can cause large errors in calculating the apparent vortex center, velocities smaller than a "cutoff" velocity are dropped. The cutoff velocity is calculated from input quantities. The remaining data set consists of the first point along the path where the velocity becomes greater than the cutoff velocity, all data points thereafter along the probe path through the vortex until that point where the velocity has dropped off again to the cutoff value. If any of the data points within this band have identically zero velocity components (for example, if the data point is judged bad and the velocity components set equal to zero), the program will treat the velocity components as zero and continue to process that point.

After printing the field point coordinates within the range defined by the first and last velocities greater than the cutoff, the program determines the set of coordinates of the points of intersection of lines normal to the resultant velocity vectors. Resultant velocity vectors with magnitudes identically equal to zero are excluded from this calculation. Intersection points with Y coordinates outside of the range spanned by the field points where the previously calculated peaks in normal velocity component occur are also excluded from further processing. The apparent vortex center is then computed from the subset of remaining intersection points by means of an averaging procedure.

Upon completion of the determination of the coordinates of the apparent vortex center, the program continues with the calculation of the distances from the center to the location of the field points. Next,

these radial distances are tabulated in the output together with the corresponding resultant velocities. These velocities are in fact the vortex tangential velocities. The program then searches for the maximum and minimum velocity values and the corresponding radial distances. A check for core or noncore penetration follows. This is done by checking on the sense of the direction of the vortex tangential velocity at the field point immediately adjacent to the maximum or minimum peak towards the vortex center.

Lastly, the program computes an average value for the total circulation from the set of circulation values obtained from equation (20) applied to all the tabulated vortex tangential velocities and corresponding radii. The program is arranged to handle cases consecutively.

Program operation.- The trailing vortex crossflow program is written in Fortran IV language and has been run on the IBM 360/67 TSS batch system at Ames Research Center. With this machine, 500 data points can be processed although this number is not necessarily a maximum. If the program is to be run on a different computer with smaller storage, dimension statements need to be changed to permit operation on that machine.

No tapes are required other than the standard input and output. The running time on the TSS batch system required to process about 300 data points is approximately 1.5 minutes.

Program limitations and precautions.- Some care must be taken in specifying the variable FACTOR in the input. This positive variable multiplied with the specified nominal value of the axial velocity UAX serves in the program as a lower bound, VMIN, for the magnitudes of the first and last resultant velocities in the crossflow planes treated by the program. When this lower bound is too low, the number of admissible vortex tangential velocities becomes unduly large in its relation to the points of intersection (Z_{ij}, Y_{ij}) determined by the program. The program is dimensioned to handle a set of 100 vortex tangential velocities with the first and last magnitudes larger than VMIN. If more than 100 are treated, the program will be stopped and the following message appears in the output: "DIMENSION OF INTERSECTION POINT COORDINATES NOT SUFFICIENT". An increase in the input variables FACTOR or UAX will raise the lower bound (cutoff) value, VMIN, and alleviate the problem. Alternatively, the array size of

the variables $ZC(Z_{ij})$ and $YC(Y_{ij})$ in the dimension statement can be enlarged if the storage capacity of the computer is large enough.

The program writes out the coordinates of all intersection points as an option. This output can be time and paper consuming if the number of admitted vortex tangential velocities is large. It is recommended that the program be run with a given set of data first without the optional output. If the value for the total number of computed intersection points specified in the output is less than 200, the program can be rerun with the inclusion of the optional output if so desired.

Description of input.- This section describes the input for the trailing vortex crossflow program. In the following discussion, the content of all input cards is described and, where appropriate, instructions on generating the input quantities are given. All input variables are summarized at the end of this section in the order of appearance in the input deck. The input format for all cards is shown in figure 11; the item numbers refer to figure 11.

The TSS 360 computer system at Ames Research Center offers an alternate way for reading in the set of field point coordinates with the two vortex perturbation velocity components. These data can be generated and stored in a data set. The trailing vortex crossflow program can be modified to read from a data set with a minimum of alterations. This method is advantageous when large amounts of data are generated.

Item 1: The first card serves as identification and may contain any alphameric information required. This information is printed on the first page of the output.

Item 2: The second card contains an axial velocity UAX and the axial location of the crossflow plane under consideration. The axial velocity can be tunnel velocity for wind-tunnel data or the speed of the vortex generating aircraft for flight data. This quantity is used only to calculate the cutoff velocity VMIN. In addition, this card specifies the fraction FACTOR of the axial velocity used to calculate the cutoff velocity, the total number of data points supplied (500 maximum) and a variable controlling the optional output of the intersection point coordinates. As was noted above in the discussion concerning program limitations and precautions, the fraction specification multiplied by the nominal axial

velocity generates the lower bound or cutoff value, VMIN, for the magnitudes of the first and last resultant velocities to be processed by the program.

The choice of the quantity FACTOR (and therefore VMIN) is motivated by the desired number of data points to be included in the analysis and perhaps by the signal-to-noise ratio. As a rule, VMIN must be high enough so that the number of admitted data points does not exceed 100. At the same time, VMIN must be low enough to allow enough data points for an accurate construction of the vortex-induced flow field in the crossflow plane. In addition, if the signal-to-noise ratio is high, one might want to use a value for VMIN a certain amount above the velocity corresponding to the noise voltage level to improve the accuracy of the calculation. For the 40- by 80-Foot Wind Tunnel tests, FACTOR was found to lie in the range of 0.20 to 0.30. The tunnel velocity UAX was 90 feet per second so that VMIN ranged from 18 to 27 feet per second. Variable IZCYC controls optional output of intersection point coordinates.

Item 3: This set of cards contains the field point coordinates and the perturbation velocity components induced at those points by the vortex in the crossflow plane. Each card contains a sequence number, the Z and Y coordinates and the velocity components coaxial and normal to the probe flight path. The sequential order of this input data must be the same as the order in which the experimental data was obtained. The coordinate system and the positive sense of the velocity components are shown in figure 10. It should be noted that any contribution to these velocity components by mechanisms other than the vortex should be excluded. The total number of cards is NFLDP (NFLDP $\leq$ 500, Item 2).

A sample input deck is shown in figure 12. This data is part of a traverse performed through a vortex in the 40- by 80-Foot Wind Tunnel and serves as input to the sample case described below. In this input, the variable IZCYC is specified to be 1; consequently, the output will include the coordinates of all intersection points.

46

Program Variable	Algebraic Symbol (if applicable)	Comment
Item 1		Any alphameric information may be put on this card for identification of the calculation.
Item 2		
UAX		Nominal axial velocity (tunnel speed); positive; feet per second
XSTAT		Axial location of crossflow plane where data is obtained; feet
FACTOR		Arbitrary positive fraction of UAX. NOTE: FACTOR × UAX = VMIN
NFLDP		Total number of supplied data points; $1 < NFLDP \leq 500$
IZCYC		IZCYC = 0: coordinates of intersection points not in output IZCYC = 1: coordinates of intersection points in output
Item 3		
IN, ZFP(IF), YFP(IF), VTANFP(IF), VNORFP(IF)	$1,2,\dots NFLDP,$ $Z(1),Z(2),\dots Z(NFLDP),$ $Y(1),Y(2),\dots Y(NFLDP),$ $V_s(1),V_s(2),\dots V_s(NFLDP),$ $V_n(1),V_n(2),\dots V_n(NFLDP)$	Data point coordinates, velocity components along and normal to the probe flight path, see figure 8 for coordinate system; feet, feet per second. $1 < IF < NFLDP$. This input requires NFLDP cards.

Description of output.- This section describes the output from the trailing vortex crossflow program. In the following, all items of output are enumerated and the contents briefly described. Sample output is shown in figure 13.

The first pages identify the run and contain all the input data in connection with the probe traverse in the crossflow plane. The peaks in the normal component velocity and the associated field point coordinates determined by the program are also specified in this part of the output. In the ideal case, the peak values should be equal and opposite.

47

The next item, printed on a new page, specifies the lower bound or cutoff value VMIN for the magnitudes of the first and last resultant velocity vectors of the set to be treated further by the program. This is followed by a tabulation of the resultant velocities and coordinates starting with the first velocity magnitude larger than the cutoff value, then proceeding along the path through the vortex until the last velocity magnitude larger than VMIN. The first column is the index IF associated with the supplied data; the second column IW is another running index which starts with the value one. Index IW enumerates the set of field points with the first and the last having resultant velocity magnitudes larger than VMIN. Some of the resultant velocity magnitudes within this band may be less than VMIN. The last three columns represent angles necessary for the geometric combination of lines normal to the resultant velocity vector. In addition, the first and last field points of the set of admitted resultant velocities or vortex tangential velocities are also printed on this page.

Optional output of coordinates appears on the next page. These coordinates locate the points of intersection of the lines erected normal to the resultant velocity vectors at the field points. This output can be lengthy and is therefore made optional through the control variable IZCYC in Item 2 of the input. The first two columns are indices of the supplied data points, the second two columns are indices associated with the admissible resultant velocity vectors. The last two columns indicate the coordinates of the intersection of the two normals identified by the indices.

On the next page, the total number of intersection points determined by the program is listed together with the number of admissible intersection points. These are points with Y coordinates falling in the range of Y spanned by the peaks of the normal components of the vortex-induced velocities as identified at the end of the first pages of output. The coordinates of the apparent vortex center are also printed as the average values of the Z and Y coordinates of the subset of admitted intersection points.

The item of the output which appears on the next page is a tabulation of vortex tangential velocities (resultant velocities) and the distance from the apparent vortex center to the associated field points. This page also lists a statement concerning a check on core or noncore penetration of the traverse under consideration.

48

The maximum and minimum values of the vortex tangential velocities and the associated radii are printed on the next page. This information is printed for both core and noncore type penetrations. In either case, the peak values should be equal and opposite and the two radii equal for the ideal case of a single vortex with concentric, circular streamlines. If the traverse resulted in a core penetration, the average of the peak magnitudes equals the maximum vortex tangential velocity v_1 and the average of the two radii is r_1. A tabulation follows of vortex strengths computed according to potential flow theory from the vortex tangential velocities and the radii. Only those velocities at radii larger than 2.50 times the radius (r_1) where the peaks in velocity occur are included in the vortex strength computation. The last item of output is the average vortex strength or circulation determined from the tabulated values.

Program listing.- The trailing vortex crossflow program is written in Fortran IV language for the IBM 360/67 computer. The program consists of a main program without subroutines.

49

```
      PROGRAM TVCRS(INPUT,OUTPUT,TAPE5=INPUT,TAPE6=OUTPUT)
C     PROGRAM TVCRS
C
C
C     THIS PROGRAM COMPUTES THE STRUCTURE OF A TURBULENT VORTEX IN THE
C     CROSSFLOW PLANE FROM EXPERIMENTAL FLOW FIELD DATA IN THE CROSSFLOW
C     PLANE
C
C     Y-AXIS TO THE RIGHT WHEN FACING FORWARD, Z-AXIS DOWN
C
      DIMENSION  YFP(500),ZFP(500),VTANFP(500),VNORFP(500),TALK(20),
     1VRSLT(500),SLOPEL(500),VVRTAN(500)
      DIMENSION ZC(100,100),YC(100,100),RAD(100)
C
C
    1 FORMAT (20A4)
    2 FORMAT (1H1,20A4//)
    3 FORMAT (3F10.5,2I5)
    4 FORMAT (///1X,I4,1X,57HFIELD POINTS ARE SPECIFIED IN THE CROSS FLO
     1W PLANE AT X= ,F10.5,1X,6H  FT. / 4X,25HNOMINAL AXIAL VELOCITY IS,
     24X,F10.5,1X,6HFT/SEC///)
    5 FORMAT (///1X, 88HTHIS ANALYSIS IS CONCERNED WITH RESULTANT VELOCI
     1TIES IN THE CROSS FLOW PLANE LARGER THAN,3X,F10.5,1X, 9HTIMES THE,
     2/1X,14HAXIAL VELOCITY///)
    6 FORMAT (I5,4F10.5)
    7 FORMAT (///1X, 84HIN THIS VORTEX PENETRATION,THE PERTURBATION VELO
     1CITY NORMAL TO THE PROBE FLIGHT PATH/1X,13HHAS A MAXIMUM,5X,F10.5,
     21X,6HFT/SEC,2X,2HAT,2X,2HZ=,5X,F10.5,1X,6H  FT. /42X,2HY=,5X,F10.5
     3,1X,6H  FT. /1X,13HAND A MINIMUM,5X,F10.5,1X,6HFT/SEC,2X,2HAT,2X,
     3                                                           2HZ=
     4,5X,F10.5,1X,6H  FT. /42X,2HY=,5X,F10.5,1X,6H  FT. ///)
    8 FORMAT (///1X,7X,20HCOORDINATES IN CROSS,13X,34HCROSS FLOW PERTURB
     1ATION VELOCITIES/12X,13HFLOW PLANE,FT,19X,22HFROM EXPERIMENT,FT/SE
     2C//4X,2HIF,3X,
     2        1HZ,14X,1HY,17X,7HCOAXIAL,13X,6HNORMAL/)
    9 FORMAT (I5,F10.5,5X,F10.5,10X,F10.5,10X,F10.5)
   10 FORMAT (1H1,62HRESULTANT VELOCITIES WITH THE FIRST AND LAST LARGER
     1 THAN VMIN=,
     1                                                         2X,F10.5,
     11X,  51HFT/SEC AT THE INDICATED FIELD POINT COORDINATES AND/ 1X,
     1                                                            46HSL
     2OPES OF LINES NORMAL TO THE VELOCITY VECTORS//3X,2HIF,8X,2HIW,8X,
     31HZ,15X,1HY, 4X,
     319HRESULT. VEL.,FT/SEC,
     3                                    2X,11HTHETAS,DEG.,4X,11HTHETAL,DE
     4G.,4X,6HSLOPEL/)
   11 FORMAT (1X,I4,6X,I4,5X,F10.5,5X,F10.5,5X,F10.5,5X,F10.5,5X,F10.5,
     15X,F10.5)
   12 FORMAT (//1X,50HTHIS FLOWFIELD ACCOUNT STARTS AT DATA POINT NUMBER
     1,6X,3HIF=,I5/1X,52HWITH FIELD POINT COORDINATES IN THE CROSS FLOW
     2PLANE,5X,2HZ=,F10.5,2X,6H  FT. /58X,2HY=,F10.5,2X,6H  FT. /1X,54HT
     3HE LAST DATA POINT NUMBER INCLUDED IN THIS ACCOUNT IS,2X,3HIF=,I5,
     4/1X,52HWITH FIELD POINT COORDINATES IN THE CROSS FLOW PLANE,5X,
```

```
      52HZ=,F10.5,2X,6H   FT. /58X,2HY=,F10.5,2X,6H   FT. //)
   13 FORMAT (1H1,
     1          3X,100HCOORDINATES OF THE POINTS OF INTERSECTION OF THE
     1LINES CONSTRUCTED AT POINTS (ZFP,YFP) NORMAL TO THE/
     1                                 10X,42HRESULTANT VELO
     2CITY VECTORS AT THOSE POINTS//9X,2HIL,8X,2HJL,8X,2HIW,8X,2HJW,13X,
     36HZC,FT.,9X,6HYC,FT./)
   14 FORMAT (9X,I3,7X,I3,7X,I3,7X,I3,8X,E12.5,5X,E12.5)
   15 FORMAT(1H1,4X,44HTOTAL NUMBER OF COMPUTED INTERSECTION POINTS,26X,
     1I5/5X,40HNUMBER OF ADMISSABLE INTERSECTION POINTS,30X,I5/5X,54HAVE
     2RAGE Z COORDINATE OF ADMISSABLE INTERSECTION POINTS,6X,F10.5,1X,3H
     3FT./5X,54HAVERAGE Y COORDINATE OF ADMISSABLE INTERSECTION POINTS,
     4          6X,F10.5,1X,3HFT.///)
   16 FORMAT (1H1,5X,38HVORTEX TANGENTIAL VELOCITIES AND RADII//9X,2HIV,
     110X,10HRADIUS,FT.,5X,27HTANGENTIAL VELOCITY,FT/SEC./)
   17 FORMAT (8X,I3,9X,F10.5,15X,F10.5)
   18 FORMAT (////5X,33HVORTEX STRENGTH,GAMMAO,FT**2/SEC.//9X,2HIV,10X,
     110HRADIUS,FT.,5X,27HTANGENTIAL VELOCITY,FT/SEC.,7X,16HGAMMAO,FT**2
     2/SEC/)
   19 FORMAT (8X,I3,9X,F10.5,15X,F10.5,15X,F10.5)
   20 FORMAT (1H1,53HIN THIS VORTEX ACCOUNT,THE VORTEX TANGENTIAL VELOCI
     1TY  /1X,13HHAS ONE PEAK ,5X,F10.5,1X,6HFT/SEC,2X,2HAT,2X,4HRAD=,F1
     20.5,2X,3HFT./1X,13HAND ANOTHER  ,5X,F10.5,1X,6HFT/SEC,2X,2HAT,2X,4
     2HRAD=,F10.5,2X,3HFT.///)
   21 FORMAT (////5X,35HAVERAGE CIRCULATION IN OUTER REGION,5X,F10.5,1X,
     19HFT**2/SEC//)
   22 FORMAT (////1X,44HTHIS TRAVERSE RESULTED IN A CORE PENETRATION///)
   23 FORMAT (////1X,48HTHIS TRAVERSE RESULTED IN A NON-CORE PENETRATION/
     1//)
   24 FORMAT (1H1,5X,59HDIMENSION OF INTERSECTION POINTS COORDINATES NOT
     1 SUFFICIENT///)
   25 FORMAT (////1X,31HABOVE TABULATION WAS STOPPED AT,2X,3HIF=,I5///)
C
 1000 READ (5,1) TALK
      WRITE (6,2) TALK
C
C     SPECIFY AXIAL FLOW VELOCITY UAX, AXIAL LOCATION, XSTAT, NUMBER OF
C     FIELD POINTS NFLDP.
C                         FACTOR IS AN ARBITRARY FRACTION OF UAX AND
C     IS DETERMINED BY THE SIGNAL NOISE LEVEL
C     IZCYC=0, INTERSECTION POINTS NOT IN OUTPUT
C     IZCYC=1, INTERSECTION POINTS IN OUTPUT
C
      READ (5,3) UAX,XSTAT,FACTOR,NFLDP,IZCYC
      VMIN=(FACTOR)*UAX
C
C     SPECIFY COORDINATES (ZFP,YFP) OF THE FIELD POINTS AND THE PERTUR-
C     BATION VELOCITIES TANGENTIAL AND NORMAL TO THE PROBE FLIGHT PATH
C     IN THE CROSS FLOW PLANE, VTANFP AND VNORFP, FT AND FT/SEC
C     VELOCITIES POSITIVE WHEN COMPONENTS ALONG Z AND Y AXIS ARE POSITIVE
C
      DO 102 IF=1,NFLDP
  102 READ (5,6) IN,ZFP(IF),YFP(IF),VTANFP(IF),VNORFP(IF)
```

51

```
C
      WRITE (6,4) NFLDP,XSTAT,UAX
      WRITE (6,5) FACTOR
C
      VNORMX=-1.0E-10
      VNORMN= 1.0E+10
      DO 131 IF=1,NFLDP
      VNORMX= AMAX1(VNORMX,VNORFP(IF))
  131 VNORMN= AMIN1(VNORMN,VNORFP(IF))
C
      WRITE (6,8)
      DO 103 IF=1,NFLDP
  103 WRITE (6,9) IF,ZFP(IF),YFP(IF),VTANFP(IF),VNORFP(IF)
C
C     LOCATE COORDINATES OF DATA POINTS WHERE MAXIMUM AND MINIMUM NORMAL
C     PERTURBATION VELOCITIES OCCUR
C
      DO 107 IF=1,NFLDP
      DIFFMX=VNORMX-VNORFP(IF)
      DIFFMN=VNORFP(IF)-VNORMN
      IF (DIFFMX.LT.1.0E-07) IFMAX=IF
      IF (DIFFMN.LT.1.0E-07) IFMIN=IF
  107 CONTINUE
      WRITE (6,7) VNORMX,ZFP(IFMAX),YFP(IFMAX),VNORMN,ZFP(IFMIN),YFP
     1(IFMIN)
      DIFFY=YFP(IFMAX)-YFP(IFMIN)
C
C
C     COMPUTE RESULTANT VELOCITIES AT POINTS (ZFP,YFP) IN THE CROSSFLOW
C     PLANE AT X=XSTATION.  IF MAGNITUDE IS LARGER THAN VMIN, CALCULATE
C     SLOPE OF THE NORMAL TO THE RESULTANT VELOCITY VECTOR AND PRINT
C     THEM AS A SUBSET OF THE SUPPLIED DATA.
C
      WRITE (6,10) VMIN
      IFIRST=0
      IW=0
      DO 100 IF=1,NFLDP
      VRSLT(IF)=SQRT(VTANFP(IF)**2+VNORFP(IF)**2)
      IF (IFIRST.EQ.0.AND.VRSLT(IF).GT.VMIN) GO TO 104
      IF (IFIRST.GT.0.AND.VRSLT(IF).LT.1.0E-07) GO TO 941
      IF (IFIRST.GT.0.AND.
     1    IFMAX.GT.IFMIN.AND.IF.GT.IFMIN.AND.IF.LT.IFMAX.AND.VRSLT(IF).
     1LT.VMIN) GO TO 941
      IF (IFIRST.GT.0.AND.
     1    IFMIN.GT.IFMAX.AND.IF.GT.IFMAX.AND.IF.LT.IFMIN.AND.VRSLT(IF).
     1LT.VMIN) GO TO 941
      IF (IFIRST.GT.0.AND.IFMIN.GT.IFMAX.AND.IF.GT.IFMIN.AND.VRSLT(IF).
     1LT.VMIN) GO TO 942
      IF (IFIRST.GT.0.AND.IFMAX.GT.IFMIN.AND.IF.GT.IFMAX.AND.VRSLT(IF).
     1LT.VMIN) GO TO 942
      IF (IFIRST.GT.0) GO TO 101
      GO TO 100
  104 IFIRST=IF
```

```
      GO TO 101
  941 VRSLT(IF)=0.0
  101 IW=IW+1
      IF (VNORFP(IF).GT.0.0) VVRTAN(IW)=VRSLT(IF)
      IF (VNORFP(IF).LT.0.0) VVRTAN(IW)=-VRSLT(IF)
      IFP1=IF+1
      DELTAY=YFP(IFP1)-YFP(IF)
      DELTAZ=ZFP(IFP1)-ZFP(IF)
      THETAS=ATAN2(DELTAY,DELTAZ)
      IF (THETAS.LT.0.0) THETAS=6.28318531+THETAS
      ALPHAV=ATAN (VTANFP(IF)/VNORFP(IF))
      THETAL=THETAS+ALPHAV
      SLOPEL(IW)= TAN (THETAL)
      THETAD=THETAS*57.2957795
      THETLD=THETAL*57.2957795
      WRITE (6,11) IF,IW,ZFP(IF),YFP(IF),VVRTAN(IW),THETAD,THETLD,SLOPEL
     1(IW)
      ILAST=IF
  100 CONTINUE
      GO TO 943
  942 WRITE (6,25) IF
  943 CONTINUE
C
C
C
      WRITE (6,12) IFIRST,ZFP(IFIRST),YFP(IFIRST),ILAST,ZFP(ILAST),
     1YFP(ILAST)
C
C     DETERMINE COORDINATES OF THE POINTS OF  INTERSECTION OF THE LINES
C     CONSTRUCTED AT POINTS (ZFP,YFP) NORMAL TO THE RESULTANT VELOCITY
C     VECTORS AT THOSE POINTS
C
      ILSTM1=ILAST-1
      DO 105 IL=IFIRST,ILSTM1
      JLS=IL+1
      DO 105 JL=JLS,ILAST
      IW=IL-IFIRST+1
      JW=JL-IFIRST+1
      IF (IW.GT.100.OR.JW.GT.100) GO TO 196
      GO TO 197
  196 WRITE (6,24)
      STOP
  197 CONTINUE
      IF (ABS(VVRTAN(IW)).LT.1.0E-07.OR.ABS(VVRTAN(JW)).LT.1.0E-07) GO
     1TO 124
      GO TO 106
  124 ZC(IW,JW)=1.0E-12
      YC(IW,JW)=1.0E-12
      GO TO 105
  106 IF (ABS(SLOPEL(JW)-SLOPEL(IW)).LT.1.0E-07) GO TO 127
      ZC(IW,JW)=-((YFP(IL)-SLOPEL(IW)*ZFP(IL))-(YFP(JL)-SLOPEL(JW)*
     1ZFP(JL)))/
     1(SLOPEL(IW)-SLOPEL(JW))
```

```
          YC(IW,JW)= YFP(IL)-SLOPEL(IW)*(ZFP(IL)-ZC(IW,JW))
          GO TO 105
      127 ZC(IW,JW)=1.0E+12
          YC(IW,JW)=1.0E+12
      105 CONTINUE
C
C         PRINT COORDINATES OF ALL POINTS OF  INTERSECTION,GOOD OR BAD
C
          IF (IZCYC.EQ.0) GO TO 198
          WRITE (6,13)
          DO 126 IL=IFIRST,ILSTM1
          JLS=IL+1
          DO 126 JL=JLS,ILAST
          IW=IL-IFIRST+1
          JW=JL-IFIRST+1
      126 WRITE (6,14) IL,JL,IW,JW,ZC(IW,JW),YC(IW,JW)
      198 CONTINUE
C
C         EXCLUDE INTERSECTION POINTS WITH YC OUTSIDE THE REGION SPANNED BY
C         YFP(IFMAX) AND YFP(IFMIN)
C
          IPIB=0
          DO 108 IL=IFIRST,ILSTM1
          JLS=IL+1
          DO 108 JL=JLS,ILAST
          IW=IL-IFIRST+1
          JW=JL-IFIRST+1
          IF (DIFFY.LT.0.0) GO TO 110
          GO TO 111
      110 IF (YC(IW,JW).LT.YFP(IFMAX). OR.YC(IW,JW).GT.YFP(IFMIN)) GO TO 113
          GO TO 108
      111 IF (YC(IW,JW).GT.YFP(IFMAX). OR.YC(IW,JW).LT.YFP(IFMIN)) GO TO 114
          GO TO 108
      113 ZC(IW,JW)=0.0
          YC(IW,JW)=0.0
          IPIB=IPIB+1
          GO TO 115
      114 ZC(IW,JW)=0.0
          YC(IW,JW)=0.0
          IPIB=IPIB+1
      115 IPIBT=IPIB
      108 CONTINUE
C
C         CALCULATE AVERAGE COORDINATES (ZCAVE,YCAVE) OF GOOD INTERSECTION
C         POINTS
C
          ZCAVE=0.0
          YCAVE=0.0
          JLTOT=(ILAST-IFIRST)+1
          NIPTOT=(JLTOT*(JLTOT-1))/2
          NIPG=NIPTOT-IPIBT
          ANIPG=NIPG
          DO 116 IL=IFIRST,ILSTM1
```

```
      JLS=IL+1
      DO 116 JL=JLS,ILAST
      IW=IL-IFIRST+1
      JW=JL-IFIRST+1
      ZCAVE=ZCAVE+ZC(IW,JW)/ANIPG
      YCAVE=YCAVE+YC(IW,JW)/ANIPG
  116 CONTINUE
C
C     PRINT COORDINATES (ZCAVE,YCAVE) OF THE AVERAGE INTERSECTION POINT,
C     ALSO THE TOTAL NUMBER OF INTERSECTION POINTS AND THE NUMBER OF
C     GOOD INTERSECTION POINTS
C
      WRITE (6,15) NIPTOT,NIPG,ZCAVE,YCAVE
C
C     COMPUTE RADII OF THE VORTEX AS THE DISTANCE FROM THE AVERAGE
C     INTERSECTION POINT (VORTEX CENTER) TO THE DATA POINTS
C
      WRITE (6,16)
      DO 117 IF=IFIRST,ILAST
      IV=IF-IFIRST+1
      RAD(IV)= SQRT((ZFP(IF)-ZCAVE)**2+(YFP(IF)-YCAVE)**2)
      IF(ABS(VVRTAN(IV)).LT.1.0E-07) RAD(IV)=0.0
  117 WRITE (6,17) IV,RAD(IV),VVRTAN(IV)
C
C
      VTANMX=-1.0E-10
      VTANMN=1.0E+10
      DO 141 IF=IFIRST,ILAST
      IV=IF-IFIRST+1
      VTANMX=AMAX1(VTANMX,VVRTAN(IV))
  141 VTANMN=AMIN1(VTANMN,VVRTAN(IV))
      DO 142 IF=IFIRST,ILAST
      IV=IF-IFIRST+1
      DIFFMX=VTANMX-VVRTAN(IV)
      DIFFMN=VVRTAN(IV)-VTANMN
      IF(DIFFMX.LT.1.0E-07) IVMAX=IV
      IF (DIFFMN.LT.1.0E-07) IVMIN=IV
  142 CONTINUE
C
C     CHECK FOR CORE PENETRATION
C
      IF (IVMAX.LT.IVMIN) GO TO 192
      IVMNP1=IVMIN+1
      IF (VVRTAN(IVMNP1).LT.0.0) WRITE (6,22)
      IF (VVRTAN(IVMNP1).GT.0.0) WRITE (6,23)
      GO TO 193
  192 IVMXP1=IVMAX+1
      IF (VVRTAN(IVMXP1).GT.0.0) WRITE(6,22)
      IF (VVRTAN(IVMXP1).LT.0.0) WRITE(6,23)
  193 CONTINUE
C
      WRITE (6,20) VTANMX,RAD(IVMAX),VTANMN,RAD(IVMIN)
C
```

```
C       CALCULATE CIRCULATION IN OUTER REGION (POTENTIAL VORTEX)
C
        RAD1=(RAD(IVMAX)+RAD(IVMIN))/2.0
        IVNG=0
        SUMGAM=0.0
        WRITE (6,18)
        RADMN=2.50*RAD1
        DO 118 IF=IFIRST,ILAST
        IV=IF-IFIRST+1
        IF(RAD(IV).LT.RADMN ) GO TO 119
        GO TO 120
119     IVNG=IVNG+1
        VORTAN=0.0
        GAMMAO=0.0
        GO TO 118
120     VORTAN=ABS(VVRTAN(IV))
        GAMMAO=6.2831*RAD(IV)*VORTAN
        SUMGAM=SUMGAM+GAMMAO
121     WRITE (6,19) IV,RAD(IV),VORTAN,GAMMAO
118     CONTINUE
        ATOT=JLTOT-IVNG
        GAMAV=SUMGAM/ATOT
        WRITE (6,21) GAMAV
        GO TO 1000
        END
```

Sample Case

The sample case concerns a segment of data obtained during one traverse through a wing tip vortex in a test performed recently in the 40- by 80-Foot Wind Tunnel at Ames Research Center (Contract NAS2-6719). The axial location of the crossflow plane was 55 chords behind a 6-inch chord, 32-inch span rectangular wing at 12° angle of attack. A three-axis, hot-wire probe measured the axial, coaxial, and normal velocity components. The probe flight path was an arc with 7.33 feet radius. For purposes of this analysis the probe flight is assumed straight during the length of vortex penetration.

The input data for this sample case is shown in figure 12; the output is listed in figure 13. A plot of the resultant velocities and the apparent vortex center is shown in figure 14. Using the data of figure 14, the magnitudes of the vortex tangential velocities are plotted as a function of radius in figure 15. This plot is a graphical representation of the corresponding tabulation in the program output of figure 13.

The input for this sample case comprises 40 data points, and the normal component of the perturbation velocity has a maximum and minimum almost equal in magnitude, an indication of a traverse through a circular vortex with concentric streamlines. The number of data points admitted by the lower bound or cutoff velocity of 18.0 feet per second is 35. This particular traverse resulted in a core penetration with nearly equal peaks in vortex tangential velocity. The total circulation strength Γ_o of this vortex calculated by the program is 21.9 feet^2 per second. With the assumption of elliptical loading on the rectangular wing model, the theoretical circulation strength for the flow conditions for this test ($\alpha = 12°$) was estimated to be 20.2 feet^2 per second, which is in good agreement with the program computed value.

CONCLUDING REMARKS

Several final observations should be made with respect to the planning and conduct of the flight tests to investigate wake vortices. First, it should be emphasized that there are essentially no reliable, comprehensive data on flight measurements of wake vortices. The ARC tests represent an excellent opportunity to make a really fundamental contribution to the

knowledge of wake vortex behavior. Although a primary goal of the tests is to measure fully developed vortex properties to assess the wake-encounter problem, it should also be a primary goal to obtain sufficient measurements to shed some light on the dissipation problem. Since the dissipation mechanisms are so poorly understood, as much auxiliary data on such effects as temperature, humidity, and turbulence should be taken as are consistent with the time and funds available. These data will serve many purposes to many investigators, and the thoroughness with which the test parameters and conditions are defined will be very important to users of the data. As an aid in planning the data collection and reduction effort, a summary of the recommended measurements, with some commentary and a reference to the discussion in this report, is presented as figure 16.

NEAR would like to emphasize the importance of good preparation in using hot-wire anemometry in a program of this sort, based on our experience in the 40- by 80-Foot Wind Tunnel tests. We had considerable difficulties with the mechanical integrity of the probe, the recording equipment, the calibration, the digitization process, and the data reduction procedure. The more experience that can be gained before the tests with the various facets of using the instrument and reducing the data, the more efficiently the data collection and reduction procedure will be.

The data reduction scheme was developed making certain assumptions regarding the symmetry of a vortex and the lack of radial velocity and ignoring effects of the other vortex of the pair and any vortex motion induced during the probe by the presence of the probe itself. This was felt to be a logical place to start. The success with which the program handled the wind-tunnel vortex data is an indication that the method should work well for the flight case. When the flight data is analyzed, however, considerable attention should be given to the behavior of the results to insure that the assumptions are not being violated.

Finally, NEAR would like to emphasize again the importance of obtaining core penetrations, since considerably more information on the structure of the vortex is obtained than if only noncore penetrations are achieved.

Nielsen Engineering & Research, Inc.
    Mountain View, California
        January, 1973

58

REFERENCES

1. De Young, J. and Harper, C. W.: Theoretical Symmetric Span Loading at Subsonic Speeds for Wings Having Arbitrary Planform. NACA Rept. 921, May 1950.

2. Kuhn, G. D. and Nielsen, J. N.: Analytical Studies of Aircraft Trailing Vortices, AIAA Paper No. 72-42.

3. MacCready, P. B.: An Assessment of Dominent Mechanisms in Vortex-Wake Decay. Aircraft Wake Turbulence and Its Detection, Plenum Press, 1971.

4. Condit, P. M. and Tracy, P. W.: Results of the Boeing Company Wake Turbulence Test Program. Aircraft Wake Turbulence and Its Detection, Plenum Press, 1971.

5. Chevalier, H.: Flight Test Studies of the Formation of Trailing Vortices and a Method to Accelerate Vortex Dissipation. AIAA Paper No. 72-988.

6. Smith, T. B. and Beesmer, K. M.: Contrail Studies for Jet Aircraft. AFCRC TR-59-251, Apr. 1959. AD 217 188.

7. MacCready, P. B., Jr.: Standardization of Gustiness Values from Aircraft. Jour. Appl. Meteorology, vol, 3, no. 4, 1964, p. 439.

8. Ryan, John P., et al: Medium Altitude Critical Atmospheric Turbulence (MEDCAT) Data Processing and Analysis. University of Dayton Research Institute, Dayton, Ohio, July 31, 1971. AD-732 878.

9. Hinze, J. O.: Turbulence. McGraw-Hill, New York, 1959, pp. 194-5.

10. MacCready, P. B., Jr.: Turbulence Measurements by Sailplane. J. Geophys. Res., vol. 67, p. 101, 1962.

11. Reed, Robert E.: Properties of the Lateral Random Oscillations of Trailing Vortices Observed in Wind-Tunnel Tests. NEAR TR-47, (to be published in 1973 as a NASA Contractor's Report).

12. McCormick, B. W., Tangler, J. L., and Sherrier, H. E.: Structure of Trailing Vortices. Jour. of Aircraft, vol. 5, no. 3, May-June 1968.

13. Baldwin, B. S., Chigier, N. A., and Sheaffer, Y. S.: Prediction of Far Flow Field in Trailing Vortices. AIAA Paper No. 72-989, presented at 2nd Atmospheric Flight Mechanics Conference, Sept. 13, 1972, Cabana Hotel, Palo Alto, CA.

14. Crow, S. C.: Stability Theory for a Pair of Trailing Vortices. AIAA Paper No. 70-53, presented at 8th Aerospace Sciences Meeting, Jan. 19-21, 1970, New York, NY.

15. Scorer, R. S. and Davenport, L. J.: Contrails and Aircraft Downwash. Journal Fluid Mechanics, vol. 43, pt. 3, Sept. 1970.

16. Tombach, I. H.: Transport of a Vortex Wake in a Stably Stratified Atmosphere. <u>Aircraft Wake Turbulence and Its Detection</u>. Plenum Press, New York, 1971.

17. Bradshaw, P.: <u>An Introduction to Turbulence and Its Measurement</u>. Pergamon Press, 1971.

18. Soderman, P. T. and Aiken, T. N.: Full-Scale Wind-Tunnel Tests of a Small Unpowered Jet Aircraft with a T-Tail. NASA TN D-6573, Nov. 1971.

19. Pilié, R. J. and Jiusto, J. E.: A Laboratory Study of Contrails. Journal of Meteorology, vol. 15, Apr. 1968.

20. Hall, M. G.: The Structure of Concentrated Vortex Cores. <u>Progress in Aeronautical Sciences</u>, vol. 7, Pergamon Press.

TABLE I

PERTINENT CHARACTERISTICS OF T-33 AIRCRAFT

Weight (at time vortices are laid down)	11,750 pounds
Wing Span	37.54 feet
Wing Taper Ratio	2.63
Wing Aspect Ratio	6.0
Wing Quarter Chord Sweep	0 degree
Wing Twist	1-1/2 degrees (washout)
Wing Airfoil Section	NACA 65-213, a = 0.5

TABLE II

PROPERTIES OF THE NACA STANDARD ATMOSPHERE
AT 12,500 FEET ALTITUDE

Density	$\rho = 0.001621$ slugs per feet^3
Temperature	$T = 14.5°$ F
Pressure	$p = 1320$ psfa
Kinematic Viscosity	$\nu = 2.14 \times 10^{-4}$ feet^2 per second
Speed of Sound	$c = 1067.4$ feet per second

TABLE III

LIST OF CONDITIONS USED IN

CONDENSATION CALCULATIONS

	DCH-2	T-33	B-47E
Gross Weight (lbs)	4,100	11,750	200,000
Span (ft)	48	37.5	116
Speed (ft/sec)	150	300	880
Altitude (ft)	1,000	12,500	35,000
Γ_o (ft^2/sec)	314	819.5	3,390
r_1 (ft)	1.1	0.86	2.66
Γ_1 (ft^2/sec)	195	509	2,100
v_1 (ft/sec)	28.2	94	126

TABLE IV

RESULTS OF CONDENSATION CALCULATIONS

	DCH-2	T-33	B-47E
p_∞ (psfa)	2,040	1,317	498
$p_\infty - p_c$ (psf)	5.8	45.5	37.1
T_∞ (° F)	55.4	14.4	-65.8
$T_\infty - T_c$ (° F)	0.3	3.5	6.3
Pounds of water vapor condensed in core per pound of mixture* $(\omega_\infty - \omega_c)$	3×10^{-5}	1.4×10^{-4}	1.3×10^{-5}
Percentage of ambient water vapor condensed in core* $\left(\dfrac{\omega_\infty - \omega_c}{\omega_\infty}\right) \times 100$	0.3%	4.6%	13%
Temperature rise in core due to condensation*(° F)	0.1	0.6	0.06
Ratio of momentum imparted to condensed water vapor to momentum of core flow	4.6×10^{-5}	2.1×10^{-4}	2×10^{-5}

*Based on the assumption that the ambient air is saturated at T_∞.
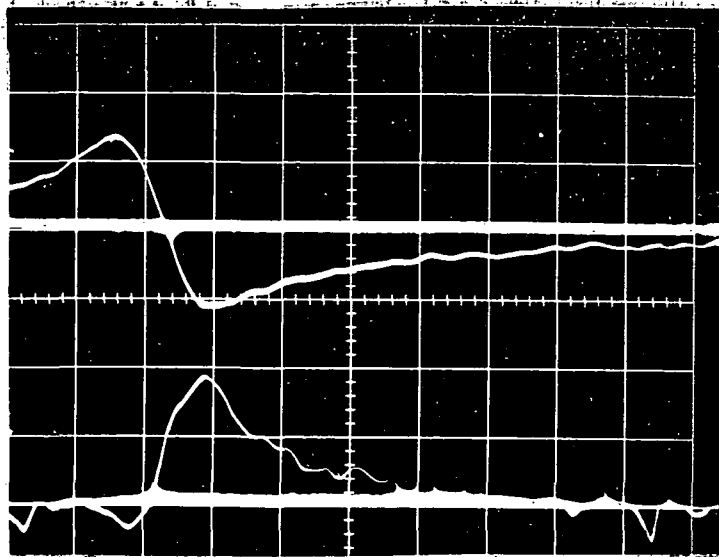
(a) Wires 1 and 3
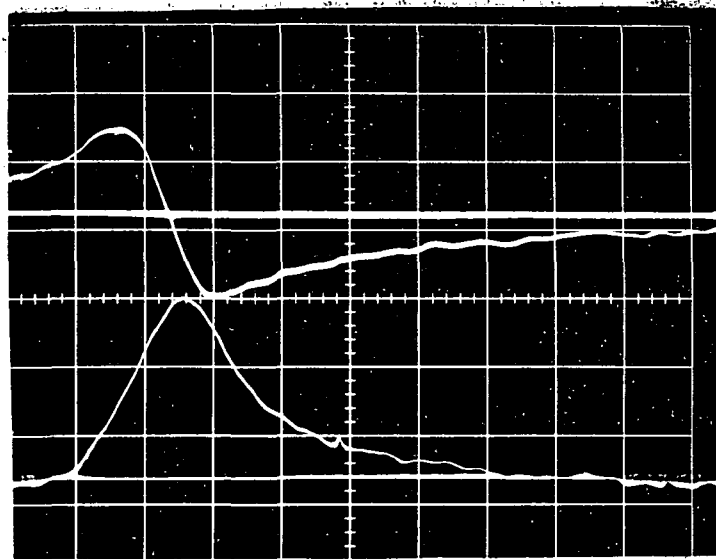
(b) Wires 2 and 3

Figure 1.- Example of a set of oscilloscope
photographs of a core penetration with a
hot-wire probe, taken in the 40- by 80-Foot
Wind Tunnel trailing vortex tests.
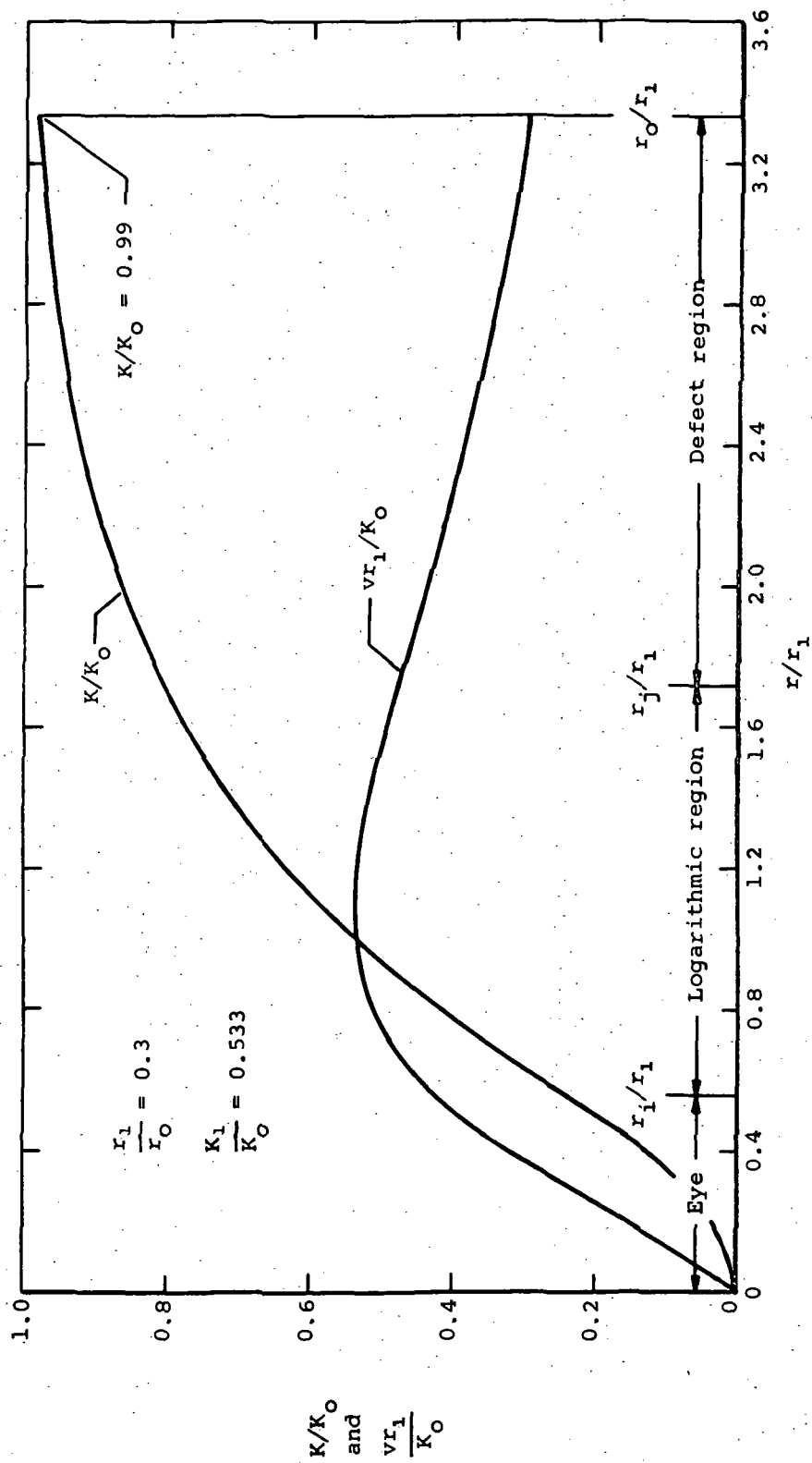
Figure 2.- Velocity and circulation profiles in a turbulent vortex.
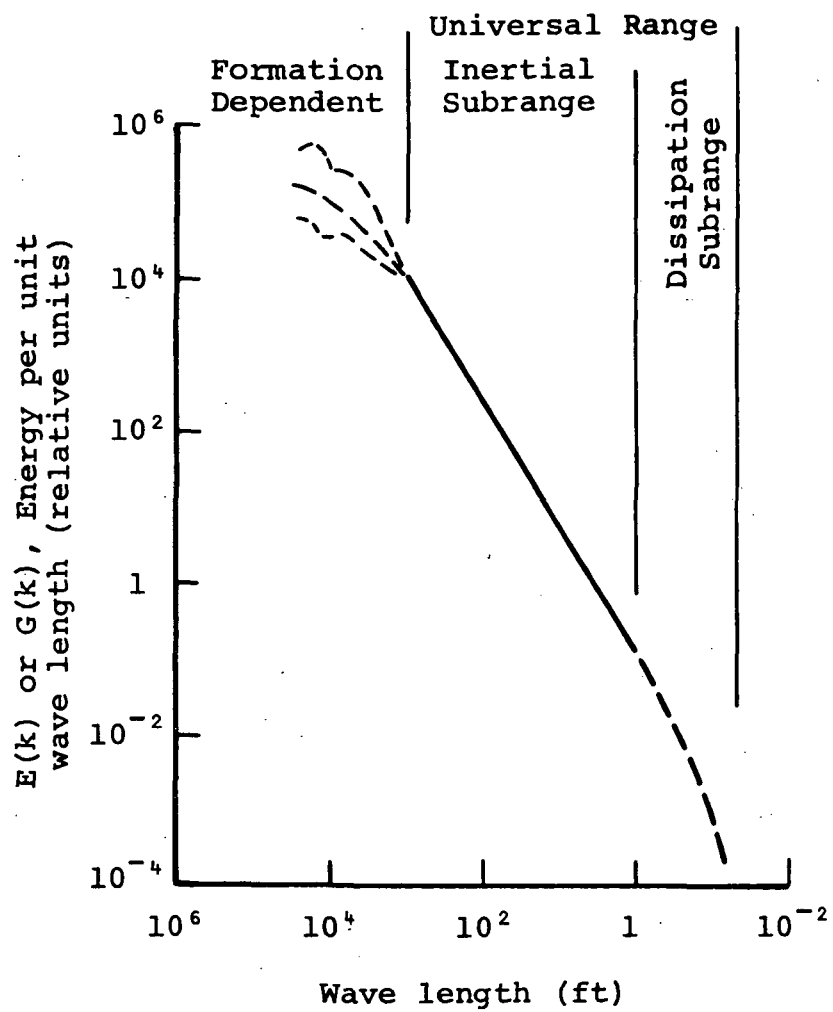
Figure 3.- Atmospheric turbulence
power spectra.

66
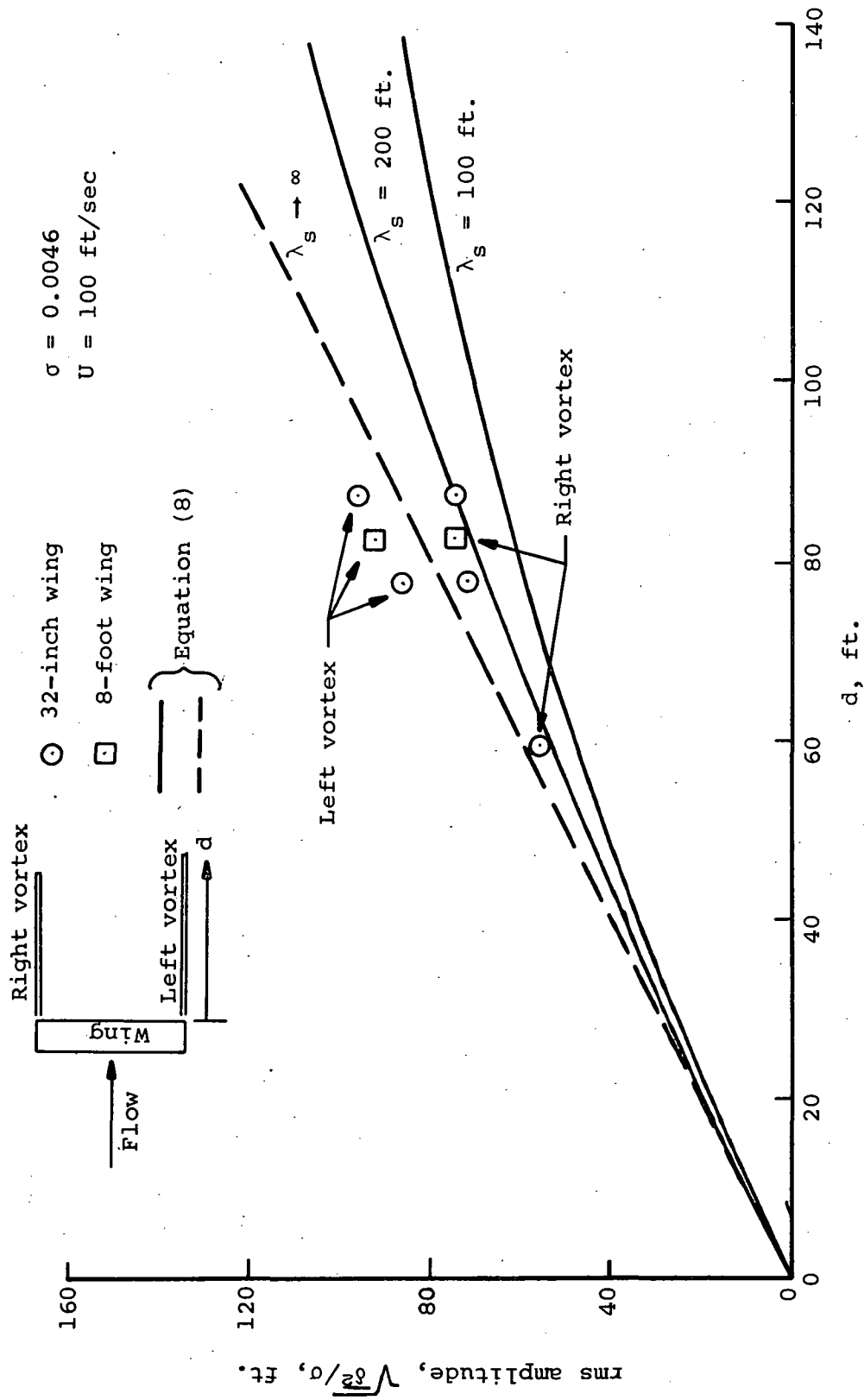
(a) 40- by 80-Foot Wind Tunnel.

Figure 4.- Comparison of theory and experiment for vortex deflection.
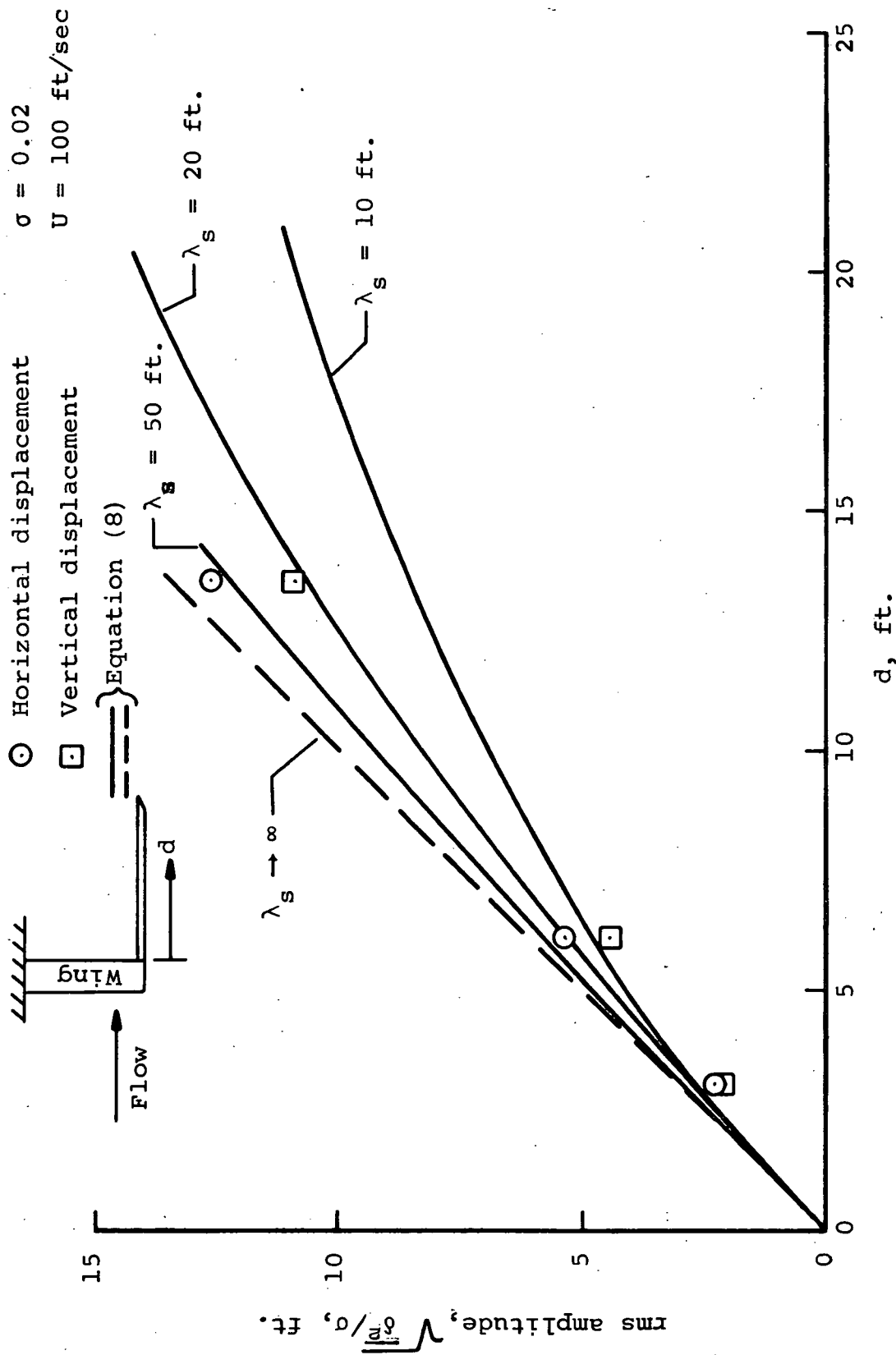
(b) 7- by 10-Foot Wind Tunnel.

Figure 4.- Concluded.

Figure 5.- Prediction of vortex deflection for flight conditions.
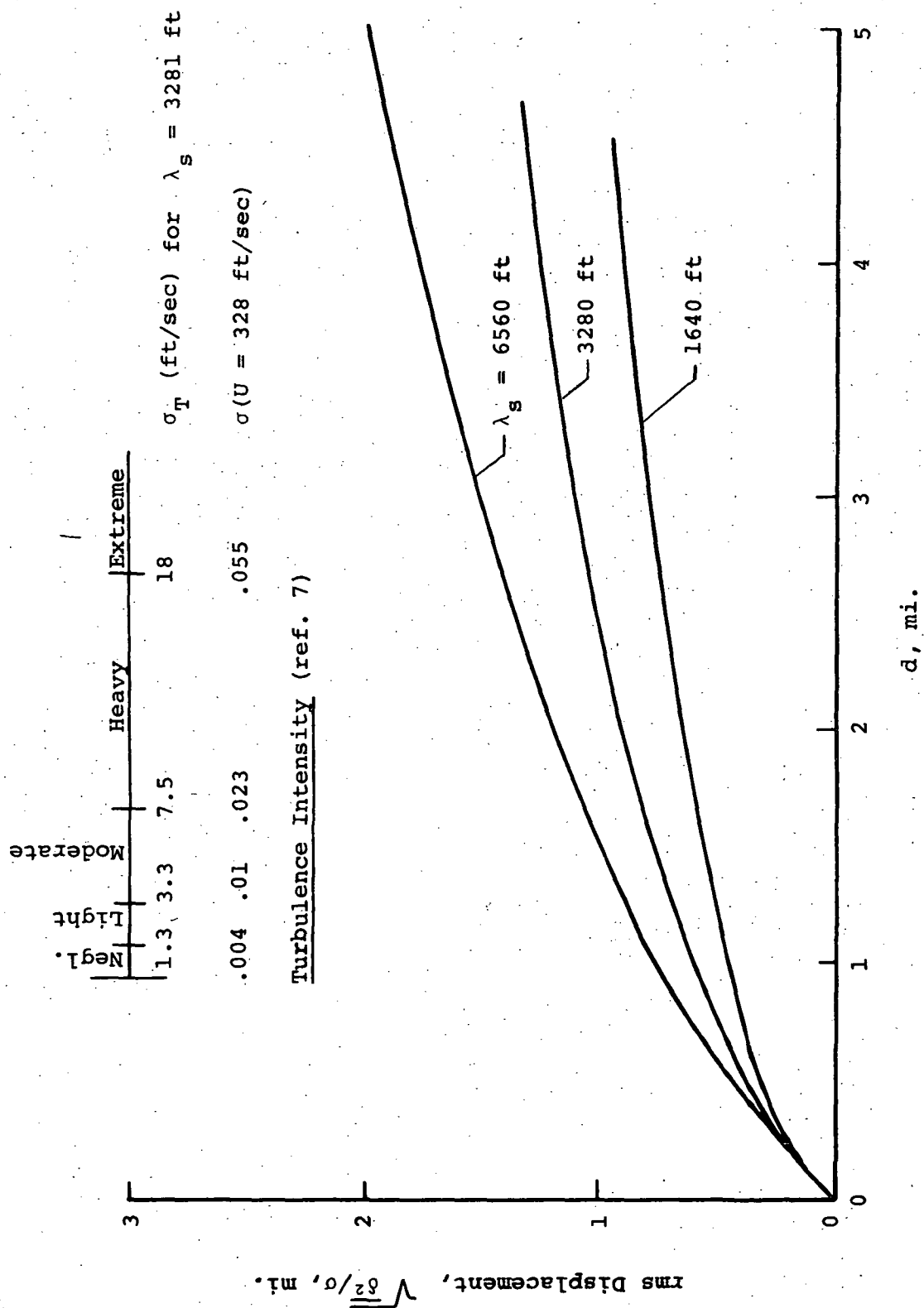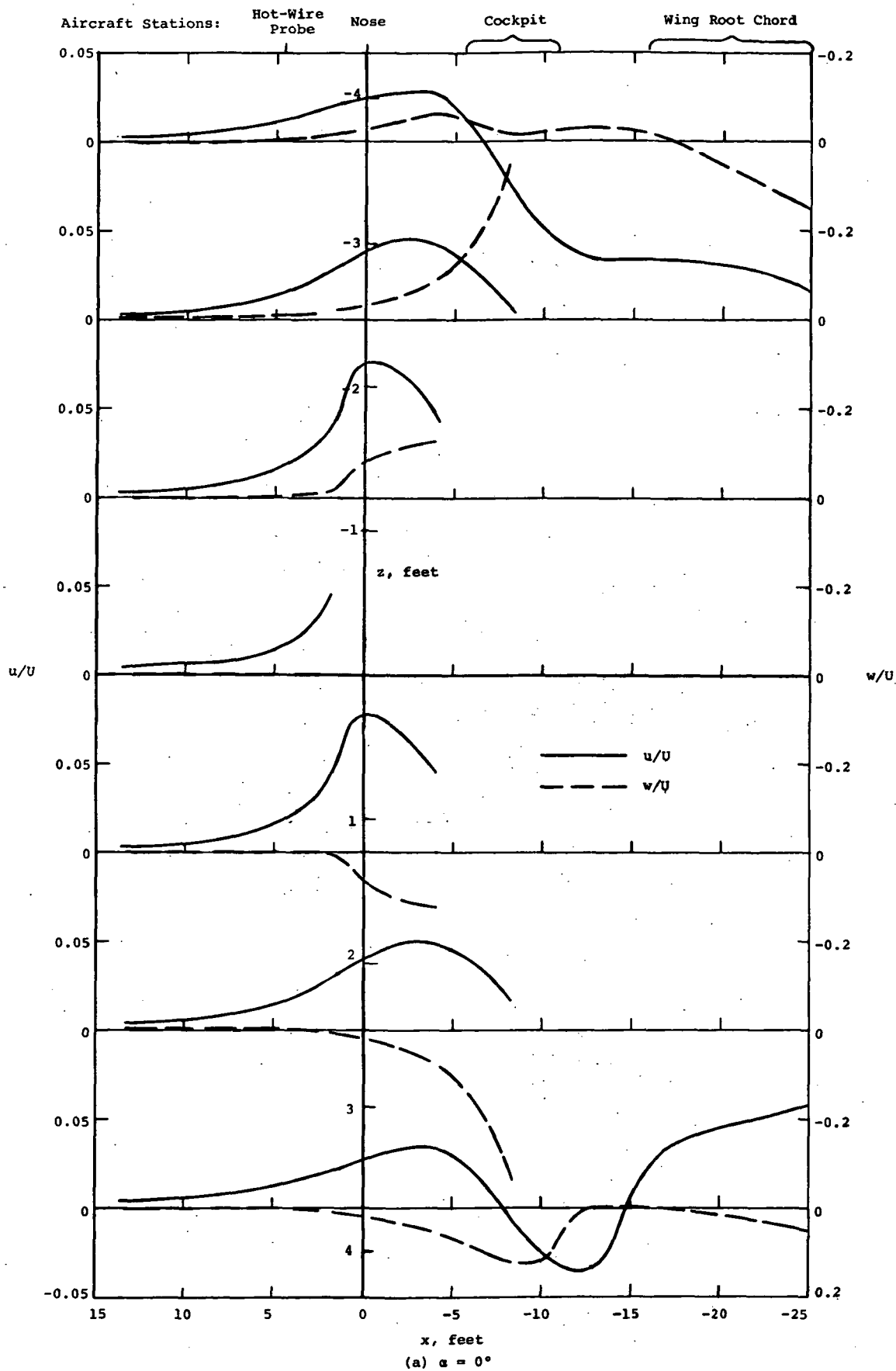
Figure 6.- Perturbation velocity components around the forward portion of the Learjet in the vertical plane of symmetry.

(b) α = 10°
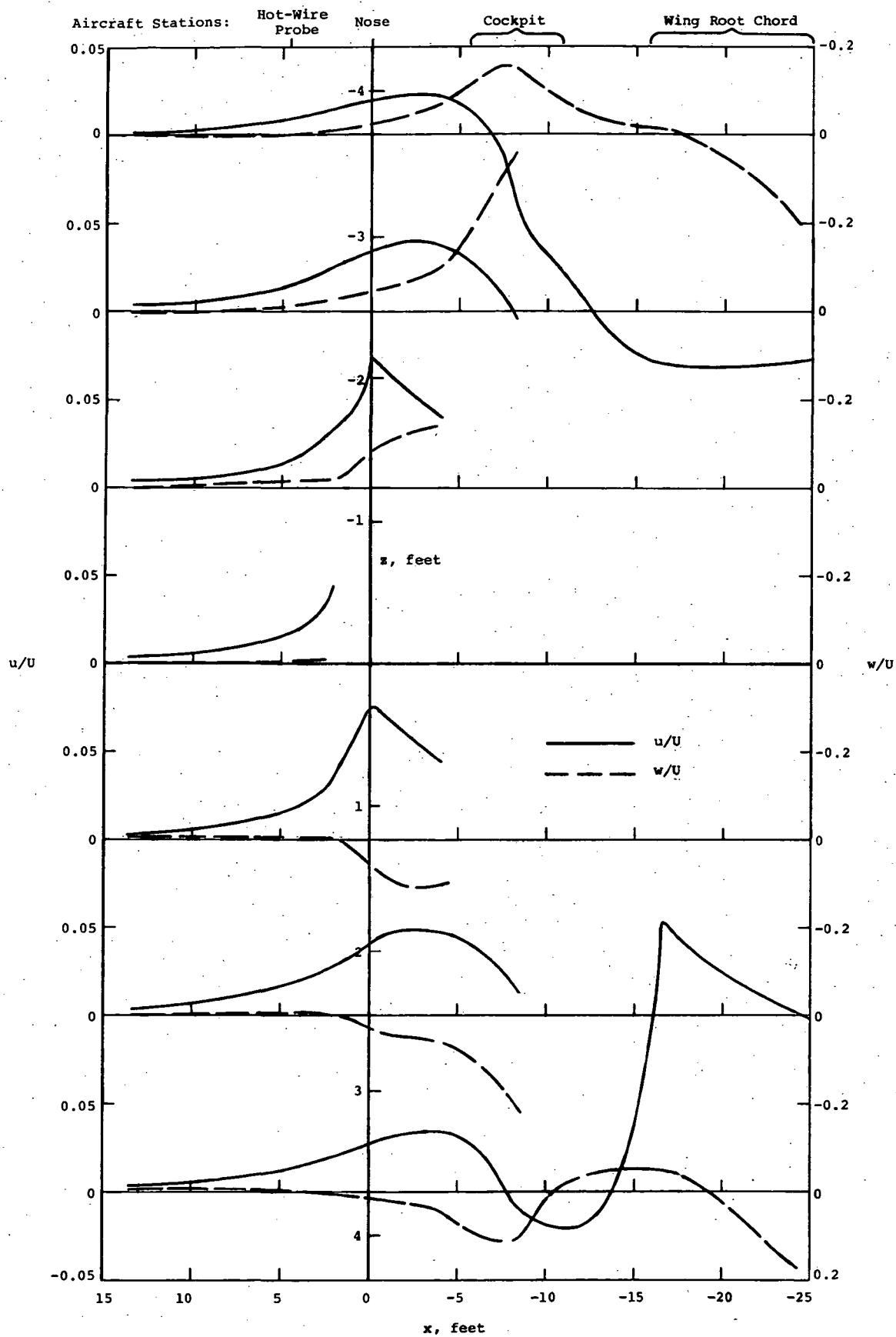
Figure 6.- Concluded.

(a) α = 0°
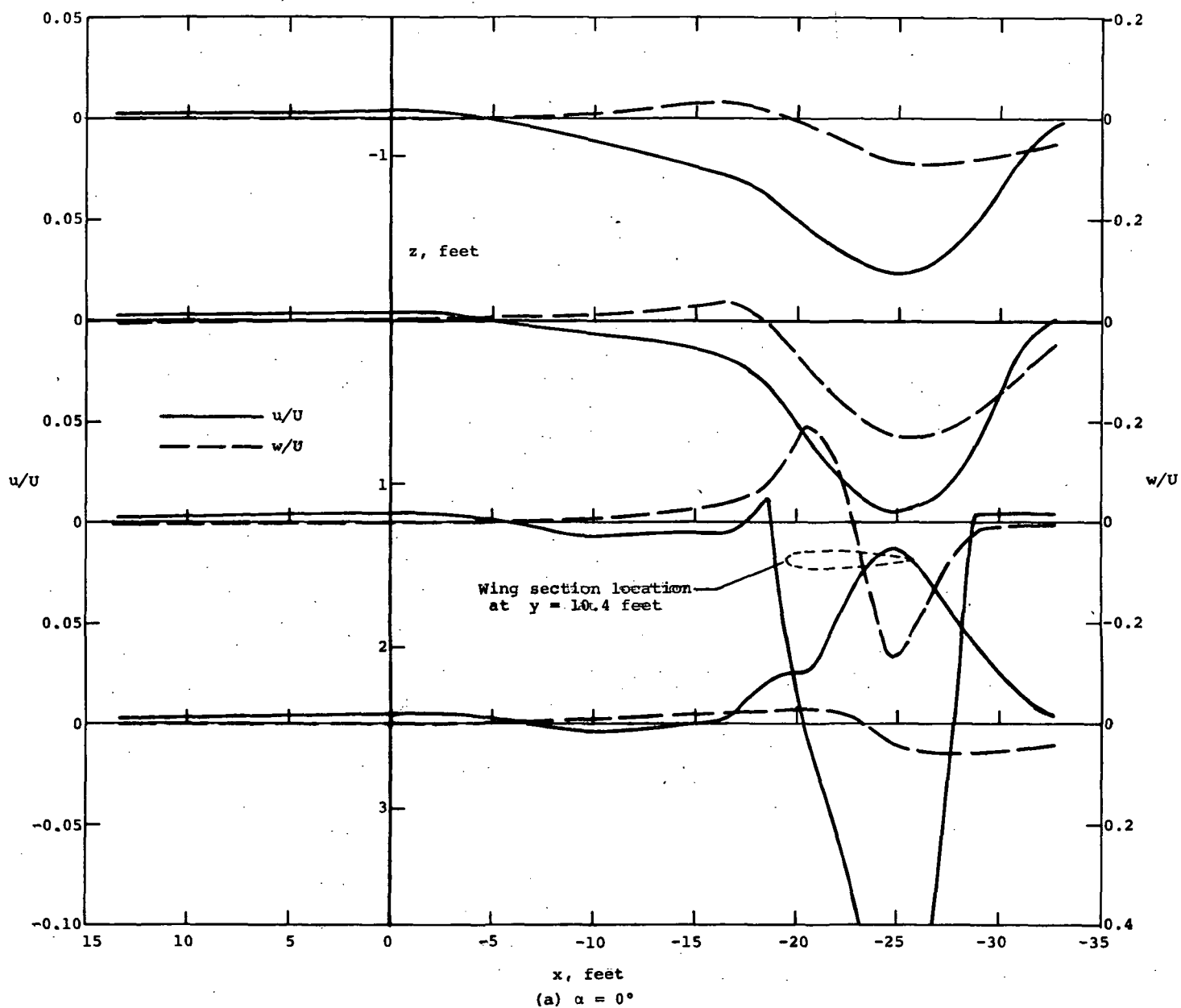
Figure 7.- Perturbation velocity components around the
forward portion of the Learjet in a vertical plane
10.25 feet outboard of the vertical plane of
symmetry (60 percent semispan).

x, feet
(b) α = 10°

Figure 7.- Concluded.

Wing section location
at y = 10.4 feet

u/U
w/U

73
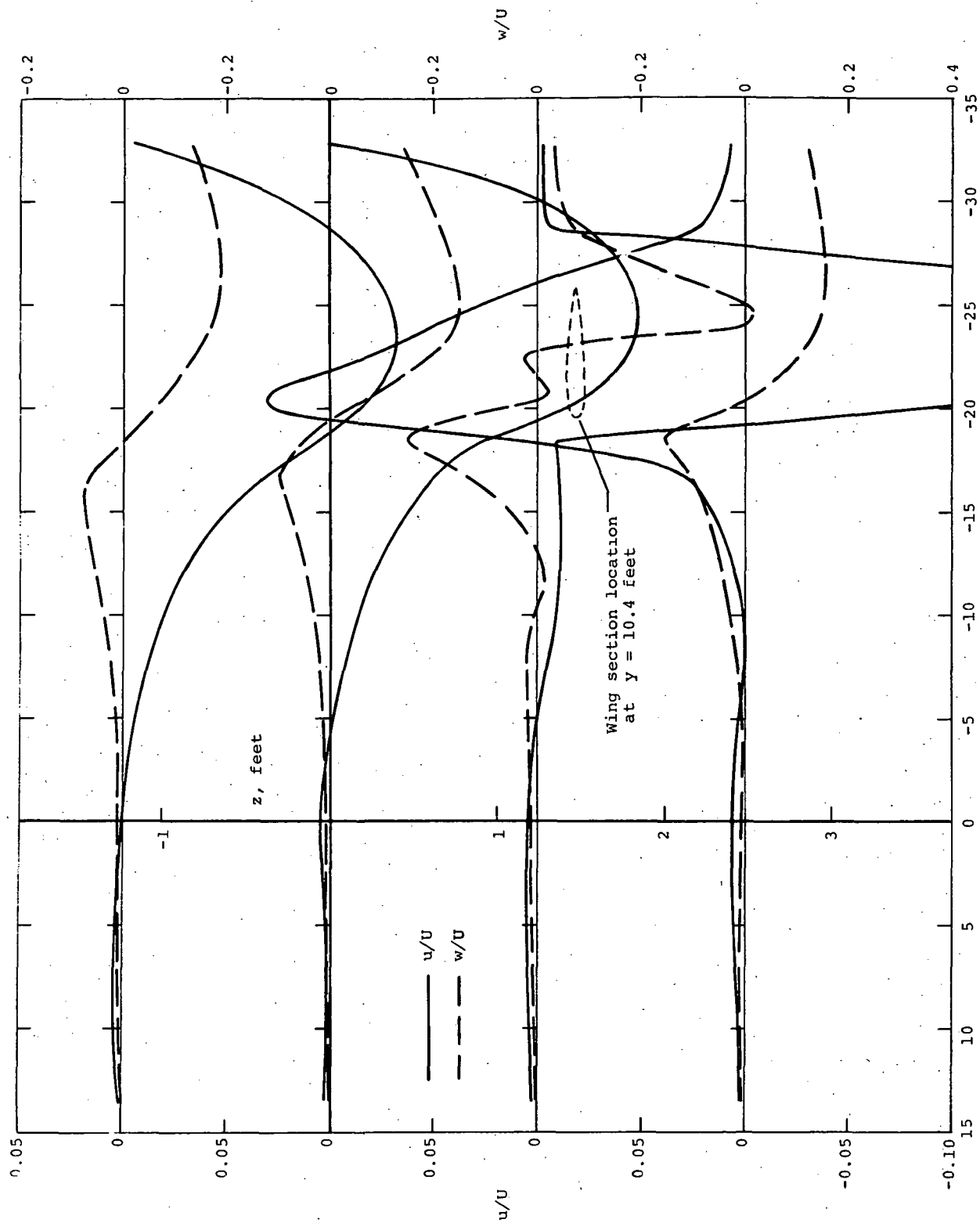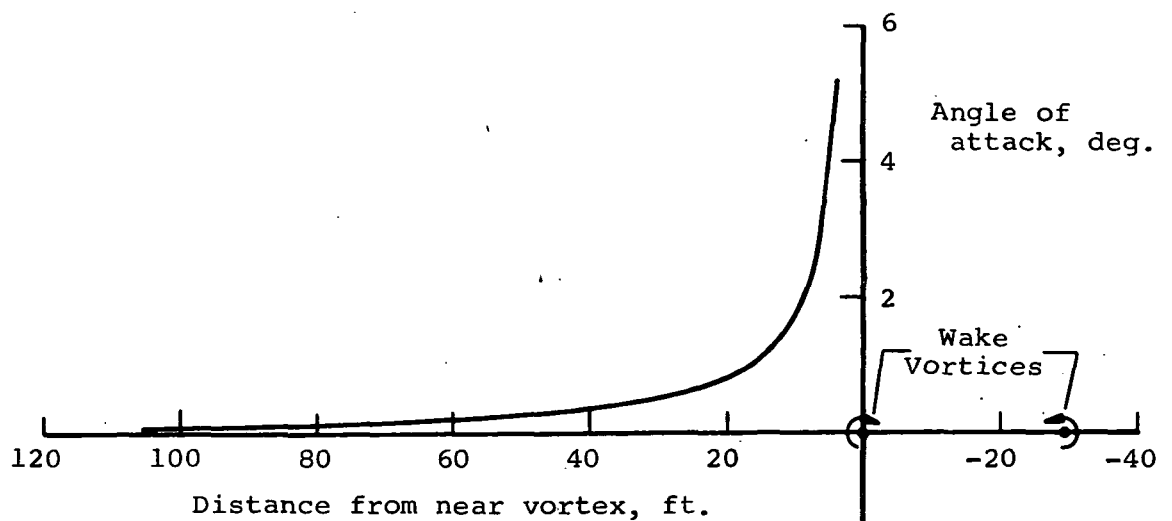
(a) Induced angle of attack.
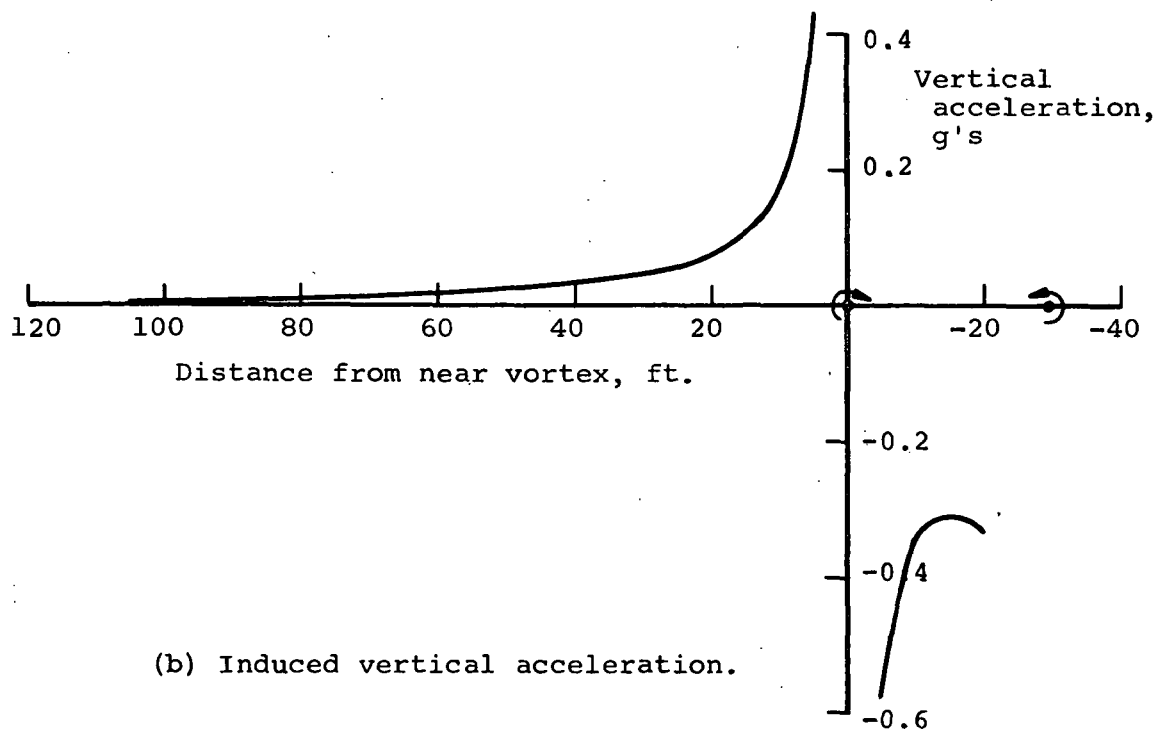
(b) Induced vertical acceleration.

Figure 8.- Angle of attack and vertical acceleration
induced on Learjet penetrating T-33 wake
at 300 ft/sec.
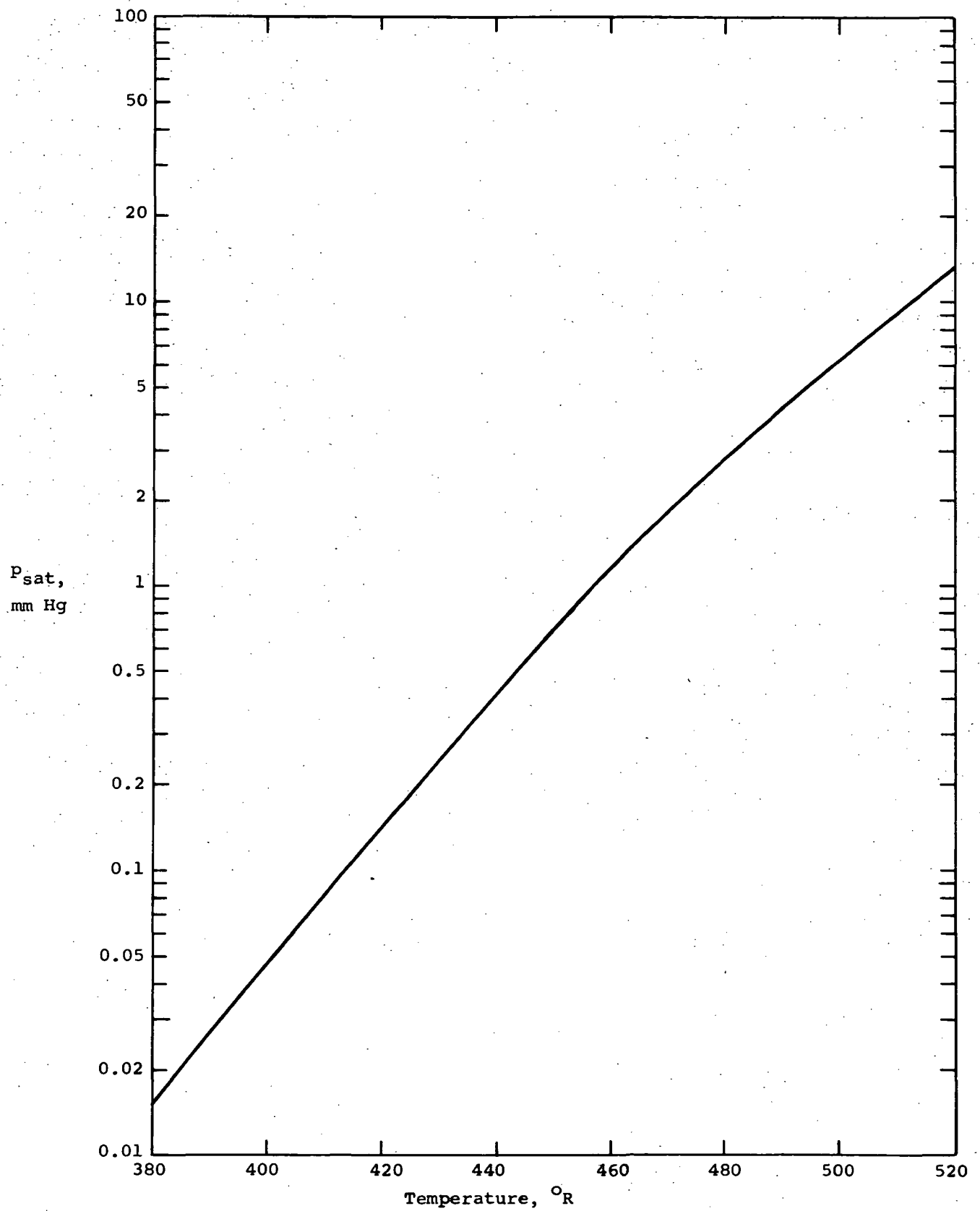
Figure 9.– Saturation pressure for water vapor
at low temperatures.
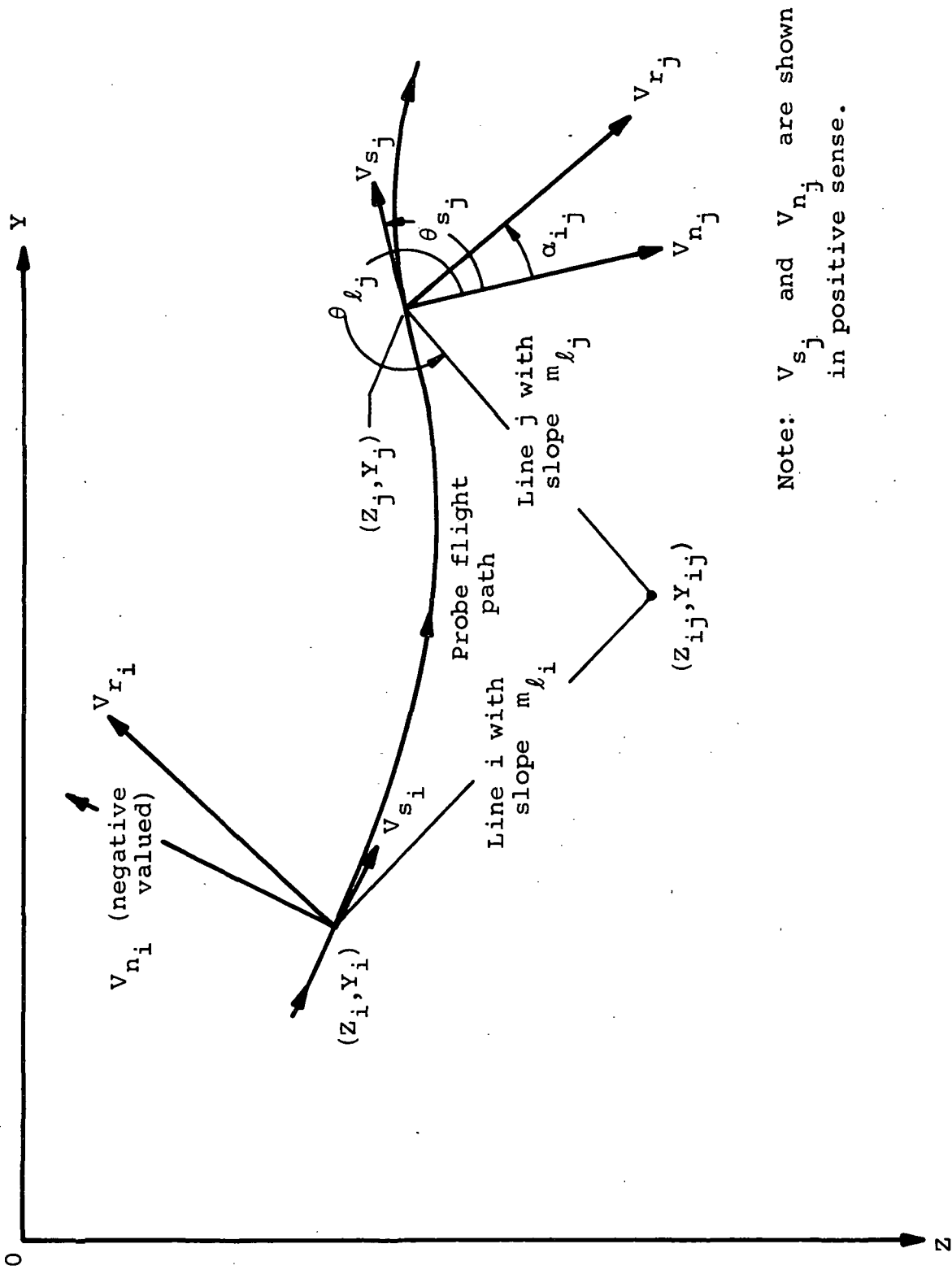
Figure 10.- Vortex crossflow plane coordinate system.

Figure 11.- Input format for trailing vortex crossflow program.

```
SAMPLE CASE, CIRCULAR VORTEX, 40X80 TUNNEL DATA,RUN 16,FILE 38,RECORD 23
 90.0        27.5        0.20        40      1
     1    0.0      1.85625    1.073     15.862
     2    0.0      1.86750   -0.205     15.131
     3    0.0      1.87875   -1.170     20.424
     4    0.0      1.890     -0.368     18.55899
     5    0.0      1.90125   -1.998     15.901
     6    0.0      1.91250   -0.498     21.21999
     7    0.0      1.92375   -1.880     25.77399
     8    0.0      1.93500   -3.678     29.97499
     9    0.0      1.94625   -3.105     27.76799
    10    0.0      1.95750   -3.830     32.81299
    11    0.0      1.96875   -5.043     39.37999
    12    0.0      1.980     -7.538     40.894
    13    0.0      1.99125  -11.493     49.23799
    14    0.0      2.0025   -17.69899   45.72400
    15    0.0      2.01375  -21.508     43.77599
    16    0.0      2.02500  -28.700     25.23099
    17    0.0      2.03625  -32.310     -2.357
    18    0.0      2.0475   -31.06799  -28.83299
    19    0.0      2.05875  -23.642    -43.63499
    20    0.0      2.070    -17.53999  -50.877
    21    0.0      2.08125   -9.3640   -51.750
    22    0.0      2.09250   -8.116    -47.42099
    23    0.0      2.10375   -4.774    -42.53799
    24    0.0      2.1150    -4.549    -36.670
    25    0.0      2.12625   -0.417    -34.06299
    26    0.0      2.13750   -0.211    -30.547
    27    0.0      2.14875   -0.883    -29.33199
    28    0.0      2.160     -0.425    -28.05399
    29    0.0      2.17125   00.367    -26.758
    30    0.0      2.1825     1.792    -24.489
    31    0.0      2.19375  -14.561    -26.64099
    32    0.0      2.205      4.087    -22.920
    33    0.0      2.21625    2.483    -21.39899
    34    0.0      2.2275     0.866    -19.51199
    35    0.0      2.23875    2.807    -18.92599
    36    0.0      2.25      -0.234    -18.713
    37    0.0      2.26125    2.2416   -20.04599
    38    0.0      2.27250    0.849    -15.956
    39    0.0      2.28375   -0.683    -15.74
    40    0.0      2.29500   -0.965    -13.279
```

Figure 12.- Listing of sample input.

SAMPLE CASE, CIRCULAR VORTEX, 40X80 TUNNEL DATA,RUN 16,FILE 38,RECORD 23

40 FIELD POINTS ARE SPECIFIED IN THE CROSS FLOW PLANE AT X=   27.50000   FT.
NOMINAL AXIAL VELOCITY IS   90.00000 FT/SEC

THIS ANALYSIS IS CONCERNED WITH RESULTANT VELOCITIES IN THE CROSS FLOW PLANE LARGER THAN   .20000 TIMES THE
AXIAL VELOCITY

	COORDINATES IN CROSS FLOW PLANE,FT		CROSS FLOW PERTURBATION VELOCITIES FROM EXPERIMENT,FT/SEC	
IF	Z	Y	COAXIAL	NORMAL
1	0.00000	1.85625	1.07300	15.86200
2	0.00000	1.86750	-.20500	15.13100
3	0.00000	1.87875	-1.17000	20.42400
4	0.00000	1.89000	-.36800	18.55899
5	0.00000	1.90125	-1.99800	15.90100
6	0.00000	1.91250	-.49800	21.21999
7	0.00000	1.92375	-1.88000	25.77399
8	0.00000	1.93500	-3.67800	29.97499
9	0.00000	1.94625	-3.10500	27.76799
10	0.00000	1.95750	-3.83000	32.81299
11	0.00000	1.96875	-5.04300	39.37999
12	0.00000	1.98000	-7.53800	40.89400
13	0.00000	1.99125	-11.49300	49.23799
14	0.00000	2.00250	-17.69899	45.72400
15	0.00000	2.01375	-21.50800	43.77599
16	0.00000	2.02500	-28.70000	25.23099
17	0.00000	2.03625	-32.31000	-2.35700
18	0.00000	2.04750	-31.06799	-28.83299
19	0.00000	2.05875	-23.64200	-43.63499
20	0.00000	2.07000	-17.53999	-50.87700
21	0.00000	2.08125	-9.36400	-51.75000
22	0.00000	2.09250	-8.11600	-47.42099
23	0.00000	2.10375	-4.77400	-42.53799
24	0.00000	2.11500	-4.54900	-36.67000
25	0.00000	2.12625	-.41700	-34.06299
26	0.00000	2.13750	-.21100	-30.54700
27	0.00000	2.14875	-.88300	-29.33199
28	0.00000	2.16000	-.42500	-28.05399
29	0.00000	2.17125	.36700	-26.75800
30	0.00000	2.18250	1.79200	-24.48900
31	0.00000	2.19375	-14.56100	-26.64099
32	0.00000	2.20500	4.08700	-22.92000
33	0.00000	2.21625	2.48300	-21.39899
34	0.00000	2.22750	.86600	-19.51199
35	0.00000	2.23875	2.80700	-18.92599
36	0.00000	2.25000	-.23400	-18.71300
37	0.00000	2.26125	2.24160	-20.04599
38	0.00000	2.27250	.84900	-15.95600
39	0.00000	2.28375	-.68300	-15.74000
40	0.00000	2.29500	-.96500	-13.27900

IN THIS VORTEX PENETRATION,THE PERTURBATION VELOCITY NORMAL TO THE PROBE FLIGHT PATH
HAS A MAXIMUM   49.23799 FT/SEC AT Z=   0.00000   FT.
                                          Y=   1.99125   FT.
AND A MINIMUM   -51.75000 FT/SEC AT Z=   0.00000   FT.
                                          Y=   2.08125   FT.

Figure 13.- Listing of sample output.

RESULTANT VELOCITIES WITH THE FIRST AND LAST LARGER THAN VMIN= 18.00000 FT/SEC AT THE INDICATED FIELD POINT COORDINATES AND SLOPES OF LINES NORMAL TO THE VELOCITY VECTORS

IF	IM	Z	Y	RESULT. VEL.,FT/SEC	THETAS,DEG.	THETAL,DEG.	SLOPEL
3	1	0.00000	1.87875	20.45748	90.00000	86.72136	17.45641
4	2	0.00000	1.89000	18.56264	90.00000	88.86405	50.43204
5	3	0.00000	1.90125	16.02604	90.00000	82.83818	7.95846
6	4	0.00000	1.91250	21.22583	90.00000	88.65560	42.61042
7	5	0.00000	1.92375	25.84246	90.00000	85.82813	13.70957
8	6	0.00000	1.93500	30.19980	90.00000	83.00464	8.14981
9	7	0.00000	1.94625	27.94105	90.00000	83.61972	8.94299
10	8	0.00000	1.95750	33.03576	90.00000	83.34244	8.56736
11	9	0.00000	1.96875	39.70158	90.00000	82.70242	7.80884
12	10	0.00000	1.98000	41.58294	90.00000	79.55589	5.42505
13	11	0.00000	1.99125	50.56153	90.00000	76.86141	4.28417
14	12	0.00000	2.00250	49.02997	90.00000	68.83942	2.58342
15	13	0.00000	2.01375	48.77429	90.00000	63.83421	2.03534
16	14	0.00000	2.02500	38.21378	90.00000	41.31963	.87913
17	15	0.00000	2.03625	-32.39586	90.00000	175.82769	-.07295
18	16	0.00000	2.04750	-42.38586	90.00000	137.13680	-.92806
19	17	0.00000	2.05875	-49.62818	90.00000	118.44941	-1.84566
20	18	0.00000	2.07000	-53.81561	90.00000	109.02178	-2.90063
21	19	0.00000	2.08125	-52.59037	90.00000	100.25651	-5.52648
22	20	0.00000	2.09250	-48.11050	90.00000	99.71195	-5.84290
23	21	0.00000	2.10375	-42.80504	90.00000	96.40346	-8.91035
24	22	0.00000	2.11500	-36.95108	90.00000	97.07155	-8.06111
25	23	0.00000	2.12625	-34.06554	90.00000	90.70138	-81.68583
26	24	0.00000	2.13750	-30.54773	90.00000	90.39576	-144.77251
27	25	0.00000	2.14875	-29.34528	90.00000	91.72429	-33.21856
28	26	0.00000	2.16000	-28.05721	90.00000	90.86793	-66.00939
29	27	0.00000	2.17125	-26.76052	90.00000	89.21421	72.91008
30	28	0.00000	2.18250	-24.55448	90.00000	85.81480	13.66574
31	29	0.00000	2.19375	-30.36058	90.00000	118.65942	-1.82961
32	30	0.00000	2.20500	-23.28154	90.00000	79.88952	5.60803
33	31	0.00000	2.21625	-21.54256	90.00000	83.38137	8.61820
34	32	0.00000	2.22750	-19.53120	90.00000	87.45871	22.53117
35	33	0.00000	2.23875	-19.13302	90.00000	81.56370	6.74243
36	34	0.00000	2.25000	-18.71446	90.00000	90.71643	-79.97009
37	35	0.00000	2.26125	-20.17093	90.00000	83.61953	8.94272

ABOVE TABULATION HAS STOPPED AT IF= 38

THIS FLOWFIELD ACCOUNT STARTS AT DATA POINT NUMBER IF= 3
WITH FIELD POINT COORDINATES IN THE CROSS FLOW PLANE Z= 0.00000 FT.
                                                      Y= 1.87875 FT.
THE LAST DATA POINT NUMBER INCLUDED IN THIS ACCOUNT IS IF= 37
WITH FIELD POINT COORDINATES IN THE CROSS FLOW PLANE Z= 0.00000 FT.
                                                      Y= 2.26125 FT.

Figure 13.- Continued.

COORDINATES OF THE POINTS OF INTERSECTION OF THE LINES CONSTRUCTED AT POINTS (ZFP,YFP) NORMAL TO THE
RESULTANT VELOCITY VECTORS AT THOSE POINTS

IL	JL	IN	JN	ZC,FT.	YC,FT.
3	4	1	2	-3.41161E-04	1.87279E+00
3	5	1	3	2.36895E-03	1.92010E+00
3	6	1	4	-1.34173E-03	1.85553E+00
3	7	1	5	1.21010E-02	2.08840E+00
3	8	1	6	6.04410E-03	1.98428E+00
3	9	1	7	7.92866E-03	2.01716E+00
3	10	1	8	8.85921E-03	2.03340E+00
3	11	1	9	9.32878E-03	2.04160E+00
3	12	1	10	8.41550E-03	2.02565E+00
3	13	1	11	8.54069E-03	2.02784E+00
3	14	1	12	8.32045E-03	2.02400E+00
3	15	1	13	8.75425E-03	2.03157E+00
3	16	1	14	8.82231E-03	2.03276E+00
3	17	1	15	8.98493E-03	2.03559E+00
3	18	1	16	9.17894E-03	2.03898E+00
3	19	1	17	9.32543E-03	2.04154E+00
3	20	1	18	9.39478E-03	2.04275E+00
3	21	1	19	8.81090E-03	2.03256E+00
3	22	1	20	9.32543E-03	2.03898E+00
3	23	1	21	9.39478E-03	2.04275E+00
3	24	1	22	9.25834E-03	2.04037E+00
3	25	1	23	2.49641E-03	1.90659E+00
3	26	1	24	1.55497E-03	1.93757E+00
3	27	1	25	5.32807E-03	1.78667E+00
3	28	1	26	3.36964E-03	3.27755E+00
3	29	1	27	-5.27467E-03	2.16387E+00
3	30	1	28	8.01309E-02	2.35942E+00
3	31	1	29	1.63331E-02	2.54535E+00
3	32	1	30	2.75356E-02	6.79102E-01
3	33	1	31	3.81865E-02	1.94527E+00
3	34	1	32	-6.87225E-02	2.66302E+00
3	35	1	33	3.36964E-02	1.90336E+00
3	36	1	34	2.64871E-04	2.46530E+00
3	37	1	35	3.81057E-03	2.03507E+00
4	5	2	3	2.87664E-03	1.93635E+00
4	6	2	4	9.19058E-04	1.94367E+00
4	7	2	5	1.06428E-03	1.95837E+00
4	8	2	6	1.35570E-03	1.97131E+00
4	9	2	7	1.61234E-03	1.98318E+00
4	10	2	8	1.04759E-03	1.99085E+00
4	11	2	9	1.99960E-03	2.00065E+00
4	12	2	10	2.19403E-03	2.00657E+00
4	13	2	11	2.35117E-03	2.01895E+00
4	14	2	12	2.55699E-03	2.01895E+00
4	15	2	13	2.72436E-03	2.02740E+00
4	16	2	14	2.89575E-03	2.03604E+00
4	17	2	15	3.06658E-03	2.04465E+00
4	18	2	16	3.22795E-03	2.05279E+00
4	19	2	17	3.37504E-03	2.06021E+00
4	20	2	18	3.41771E-03	2.06236E+00
4	21	2	19	3.59840E-03	2.07147E+00
4	22	2	20	3.60198E-03	2.07166E+00
4	23	2	21	3.84660E-03	2.08399E+00
4	24	2	22	1.78810E-03	1.98018E+00
4	25	2	23	1.26790E-03	1.95394E+00
4	26	2	24	3.09322E-03	2.04600E+00
4	27	2	25	3.06658E-03	2.00694E+00
4	28	2	26	-1.25122E-02	1.25899E+00
4	29	2	27	7.95565E-03	2.29122E+00
4	30	2	28	7.02748E-03	2.18312E+00
4	31	2	29	7.80244E-03	2.24441E+00
4	32	2	30	1.20966E-02	2.28369E+00
4	33	2	31	7.98245E-03	2.50005E+00
4	34	2	32	2.76069E-03	2.29423E+00
4	35	2	33	8.94809E-03	2.02923E+00
4	36	2	34		2.34127E+00
4	37	2	35		

IL	JL	IN	JN		
3	6	5	4	-3.24657E-04	1.89857E+00
3	7	5	5	-3.91229E-03	1.87011E+00
3	8	5	6	-1.76380E-01	4.97539E-01
3	9	5	7	-4.57069E-02	1.53749E-01
3	10	5	8	-9.23794E-02	1.16605E+00
3	11	5	9	4.51153E-01	5.49174E+00
3	12	5	10	3.10846E-02	2.14864E+00
3	13	5	11	2.44946E-02	2.09619E+00
3	14	5	12	1.68371E-02	2.05116E+00
3	15	5	13	1.09934E-02	2.05241E+00
3	16	5	14	1.74805E-02	2.04037E+00
3	17	5	15	1.68090E-02	2.03502E+00
3	18	5	16	1.64575E-02	2.03223E+00
3	19	5	17	1.55400E-02	2.02492E+00
3	20	5	18	1.33482E-02	2.02910E+00
3	21	5	19	1.33431E-02	2.00768E+00
3	22	5	20	1.35753E-02	2.00155E+00
3	23	5	21	1.20046E-02	1.99679E+00
3	24	5	22	1.33431E-02	2.00744E+00
3	25	5	23	2.50925E-03	1.92123E+00
3	26	5	24	1.54686E-03	1.91356E+00
3	27	5	25	6.01063E-03	1.94909E+00
3	28	5	26	3.49814E-03	1.92909E+00
3	29	5	27	-4.15694E-03	1.86817E+00
3	30	5	28	-4.92792E-02	1.50906E+00
3	31	5	29	2.98833E-02	2.13908E+00
3	32	5	30	1.29232E-01	2.92973E+00
3	33	5	31	-4.77460E-01	-1.09859E+00
3	34	5	32	-2.23877E-02	1.72308E+00
3	35	5	33	2.77542E-01	4.11006E+00
3	36	5	34	3.96629E-03	1.93282E+00
3	37	5	35	3.65758E-01	-1.00962E+00
4	8	5	6	3.89622E-04	1.92909E+00
4	9	6	7	6.52919E-04	1.94032E+00
4	10	6	8	1.81523E-03	1.95521E+00
4	11	6	9	1.32186E-03	1.96682E+00
4	12	6	10	1.61631E-03	1.98137E+00
4	13	6	11	1.81523E-03	1.98985E+00
4	14	6	12	2.05473E-03	2.00005E+00
4	15	6	13	2.24868E-03	2.00831E+00
4	16	6	14	2.49537E-03	2.01883E+00
4	17	6	15	2.69582E-03	2.02737E+00
4	18	6	16	2.89926E-03	2.03604E+00
4	19	6	17	3.10071E-03	2.04462E+00
4	20	6	18	3.28976E-03	2.05268E+00
4	21	6	19	3.46070E-03	2.05996E+00
4	22	6	20	3.50563E-03	2.06188E+00
4	23	6	21	3.71472E-03	2.07079E+00
4	24	6	22	3.71210E-03	2.07061E+00
4	25	6	23	3.99633E-03	2.08279E+00
4	26	6	24	1.71968E-03	1.98578E+00
4	27	6	25	1.20075E-03	1.96366E+00
4	28	6	26	3.11556E-03	2.04526E+00
4	29	6	27	2.27859E-03	2.00959E+00
4	30	6	28	-8.53970E-03	1.54862E+00
4	31	6	29	6.32814E-03	2.30998E+00
4	32	6	30	6.32875E-03	2.18217E+00
4	33	6	31	7.90469E-03	2.24933E+00
4	34	6	32	8.93587E-03	2.29326E+00
4	35	6	33	1.56878E-02	2.58097E+00
4	36	6	34	9.09585E-03	2.30008E+00
4	37	6	35	2.75329E-03	2.02982E+00
5	8	7	36	1.03586E-02	2.35388E+00
5	9	7	37	-4.02347E-03	1.95149E+00
5	10	7	8	-4.72037E-03	1.98846E+00
5	11	7	9	6.56333E-03	2.01373E+00
5		7	10	7.62618E-03	2.02830E+00

Figure 13.- Continued.

81

Figure 13.- Continued.

The following data are printed in a rotated listing of numeric columns. Each data block lists a mode-group index, a point index, and two floating-point values.

Left data block

group	index	value 1	value 2
5	10	2.01683E+00	6.78977E-03
5	11	2.02193E+00	7.16150E-03
5	12	2.02079E+00	7.07792E-03
5	13	2.02944E+00	7.70929E-03
5	14	2.03194E+00	7.89139E-03
5	15	2.03565E+00	8.16251E-03
5	16	2.03965E+00	8.45424E-03
5	17	2.04273E+00	8.67876E-03
5	18	2.04446E+00	8.80483E-03
5	19	2.03600E+00	8.18775E-03
5	20	2.04207E+00	8.63062E-03
5	21	2.03285E+00	7.95759E-03
5	22	2.04419E+00	8.78475E-03
5	23	1.95285E+00	2.12274E-03
5	24	1.94224E+00	1.34873E-03
5	25	1.98948E+00	4.79457E-03
5	26	1.96438E+00	2.96354E-03
5	27	1.86643E+00	-4.18071E-03
5	28	6.28534E+01	5.90315E+00
5	29	1.96354E+00	1.73756E-02
5	30	2.39969E+00	3.47156E-02
5	31	2.71137E+00	5.74502E-02
5	32	1.45169E+00	-3.44325E-02
5	33	2.54359E+00	4.52122E-02
5	34	1.97150E+00	3.48261E-02
5	35	2.89461E+00	7.08014E-02
6	7	1.81941E+00	-1.41833E-02
6	8	1.49584E+00	-5.38855E-02
6	9	2.74170E+00	9.89838E-02
6	10	2.06960E+00	1.65192E-02
6	11	2.05359E+00	1.45513E-02
6	12	2.03383E+00	1.21264E-02
6	13	2.03996E+00	1.28793E-02
6	14	2.03535E+00	1.23134E-02
6	15	2.03600E+00	1.23928E-02
6	16	2.03590E+00	1.23806E-02
6	17	2.03456E+00	1.22167E-02
6	18	2.02215E+00	1.06937E-02
6	19	2.02673E+00	1.12559E-02
6	20	2.01561E+00	9.89147E-03
6	21	2.02549E+00	1.11036E-02
6	22	1.95235E+00	2.12869E-03
6	23	1.94579E+00	1.32420E-02
6	24	1.97711E+00	5.16699E-03
6	25	1.95973E+00	3.03401E-02
6	26	1.90527E+00	-3.64807E-02
6	27	1.56932E+00	-4.48700E-02
6	28	2.14631E+00	2.59284E-02
6	29	2.80071E+00	1.06225E-01
6	30	2.95861E+00	-6.00458E-01
6	31	1.76924E+00	-2.03388E-02
6	32	3.69394E+00	2.15826E-01
6	33	1.96413E+00	3.57468E-01
6	34	-1.41832E+00	-4.11460E-01
6	35	2.21409E+00	2.99496E-02
7	8	2.12367E+00	1.98386E-02
7	9	2.03205E+00	9.65910E-03
7	10	2.03263E+00	8.84494E-03
7	11	2.03364E+00	9.77177E-03
7	12	2.03359E+00	9.76579E-03
7	13	2.03552E+00	9.98232E-03
7	14	2.03798E+00	1.02573E-02
7	15	2.03950E+00	1.04276E-02
7	16	2.02969E+00	1.04876E-02
7	17	2.02969E+00	9.32999E-03
7	18	2.03471E+00	9.89118E-03
7	19	2.02514E+00	8.82188E-03
7	20	2.03520E+00	9.92407E-03
7	21	1.96401E+00	1.98612E-03

Right data block

group	index	value 1	value 2
7	24	1.95738E+00	1.24418E-03
7	25	1.98920E+00	4.80295E-03
7	26	1.97175E+00	2.85181E-03
7	27	1.91479E+00	-3.51743E-03
7	28	1.49889E+00	-5.00239E-02
7	29	2.64011E+00	-2.29749E-02
7	30	9.38057E+00	7.75870E-02
7	31	1.76115E+00	8.31301E-01
7	32	-2.06981E-02	-2.06981E-02
7	33	1.32920E-01	1.32920E-01
7	34	3.14496E+00	3.41626E-03
7	35	1.97680E+00	1.13750E+03
8	9	1.01766E+04	1.48315E-02
8	10	2.08457E+00	7.16033E-03
8	11	2.01885E+00	7.87964E-03
8	12	2.02501E+00	7.52013E-03
8	13	2.02193E+00	8.61142E-03
8	14	2.03128E+00	8.77965E-03
8	15	2.03272E+00	9.11426E-03
8	16	2.03559E+00	9.47825E-03
8	17	2.04080E+00	9.72341E-03
8	18	2.04155E+00	9.80992E-03
8	19	2.03223E+00	8.78043E-03
8	20	2.02919E+00	9.36832E-03
8	21	2.03776E+00	8.36780E-03
8	22	2.03865E+00	9.47171E-03
8	23	1.97352E+00	1.86974E-03
8	24	1.96756E+00	1.17386E-03
8	25	1.99671E+00	4.57690E-03
8	26	1.98076E+00	-2.71532E-03
8	27	1.92904E+00	-3.32205E-03
8	28	1.57941E+00	-4.41317E-02
8	29	2.15218E+00	8.36337E-02
8	30	2.67402E+00	-5.08955E+00
8	31	-4.16465E+01	-1.93357E-02
8	32	1.79184E+00	1.54115E-01
8	33	3.27786E+00	3.30369E-03
8	34	-4.97550E+00	-8.09235E-01
9	10	2.00560E+00	4.71936E-03
9	11	2.01919E+00	6.38358E-03
9	12	2.02961E+00	7.79422E-03
9	13	2.02214E+00	8.11722E-03
9	14	2.03563E+00	8.56404E-03
9	15	2.03913E+00	9.01349E-03
9	16	2.04154E+00	9.45425E-03
9	17	2.04258E+00	8.43624E-03
9	18	2.03463E+00	9.06478E-03
9	19	2.03954E+00	8.07456E-03
9	20	2.03180E+00	9.21553E-03
9	21	2.04071E+00	1.75988E-03
9	22	1.98249E+00	1.10597E-03
9	23	1.97739E+00	4.38731E-03
9	24	2.00301E+00	2.59082E-03
9	25	1.98898E+00	-3.11054E-03
9	26	1.94446E+00	-3.64954E-02
9	27	1.68376E+00	2.33440E-02
9	28	2.15104E+00	1.07367E+00
9	29	2.80700E+00	-3.05798E-01
9	30	-4.19178E-01	-1.75753E-02
9	31	1.83151E+00	3.20407E-03
9	32	3.94583E+00	-2.57965E-01
9	33	1.99377E+00	7.91801E-03
10	13	-4.56609E-02	9.95660E-03
10	14	2.03550E+00	9.89899E-03
10	15	2.03550E+00	1.02310E-02
10	16	2.03764E+00	1.06247E-02

Left block

i	j	value 1	value 2
12	19	1.08311E-02	2.03876E+00
12	20	1.08099E-02	2.03864E+00
12	21	9.24528E-03	2.03016E+00
12	22	9.98407E-03	2.03416E+00
12	23	8.63248E-03	2.02683E+00
12	24	1.00103E-02	2.03431E+00
12	25	1.67889E-03	1.98911E+00
12	26	1.04862E-03	1.98569E+00
12	27	4.36663E-03	2.00369E+00
12	28	2.51979E-03	1.99367E+00
12	29	-2.83396E-03	1.96463E+00
12	30	2.94633E-02	1.84669E+00
12	31	-2.45732E-02	2.13984E+00
12	32	-1.22965E+00	-4.69090E+00
12	33	-7.39864E-02	1.57862E-01
12	34	-1.44685E-02	1.90151E+00
12	35	-1.96413E-01	9.14452E-01
12	36	3.16177E-03	1.99715E+00
12	37	-7.99535E-02	1.54625E+00
13	15	6.61474E-03	2.01959E+00
13	16	1.00050E-02	2.03411E+00
13	17	9.91177E-03	2.03371E+00
13	18	-1.03279E-02	2.03550E+00
13	19	1.07919E-02	2.03768E+00
13	20	1.10117E-02	2.03843E+00
13	21	1.09606E-02	2.03821E+00
13	22	9.17370E-03	2.03055E+00
13	23	9.99795E-03	2.03408E+00
13	24	8.52627E-03	2.02778E+00
13	25	1.57032E-03	1.99798E+00
13	26	9.81170E-04	1.99545E+00
13	27	4.19966E-03	2.00153E+00
13	28	-2.40065E-03	1.98001E+00
13	29	-2.62292E-03	1.90391E+00
13	30	-2.03857E-02	2.13315E+00
13	31	-3.31219E-02	1.76884E+00
13	32	-1.61460E-01	1.55991E+00
13	33	-5.19148E-02	1.74295E+00
13	34	-1.29473E-02	2.05553E+00
13	35	-1.00681E-02	2.03661E+00
13	36	-3.07106E-02	2.03532E+00
13	37	-5.79580E-02	2.03561E+00
14	15	2.05259E-02	2.03531E+00
14	16	1.32010E-02	2.03630E+00
14	17	-1.27053E-02	2.02759E+00
14	18	1.28151E-02	2.03009E+00
14	19	1.27002E-02	2.02526E+00
14	20	1.23084E-02	2.02980E+00
14	21	9.71034E-03	2.00629E+00
14	22	1.06808E-02	2.00487E+00
14	23	8.80912E-03	2.01305E+00
14	24	1.05688E-03	1.99030E+00
14	25	1.46851E-03	1.96054E+00
14	26	9.16149E-04	1.82954E+00
14	27	4.33375E-02	1.91100E+00
14	28	-6.69510E-02	1.97336E+00
14	29	-3.54197E-02	1.85575E+00
14	30	-1.12795E-02	2.01025E+00
14	31	-5.68045E-02	1.89738E+00
14	32	-2.99806E-03	2.03355E+00
14	33	-4.06885E-02	2.03547E+00
14	34	9.73009E-03	2.03693E+00
14	35	-1.06722E-02	2.03735E+00
15	18	1.13890E-02	2.03694E+00
15	19	1.15950E-02	2.03935E+00
15	20	1.13960E-02	2.03994E+00

Right block

i	j	value 1	value 2
15	21	8.92642E-03	2.03192E+00
15	22	9.99589E-03	2.03439E+00
15	23	8.22242E-03	2.03049E+00
15	24	1.00283E-02	2.03416E+00
15	25	1.34375E-03	2.01648E+00
15	26	8.42939E-04	2.01547E+00
15	27	2.14932E-03	2.02154E+00
15	28	2.22223E-03	2.01812E+00
15	29	-1.45094E-02	2.00923E+00
15	30	4.65724E-02	1.98422E+00
15	31	-5.35311E-02	2.10854E+00
15	32	-3.07617E-02	1.90480E+00
15	33	-1.04290E-02	1.99252E+00
15	34	-4.78002E-02	1.91646E+00
15	35	2.88091E-03	2.01961E+00
15	36	-3.58112E-02	1.95114E+00
15	37	1.18163E-02	1.94082E+00
16	18	1.24503E-02	2.03595E+00
16	19	1.23863E-02	2.03589E+00
16	20	1.19055E-02	2.03547E+00
16	21	8.78136E-03	2.03277E+00
16	22	1.04416E-02	2.03383E+00
16	23	8.04635E-03	2.03207E+00
16	24	1.00668E-02	2.03385E+00
16	25	1.22631E-03	2.02606E+00
16	26	7.72591E-04	2.02568E+00
16	27	3.62928E-03	2.02819E+00
16	28	2.01828E-03	2.02677E+00
16	29	-2.03038E-03	2.02322E+00
16	30	-1.23176E-02	2.01417E+00
16	31	6.22983E-02	2.07977E+00
16	32	-2.47123E-03	1.99154E+00
16	33	-9.35247E-03	2.01678E+00
16	34	-3.66556E-02	1.99295E+00
16	35	-2.92984E-02	1.99924E+00
17	17	1.31562E-02	2.03529E+00
17	18	1.26925E-02	2.03538E+00
17	19	1.19356E-02	2.03565E+00
17	20	8.25153E-03	2.03569E+00
17	21	9.74078E-03	2.03553E+00
17	22	9.85834E-03	2.03617E+00
17	23	1.10277E-02	2.03620E+00
17	24	6.99726E-03	2.03600E+00
17	25	3.39411E-03	2.03611E+00
17	26	1.87681E-03	2.03638E+00
17	27	-1.84975E-03	2.03703E+00
17	28	-1.06451E-02	2.02971E+00
17	29	8.96566E-02	2.03842E+00
17	30	-2.97044E-02	2.03776E+00
17	31	-2.07107E-02	2.03687E+00
18	17	-8.46085E-03	2.03605E+00
18	18	-2.97122E-02	2.03877E+00
18	19	2.67531E-03	2.03812E+00
18	20	-2.49566E-02	2.03691E+00
18	21	1.22603E-02	2.04069E+00
18	22	1.14065E-02	2.03990E+00
18	23	7.33947E-03	2.04096E+00
18	24	9.15594E-03	2.03872E+00
18	25	7.04685E-03	2.04460E+00
18	26	9.46299E-03	2.04692E+00
18	27	9.75138E-04	2.04459E+00
18	28	6.25676E-04	2.04590E+00
18	29	3.13560E-03	2.04906E+00
18	30	1.72861E-03	2.05609E+00
18	31	-1.67596E-03	1.89695E+00
18	32	-9.25051E-03	
18	33	1.62220E-01	

Figure 13.- Continued.

83

Table — Figure 13 (continued). Numerical data listing.

Value	Value	i	j	k	l	Value	Value	i	j	k	l
2.22179E+00	-1.32472E-02	22	21	24	23	2.06986E+00	-2.40970E-02	30	16	32	18
2.10130E+00	3.09170E-04	23	21	25	23	2.06391E+00	-1.76771E-02	31	16	33	18
2.10154E+00	2.48414E-04	24	21	26	23	2.05462E+00	-7.67289E-03	32	16	34	18
2.08725E+00	1.85123E-03	25	21	27	23	2.07064E+00	-2.49332E-02	33	16	35	18
2.09497E+00	9.85130E-04	26	21	28	23	2.04512E+00	-2.56193E-03	34	16	36	18
2.11110E+00	-8.24977E-04	27	21	29	23	2.06760E+00	-2.16548E-02	35	16	37	18
2.13483E+00	-3.48206E-03	28	21	30	23	2.03907E+00	1.06638E-02	18	17	20	19
2.21701E+00	-1.27105E-02	29	21	31	23	2.04747E+00	6.11275E-03	19	17	21	19
2.16589E+00	-6.97392E-03	30	21	32	23	2.04311E+00	8.44311E-03	20	17	22	19
2.16094E+00	-6.41810E-03	31	21	33	23	2.04699E+00	6.36971E-03	21	17	23	19
2.13882E+00	-3.93588E-03	32	21	34	23	2.04295E+00	9.05002E-03	22	17	24	19
2.18060E+00	-8.62467E-03	33	21	35	23	2.05719E+00	8.45439E-03	23	17	25	19
2.08541E+00	2.05813E-03	34	21	36	23	2.05773E+00	5.50981E-03	24	17	26	19
2.18236E+00	-8.82202E-03	35	21	37	23	2.05346E+00	2.86872E-03	25	17	27	19
2.11377E+00	1.52802E-04	23	22	25	24	2.05584E+00	-1.57799E-03	26	17	28	19
2.11367E+00	1.64580E-04	24	22	26	24	2.06153E+00	-1.50490E-03	27	17	29	19
2.10419E+00	1.34155E-03	25	22	27	24	2.07367E+00	-7.97801E-01	28	17	30	19
2.10874E+00	7.76555E-04	26	22	28	24	1.75898E+01	-8.41491E+00	29	17	31	19
2.12060E+00	-6.94691E-04	27	22	29	24	2.09496E+00	-1.96212E-02	30	17	32	19
2.14004E+00	-3.10676E-03	28	22	30	24	2.08653E+00	-1.50508E-02	31	17	33	19
2.21687E+00	-1.26374E-02	29	22	31	24	2.07153E+00	-6.92256E-03	32	17	34	19
2.16608E+00	-6.58418E-03	30	22	32	24	2.09743E+00	-2.09593E-02	33	17	35	19
2.16393E+00	-6.07039E-03	31	22	33	24	2.05423E+00	-2.44802E-03	34	17	36	19
2.14464E+00	-3.67740E-03	32	22	34	24	2.09339E+00	-1.87702E-02	35	17	37	19
2.18239E+00	-8.35949E-03	33	22	35	24	2.05757E+00	4.28432E-03	19	18	21	20
2.09987E+00	1.87737E-03	24	22	36	24	2.04782E+00	7.06715E-03	20	18	22	20
2.18433E+00	-8.60100E-03	35	22	37	24	2.05371E+00	5.61591E-03	21	18	23	20
2.11168E+00	1.78326E-04	24	23	26	25	2.04471E+00	8.72011E-03	22	18	24	20
2.16417E+00	-4.64231E-04	25	23	27	25	2.06793E+00	7.13967E-04	23	18	25	20
2.30211E+00	-2.15291E-03	26	23	28	25	2.06862E+00	4.75781E-04	24	18	26	20
2.15003E+00	-2.91081E-03	27	23	29	25	2.06247E+00	2.59747E-03	25	18	27	20
2.17444E+00	-5.89922E-04	28	23	30	25	2.06586E+00	1.42611E-02	26	18	28	20
2.19530E+00	-8.45269E-04	29	23	31	25	2.07387E+00	-1.33556E-03	27	18	29	20
2.19994E+00	-9.02125E-04	30	23	32	25	2.08970E+00	-6.79087E-03	28	18	30	20
2.20766E+00	-9.96633E-04	31	23	33	25	2.40515E+00	-1.15544E-01	29	18	31	20
2.20561E+00	-9.71531E-04	32	23	34	25	2.11602E+00	-1.58662E-02	30	18	32	20
2.23017E+00	-1.27222E-03	33	23	35	25	2.10683E+00	-1.26966E-02	31	18	33	20
8.01794E+00	-7.21262E-02	34	23	36	25	2.08796E+00	-6.19304E-03	32	18	34	20
2.24793E+00	-1.48960E-03	35	23	37	25	2.06323E+00	-2.33556E-03	33	18	35	20
2.15210E+00	-1.00848E-04	25	24	27	26	2.11684E+00	-1.61483E-02	34	18	36	20
2.17866E+00	-2.85667E-04	26	24	28	26	1.88476E+00	3.55543E-03	35	18	37	20
2.15995E+00	-1.55042E-04	27	24	29	26	2.04450E+00	6.64921E-03	20	19	22	21
2.17862E+00	-2.84022E-04	28	24	30	26	2.00766E+00	5.90868E-04	21	19	23	21
2.19467E+00	-3.93516E-04	29	24	31	26	2.07798E+00	4.03961E-04	22	19	24	21
2.20248E+00	-4.48861E-04	30	24	32	26	2.07902E+00	1.30202E-03	23	19	25	21
2.21133E+00	-5.13395E-04	31	24	33	26	2.06778E+00	2.43752E-03	24	19	26	21
2.22424E+00	-6.68251E-04	32	24	34	26	2.07405E+00	-1.14742E-03	25	19	27	21
2.30883E+00	-1.73605E-03	33	24	35	26	2.08759E+00	-5.25557E-03	26	19	28	21
2.25405E+00	-8.05060E-04	34	24	36	26	2.11041E+00	-3.04311E-02	27	19	29	21
2.13735E+00	3.63086E-04	26	25	28	27	2.24943E+00	-1.11141E-02	28	19	30	21
2.15579E+00	-2.12007E-04	27	25	29	27	2.14267E+00	-9.54422E-04	29	19	31	21
2.17266E+00	-7.19857E-04	28	25	30	27	2.11006E+00	-5.21248E-03	30	19	32	21
2.19637E+00	-1.43363E-03	29	25	31	27	2.13400E+00	-1.12189E-03	31	19	33	21
2.19688E+00	-1.44875E-03	30	25	32	27	2.15220E+00	-9.99962E-04	32	19	34	21
2.20235E+00	-1.61341E-03	31	25	33	27	2.06872E+00	-1.24402E-02	33	19	35	21
2.19567E+00	-1.41256E-03	32	25	34	27	2.15000E+00	3.66755E-03	34	19	36	21
2.22995E+00	-2.25220E-03	33	25	35	27	2.07107E+00	1.01433E-02	35	19	37	21
2.07681E+00	-2.16570E-04	26	26	28	28	2.03323E+00	4.44999E-04	21	20	23	22
2.23739E+00	-2.66835E-03	27	26	29	28	2.08990E+00	3.23905E-04	22	20	24	22
2.16535E+00	-8.09822E-05	28	26	30	28	2.09061E+00	2.05474E-03	23	20	25	22
2.17864E+00	-2.82397E-04	29	26	31	28	2.08049E+00	1.12189E-03	24	20	26	22
2.19471E+00	-5.25867E-05	30	26	32	28	2.09834E+00	-9.99962E-04	25	20	27	22
2.20148E+00	-6.20339E-04	31	26	33	28	2.11946E+00	-4.61334E-03	26	20	28	22
2.20975E+00	-7.53743E-04	32	26	34	28	2.23991E+00	-2.52287E-02	27	20	29	22
2.21032E+00	-7.62363E-04	33	26	35	28	2.14990E+00	-9.82453E-03	28	20	30	22
2.23145E+00	-1.08245E-03	34	26	36	28	2.14250E+00	8.57744E-03	29	20	31	22
1.73446E+00	6.44667E-03	35	26	37	28	2.12030E+00	-4.75786E-03	30	20	32	22
2.24917E+00	-1.35086E-03	28	27	30	29	2.16040E+00	-1.16207E-02	31	20	33	22
2.18510E+00	1.89892E-04	29	27	31	29	2.08009E+00	2.14131E-03	34	20	36	22
2.19320E+00	3.01045E-04	29	27	32	29	2.15919E+00	-1.14131E-02	35	20	37	22
2.20781E+00	5.01471E-04	30	27								

Figure 13.- Continued.

TOTAL NUMBER OF COMPUTED INTERSECTION POINTS   595
NUMBER OF ADMISSABLE INTERSECTION POINTS   284
AVERAGE Z COORDINATE OF ADMISSABLE INTERSECTION POINTS   .00564 FT.
AVERAGE Y COORDINATE OF ADMISSABLE INTERSECTION POINTS   2.03502 FT.

29	33	27	31	6.99933E-04	2.22228E+00
29	34	27	32	1.11654E-03	2.25266E+00
29	35	27	33	1.02014E-03	2.24563E+00
29	36	27	34	5.15109E-04	2.20081E+00
29	37	27	35	1.40697E-03	2.27383E+00
30	31	28	29	7.26024E-04	2.19242E+00
30	32	28	30	2.79236E-03	2.20066E+00
30	33	28	31	6.68643E-03	2.27387E+00
30	34	28	32	-5.07590E-03	2.11313E+00
30	35	28	33	8.14473E-03	2.29353E+00
31	32	29	30	7.20878E-04	2.19235E+00
31	33	29	31	-1.66736E-02	2.41036E+00
31	34	29	32	-1.51258E-03	2.19652E+00
31	35	29	33	-2.15356E-03	2.19769E+00
31	36	29	34	-1.38542E-03	2.19628E+00
31	37	29	35	-5.24963E-03	2.20335E+00
32	33	30	31	7.19857E-04	2.19243E+00
32	34	30	32	-6.26606E-03	2.20521E+00
32	35	30	33	-3.73733E-03	2.18404E+00
32	37	30	34	-1.32954E-03	2.19754E+00
33	34	30	35	-2.97514E-02	2.03815E+00
33	35	31	32	5.28358E-04	2.20795E+00
33	36	31	33	-1.68681E-02	2.11040E+00
33	37	31	34	-8.05598E-04	2.20928E+00
34	35	31	35	1.19951E-02	2.31963E+00
34	36	32	32	3.80976E-04	2.21955E+00
34	37	32	33	-1.38668E-01	1.02118E+00
35	36	32	34	7.12533E-04	2.24355E+00
35	37	33	35	2.19510E-04	2.23245E+00
				2.48373E-03	2.28346E+00
				1.29739E-03	2.23962E+00
				-1.02259E-02	2.16980E+00
				-1.26528E-04	2.26012E+00

Figure 13.- Continued.

85

VORTEX TANGENTIAL VELOCITIES AND RADII

IV	RADIUS,FT.	TANGENTIAL VELOCITY,FT/SEC.
1	.15638	20.45748
2	.14513	18.56264
3	.13389	16.02604
4	.12265	21.22583
5	.11142	25.84246
6	.10018	30.19980
7	.08895	27.94105
8	.07773	33.03576
9	.06651	39.70158
10	.05531	41.58294
11	.04414	50.56153
12	.03301	49.02997
13	.02201	48.77429
14	.01150	38.21378
15	.00577	-32.39586
16	.01369	-42.38586
17	.02439	-49.62818
18	.03543	-53.81561
19	.04657	-52.59037
20	.05775	-48.11050
21	.06896	-42.80504
22	.08017	-36.95108
23	.09140	-34.06554
24	.10263	-30.54773
25	.11387	-29.34528
26	.12510	-28.05721
27	.13634	-26.76052
28	.14758	-24.55448
29	.15883	-30.36058
30	.17007	-23.28154
31	.18131	-21.54256
32	.19256	-19.53120
33	.20380	-19.13302
34	.21505	-18.71446
35	.22630	-20.17093

THIS TRAVERSE RESULTED IN A CORE PENETRATION

IN THIS VORTEX ACCOUNT, THE VORTEX TANGENTIAL VELOCITY
HAS ONE PEAK   50.56153 FT/SEC AT RAD=   .04414 FT.
AND ANOTHER   -53.81561 FT/SEC AT RAD=   .03543 FT.

VORTEX STRENGTH,GAMMAO,FT**2/SEC.

IV	RADIUS,FT.	TANGENTIAL VELOCITY,FT/SEC.	GAMMAO,FT**2/SEC.
1	.15638	20.45748	20.10006
2	.14513	18.56264	16.92714
3	.13389	16.02604	13.48216
4	.12265	21.22583	16.35768
5	.11142	25.84246	18.09094
6	.10018	30.19980	19.00966
24	.10263	30.54773	19.69831
25	.11387	29.34528	20.99436
26	.12510	28.05721	22.05385
27	.13634	26.76052	22.92441
28	.14758	24.55448	22.76886
29	.15883	30.36058	30.29733
30	.17007	23.28154	24.07771
31	.18131	21.54256	24.54146
32	.19256	19.53120	23.63003
33	.20380	19.13302	24.50015
34	.21505	18.71446	25.28654
35	.22630	20.17093	28.67980

AVERAGE CIRCULATION IN OUTER REGION   21.90114 FT**2/SEC
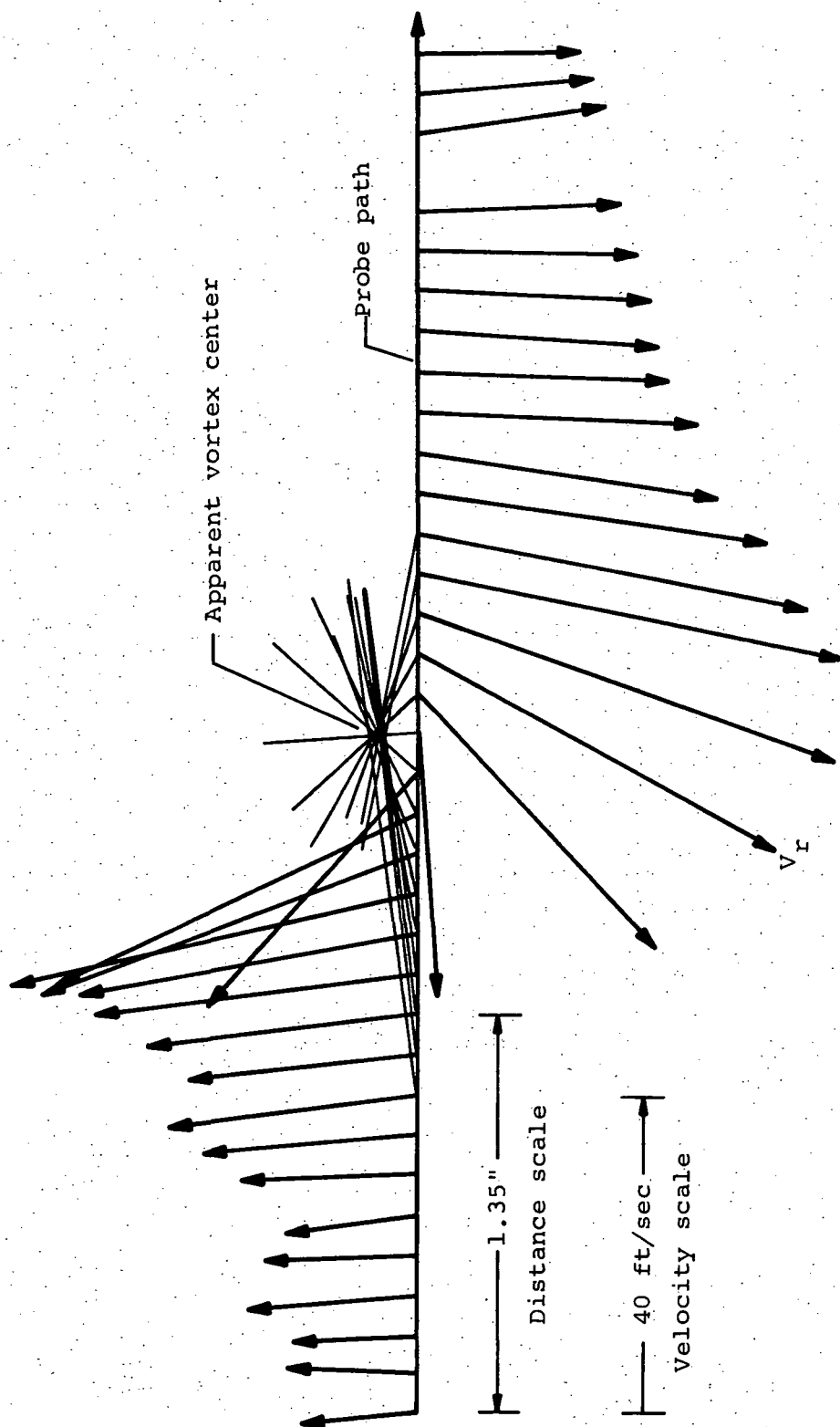
Figure 13.- Concluded.

Figure 14.— Resultant velocity vector and vortex center construction in the crossflow plane 55 chord lengths behind tip of a rectangular wing with 32-inch span and 6-inch chord (data taken in 40×80 tunnel at Ames at $\alpha = 12^\circ$).
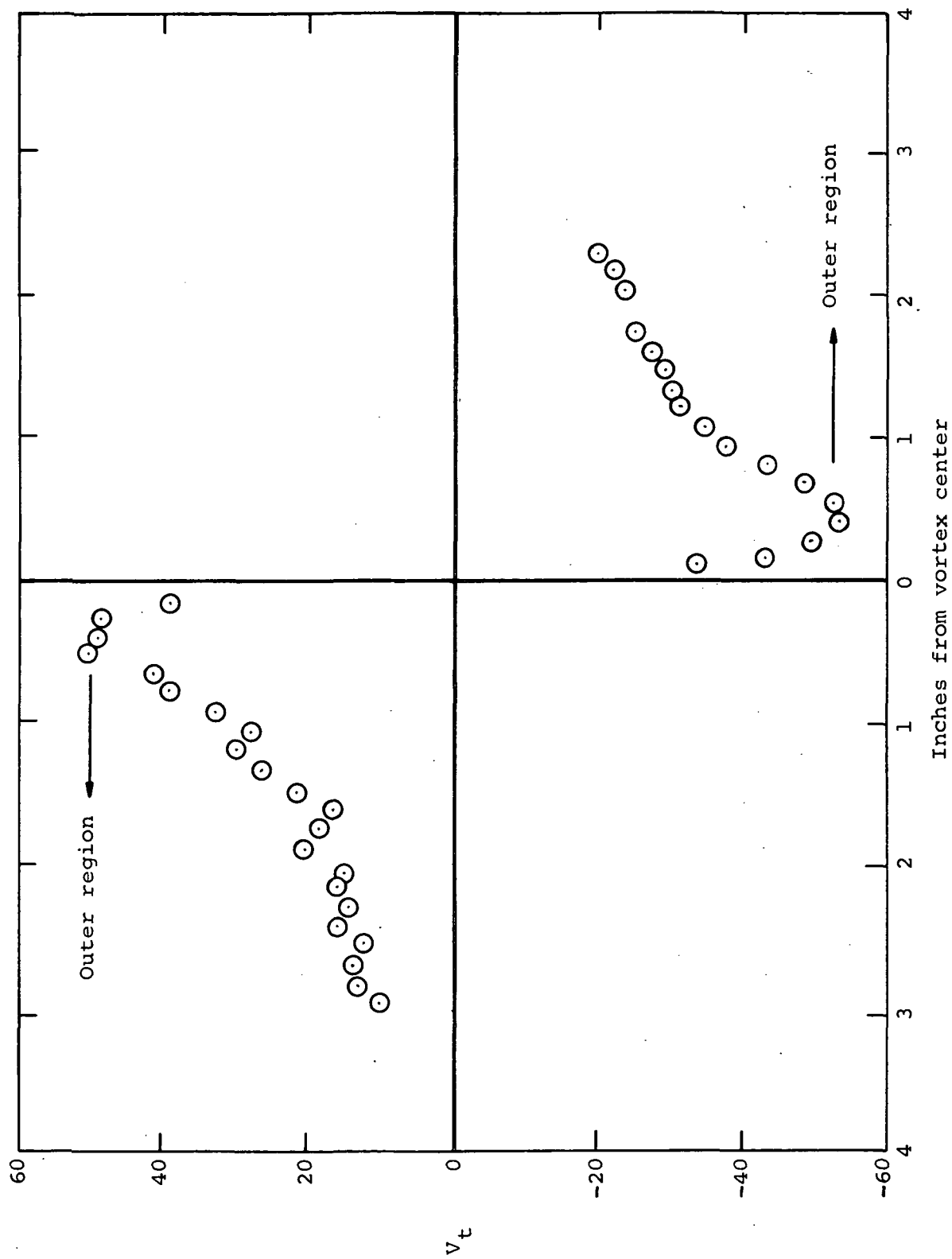
87

Figure 15.— Vortex tangential velocities as a function of radial distance from vortex center using data from figure 14.

Measurement	Instrument	Comments	Page Refs.
Vortex Velocity, 3 components	DISA 3-wire anemometer	Should be calibrated both on ground and in flight	19-21
		Tape recorder speed should reflect digitizing required	21-22
		Recommend using an oscilloscope with a "memory"	21
Vortex Temperature	DISA Single-Wire anemometer	Must have constant current electronics for frequency response	20
Distance of Probe behind T-33	LRC airborne DME		22
Vertical Displacement of Wake	Altimeters	Difference the Learjet and T-33 altimeter readings	22
T-33 Weight	Calculated	Required to get theoretical Γ_o	18
T-33 Lift Constancy	Pilot assessment	Vertical acceleration of T-33 should be minimized	18
T-33 Air Speed	Cockpit instruments	Value and constancy should be monitored and tape recorded	18
Air Density	Learjet ambient temp and pressure probes	Required to get theoretical Γ_o	18
Air Turbulence Levels	DISA 3-wire anemometer	Problem is low output voltage	13-15
	DISA Voltmeter	Has a 1 millivolt scale	14-15
	Vanes on nose boom	Limited to about 15 Hz	15-16
Air Humidity	On-Board meter or sampler	Ambient levels and within vortex, if possible	25,31-36
Air Temperature	Learjet Temperature probe	Need temperature distribution over ~ 2000 feet height	24
Vertical Air Currents	Learjet Accelerometers and hot-wire probes	Any estimates of vertical air currents will be done from indirect measurements or isotropy of turbulence	24-25
Crow Instability	Movie camera	Fly Learjet along wake and take movies	23
Learjet - Wake Interaction	Movie Camera	Done from chase plane filming the Learjet penetration	24
Vortex Dissipation Mechanisms	Movie camera and Learjet penetration	Film dissipation region and fly Learjet probes through region	24
Learjet Trajectory	Accelerometers on board Learjet	Single and double integration necessary to establish position versus time for wake probes and corrections to hot-wire velocities	--

Figure 16.- Summary of recommendations on data collection.

89